3-24-2016

Capturing Atmospheric Effects on 3-D Millimeter Wave Radar Propagation Patterns

Richard D. Cook

Follow this and additional works at: https://scholar.afit.edu/etd

Part of the Engineering Physics Commons

Recommended Citation

**CAPTURING ATMOSPHERIC EFFECTS ON
3-D MILLIMETER WAVE RADAR
PROPAGATION PATTERNS**

THESIS

Richard Daniel Cook, Second Lieutenant, USAF

AFIT-ENP-MS-16-M-063

**DEPARTMENT OF THE AIR FORCE
AIR UNIVERSITY**

AIR FORCE INSTITUTE OF TECHNOLOGY

Wright-Patterson Air Force Base, Ohio

AFIT-ENP-MS-16-M-063

CAPTURING ATMOSPHERIC EFFECTS ON 3-D

MILLIMETER WAVE RADAR PROPAGATION PATTERNS

THESIS

Presented to the Faculty

Department of Engineering Physics

Graduate School of Engineering and Management

Air Force Institute of Technology

Air University

Air Education and Training Command

in Partial Fulfillment of the Requirements for the

Degree of Master of Science in Applied Physics

Richard Daniel Cook, B.S.

Second Lieutenant, USAF

March 2016

AFIT-ENP-MS-16-M-063

CAPTURING ATMOSPHERIC EFFECTS ON 3-D

MILLIMETER WAVE RADAR PROPAGATION PATTERNS

THESIS

Richard Daniel Cook, B.S.
Second Lieutenant, USAF

Committee Membership:

Dr. S.T. Fiorino
Chair

Dr. K.J. Keefer
Member

Lt Col J. Stringer, PhD
Member

AFIT-ENP-MS-16-M-063

Abstract

The need to model millimeter wave (MMW) radar propagation is imperative to proper design of aeronautical, civil, and military systems. Traditional radar propagation modeling is done using a path transmittance with little to no input for weather and atmospheric conditions. As radar advances into the MMW regime, atmospheric effects, such as attenuation and refraction, become more pronounced than at traditional radar wavelengths. The DoD High Energy Laser Joint Technology Offices High Energy Laser End-to-End Operational Simulation (HELEEOS), in combination with the Laser Environmental Effects Definition and Reference (LEEDR) code, is a powerful tool for simulating laser propagation and effects tied to atmospheric phenomena such as turbulence and extinction. Although LEEDR is already developed to characterize radiative transfer effects, this research attempts to extend HELEEOS to characterize the far field radar pattern in three dimensions as a signal propagates from an antenna through realistic atmospheres and weather conditions. The latter are derived from NOAA numerical weather prediction models or the Extreme and Percentile Environmental Reference Tables (ExPERT) climatological database. The results from these simulations are compared to those from traditional radar propagation software packages. In summary, this research explored adapting a laser propagation model to extend understanding of MMW propagation through various atmospheric and weather conditions.

iv

Acknowledgements

Table of Contents

List of Figures

List of Tables

CAPTURING ATMOSPHERIC EFFECTS ON 3-D

MILLIMETER WAVE RADAR PROPAGATION PATTERNS

I. Introduction

Radar applications in the millimeter wave (MMW) (30 - 300 GHz) band tradition-ally have been limited due to high atmospheric absorption and insufficient transmitter power. As radar technology progresses, MMW is finding itself at the forefront of radar innovation. Numerous applications, both civil and military, are found in Section 1.2. From a military standpoint, being able to quickly and accurately predict the three dimensional pattern of MMW propagation in various atmospheric scenarios is nec-essary to fully exploit design of radar weapon systems, electronic countermeasures (ECM), and electronic counter-countermeasures (ECCM).

This research addresses the complexities and shortcomings involved with using software to model MMW radar propagation in not only the traditional range-power relationships, but also the change in shape of the waveform and pattern over three dimensions as a signal propagates from an antenna towards a target. The High Energy Laser End-to-End Operational Simulation (HELEEOS) [7], developed by Air Force Institute of Technology's Center for Directed Energy, with the support of the High Energy Laser Joint Technology Office (HEL-JTO), is investigated as a potential tool to be adapted and modified in order to help predict the highly atmospheric dependent behavior of MMW radiation. Much is understood about the behavior of traditional radar wavelengths at the aperture and target. However, this research seeks to address gaps in knowledge of scattering, diffraction, and absorption that affect the propagation of a MMW radar beam. Due to shorter wavelength and phenomena

discussed in Chapter II, MMW radar is more sensitive to atmospheric effects than traditional wavelengths. Various radar modeling techniques are evaluated relative to the investigation of fundamental atmospheric processes that affect the propagation of MMW radar patterns. A MATLAB script is generated and optimized that allows HELEEOS to model a MMW radar pattern in various atmospheres and scenarios. The results from these HELEEOS calculations are compared amongst themselves and with existing radar models. Finally, future endeavors for research and capability enhancement are proposed. This thesis seeks to evaluate the problem statement of to what degree is HELEEOS able to be used to provide accurate modeling of EM Radiation propagation and scattering in the MMW regime, specifically with regards to impacts on MMW radar performance. A thorough analysis and evaluation of HELEEOS' ability to model MMW radiation will provide a springboard to future research and tools to accurately characterize the propagation of MMW radiation through a realistic atmosphere.

1.1   Background

As radar evolves into higher frequency bands, specific assumptions that engineers have been using for decades become outdated and inaccurate for the new wavelengths being explored. Being able to accurately model radar and other electromagnetic (EM) propagation is fundamental to proper system design for communications, radar, and other electrical applications such as satellite links and even vehicle design. Furthermore, with increasing sensitivities of electronic systems, the pattern with which EM waves propagate will become more of a factor to determine performance of systems.

Today, a large majority of radars operate between 300 MHz and 25 GHz [24]. Various ranges of radar frequencies, or bands, are used for many different applications from air traffic control, terrain avoidance, traffic collision avoidance (in air and land

vehicles), automotive parking assistance, automated landing guidance, police speed detection radar, and many other applications [25]. These radar systems are still expensive to operate and test and being able to model their propagation will save time and money. However, assumptions and approximations built into current propagation models for the traditional radar frequencies listed included in the band are reliable and accurate in most atmospheric conditions. However, moving outside of this band sends the designer into uncharted territory.
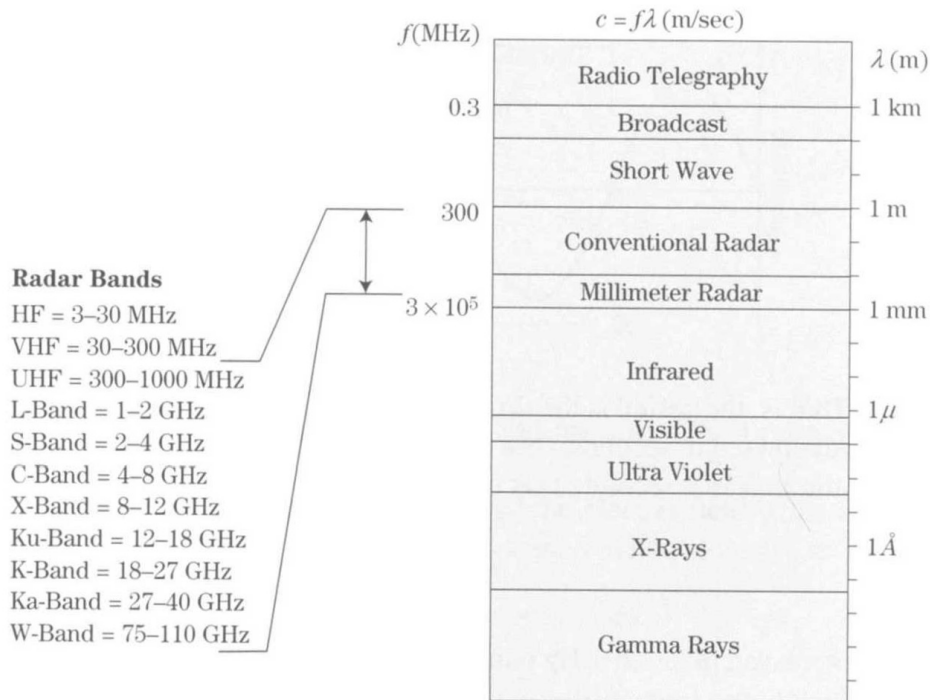
Figure 1. Placement of MMW Radar in EM Spectrum (Reproduced by permission of the Institution of Engineering & Technology [24])

Traditionally, frequencies between 30 GHz to 300 GHz (1 cm to 1 mm) have been avoided due to difficulties in signal processing, available power, and strong atmospheric absorption. However, as solid state transmitters are developed to provide adequate power, many industries are beginning to experiment with using the MMW part of the EM spectrum. This regime offers unique atmospheric propagation and antenna side-lobe pattern effects. It is necessary to investigate these effects to fur-

ther determine various operating parameters for a system and avoid interference with other electronic systems.

Because HELEEOS accounts for first principles of radiative transfer, potential exists for HELEEOS to be an improvement over existing methods. Despite this, future research will need to address any potential discrepancies that are brought up when switching from a laser propagation to RF propagation simulation. By using HELEEOS to model MMW radar, the capability to provide a full picture of the three dimensional pattern can be generated in order to predict radar propagation in various real-time weather and atmospheric scenarios. Examining turbulence effects on the MMW, refractive bending, multiple scattering, and attenuation correlation to experimentally measured strengths are all research areas that HELEEOS can interrogate. By providing first principle physical analysis HELEEOS gives promise to providing information that can be used to evaluate MMW radar signals.

1.2 Applications and Employment Considerations

Today, many applications of MMW radiation are finding their way into everyday life as well as defense applications. Cellular phone frequencies, wireless internet, digital radio, satellite communications, TSA full body scanners, collision avoidance radar on aircraft, and newer automobile features that sense collision hazards around the vehicle all at least partially employ the MMW regime [13]. However, this regime is heavily weather and atmosphere dependent which requires a thorough knowledge of the behavior and radiative transfer in the MMW regime. If one can effectively predict the radar pattern at any point down-range of the antenna, it will assist designers and engineers in optimizing systems based on terrain and weather extremes.

In addition to power propagated to an area of interest, radar cross section (RCS) is also highly wavelength dependent. RCS is used to give a representation of how large

an object appears on a radar return and is directly related to how well an object scatters energy in various directions from an incident angle. RCS measurements are based on traditional radar frequencies. Thus, it is not as widely understood how objects may look to a radar at MMW frequencies. Due to the much smaller wavelength, it is likely that small objects may impact the RCS much larger than anticipated. The scattering of MMW radiation will help answer questions about how objects will appear to a MMW radar. For instance, approximately 50% of a total target return at 96 GHz is due to nuts, bolts, rivets, and cracks [13]. This means that traditional models of RCS can be radically changed due to the fact that the "barn door" is no longer providing most of the radar return; it may, in fact, be the "doorknob" that will reflect the most.

Another advantage of MMW radar frequencies is the increased radar performance in areas of resolution and gain. The angular resolution of an antenna is directly proportional to wavelength, assuming antenna dimensions are not changed. Because of this, a smaller wavelength allows for smaller angular resolution which results in finer target identification and separation. Gain, (G) is the concentration of power which allows for a more directed beam of radar energy. An expression for gain is shown in Equation 1. Therefore, gain will increase in an antenna as the wavelength decreases [28].

$$G = 4\pi \frac{A\eta}{\lambda^2} \tag{1}$$

Weather satellites also use the microwave regime for cloud and precipitation detection. CloudSat, ProSensing Cloud Profiler, and many other space-based weather platforms operate with a 94 GHz channel [13]. A comparison of the increased effects from weather with increase in frequency is seen in Table 1. Note the difference in attenuation between 35 GHz compared with 94 GHz: the higher the frequency, the

higher the attenuation difference when weather effects are considered. The variance around 10 GHz are not as pronounced. Additionally, note the drastic change that is dependent upon intensity of weather effects such as rain; quadrupling the rain rate from 0.25 to 1.0 mm/hr increases the attenuation sevenfold. These effects support the reasoning that real-time weather and climatology modeling must be implemented into a MMW propagation model.

Table 1. LEEDR Generated Comparison of Atmospheric Effects on EM Attenuation at Traditional and MMW Radar Frequencies

	One-Way Loss (dB/km)		
Parameter	10 GHz	35 GHz	94 GHz
Standard Atmosphere	0.012	0.099	0.383
Rain (mm/hr)			
5	0.089	1.489	5.186
25	0.591	6.943	15.863
75	2.145	18.420	32.891
Clean Continental Cumulus	0.027	0.281	1.387
Fog	0.014	0.126	0.532

1.3 Thesis Outline

Chapter II reviews previous research in MMW propagation and radar theory. Furthermore, it examines work that has been done in EM wave propagation modeling. Concepts of operation are reviewed for models such as Advanced Refractive Effects Prediction System (AREPS) [22], Improved Many-on-Many (IMOM) [18], Laser Environmental Effects Definition and Reference (LEEDR) [9], and HELEEOS. Chapter III covers research methodology and layout of the experiment. Chapter IV evaluates the strengths and weaknesses of using HELEEOS to model a MMW radar pattern along with comparison to current radar models. A summary and conclusion of findings are presented in chapter V, along with prospects for future research. Finally, an appendix contains applicable MATLAB scripts used and information on how to use MATLAB's Sensor Array Toolbox to generate radar patterns for import into HELEEOS or other applications of interest.

II. Literature Review

2.1 EM Wave Propagation Theory

Radar employs EM waves that propagate at relatively high frequencies (see Figure 1), and investigations into how the waves propagate in the atmosphere originate with radiative transfer theory. In vacuum, EM radiation propagates at the speed of light and does not experience refraction absorption, or scattering. However, Earth's atmosphere is anything but a vacuum. Especially at the lower altitudes, various processes occur which either scatter, absorb, re-emit, or otherwise alter the photons as they travel through the atmosphere. Therefore, a thorough understanding of radiative transfer as it applies to MMW radar is required.

Index of Refraction.

Solving the wave equation, Equation 2 for an EM wave in vacuum, the speed of light (in meters per second) is found to be Equation 3.

$$\frac{\partial^2 u}{\partial t^2} - c^2 \nabla^2 u = 0 \tag{2}$$

$$c \equiv \frac{1}{\sqrt{\varepsilon_o \mu_o}} \tag{3}$$

where $\varepsilon_o = 8.854 \times 10^{-12} \frac{F}{m}$ is the permittivity of free space and $\mu_o = 1.257 \times 10^{-6} \frac{N}{A^2}$ is the permeability of free space.

When considering propagation in a non-vacuum, the expression for the wave propagation direction vector $\vec{k}$ becomes

$$\left| \vec{k} \right| + i \left| \vec{k} \right| = \omega \sqrt{\frac{\varepsilon \mu}{\varepsilon_o \mu_o}} \sqrt{\varepsilon_o \mu_o} = \frac{\omega N}{c} \tag{4}$$

where ω is the angular frequency of the wave and N is the complex index of refraction defined by $N = \frac{c}{c'}$ where c' is the phase speed (approximately, if the medium is non-absorbing) of the wave through a medium. N is a complex number and the real part of N defines the phase velocity whereas the imaginary part represents attenuation of the wave. The magnitude of N is generally greater than 1, which implies the wave slows down through the medium. It is important to remember that N is heavily dependent not only upon the medium, but also the frequency of the wave [23].

Scattering.

In addition to absorption, EM radiation can be scattered out of the path as depicted in Figure2. This clearly reduces the effect of MMW radiation because the energy is no longer on the path between the receiver (or target) and transmitter. The likelihood of EM radiation scattering is heavily dependent upon the size and number of the scatterers and the wavelength of radiation.
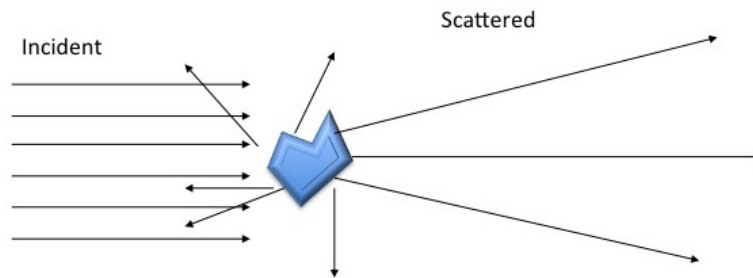
Figure 2. Single Scattering of Incident Wave by Particle (Adapted from Petty [23])

Because sensors do not differentiate between energy that has been absorbed or scattered, an extinction coefficient will be defined as the sum of energy absorbed and scattered out of the line-of-sight.

$$\beta_e = \beta_a + \beta_s \tag{5}$$

In order to characterize the extinction as absorption or scattering, the term single scatter albedo, $\tilde{\omega}$ is defined as

$$\tilde{\omega} = \frac{\beta_s}{\beta_e} = \frac{\beta_s}{\beta_s + \beta_a} \tag{6}$$

$\tilde{\omega}$ has a range of zero in purely absorbing medium and one in purely scattering medium.

Because scattering of light depends upon the wavelength of the incident radiation as well as the size of the scatterer, it is convenient to describe scattering behavior in relation to a dimensionless size parameter, χ.

$$\chi \equiv \frac{2\pi r}{\lambda} \tag{7}$$

where r is the radius of the scattering particle. Figure 3 shows various types of scattering as defined according to their size parameter; note the traditional and MMW radar regimes shaded on the dark and light gray respectively. Even with wavelengths on the millimeter scale, it is still typical to only address Rayleigh and Mie scattering, and ignore geometric optics. As the wavelengths get shorter, there are fewer constituents commonly found in the atmosphere that produce negligible scattering. As this research focuses on wavelengths on the order of a millimeter, we see that scattering will begin to become an issue once on the order of radii equal to $0.1\mu m$ or greater. This corresponds to Rayleigh Scattering for dust, smoke, haze, and cloud droplets. In the MMW regime, drizzle, raindrops, and hail act as Mie Scatterers. It is crucial to consider the wavelength with respect to the size of the scatterer when considering radar applications as they move into the MMW regime. For instance, realizing that as χ increases, forward scattering starts to dominate, which means that there is less energy returned to the receiver, which, in turn, means that there may be no return

for a particular target or weather phenomena.

The differences between Rayleigh and Mie Scattering are shown below in Figure 4. For Mie Scattering,photons are scattered primarily in the forward direction and the larger the particle, the greater forward scattering of energy. Note that the phase function (where the energy is likely to scatter with respect to incident angle) denotes a relatively isotropic distribution for Rayleigh Scattering whereas Mie Scattering is characterized by mostly forward scattering.

Rayleigh Scattering   Mie Scattering
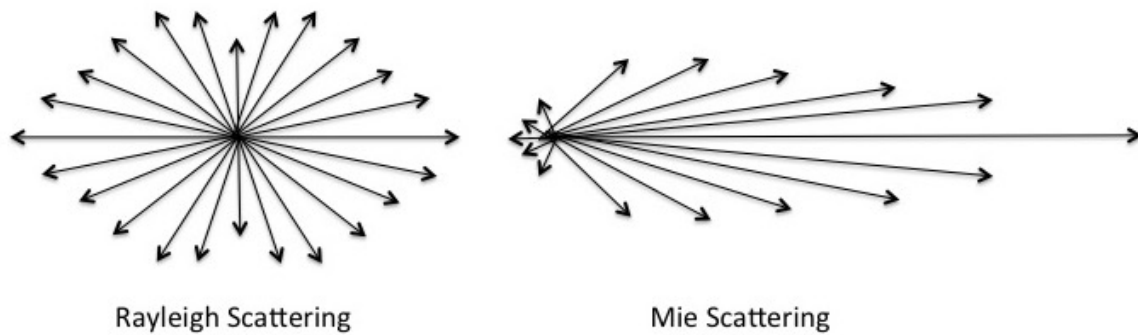
Figure 4. Comparison of Rayleigh and Mie Scattering. For Mie Scattering, larger particles create a more pointed forward scattering pattern (Adapted from Petty [23])

Scattering will be important to model because it is vital to forming a 3-D picture of the radar pattern as it propagates. Furthermore, the various sidelobes in a radar transmitter will cause very complex patterns developed when scattering takes effect. This was not normally a factor for traditional radar because the wavelengths were longer and most atmospheric constituents had negligible contributions to scattering.

Multiple Scattering.

The phenomena of multiple scattering occurs when radiation scatters several times after the initial incidence with a scatterer. With multiple scattering, it is possible for a photon to scatter out of line of sight and back into the line of sight. Modeling
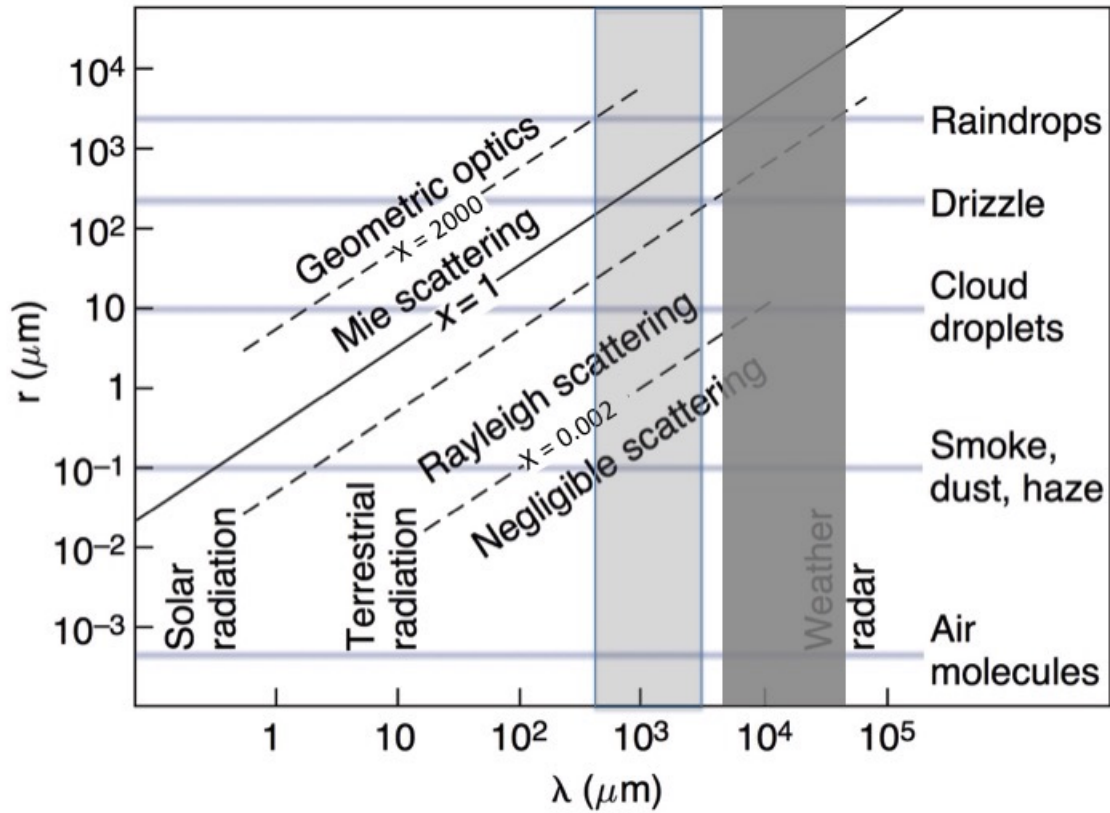
Figure 3. Comparison of Size of Scatterer vs. Wavelength and the various scattering regimes. The shaded box represents the MMW regime. Note that $\chi \equiv \frac{2\pi r}{\lambda}$. Modified from Atmospheric Science, 2nd Edition, John M. Wallace and Peter V. Hobbs, Figure 4.11, Pg. 123, Copyright 2006, with permission from Elsevier [34].

this is very difficult and computationally demanding; however, at higher density of scatterers, it becomes more important to consider multiple scattering effects.

As of the writing of this thesis in January 2016, HELEEOS only accounts for single scattering. However, especially with the density of lower atmospheric levels, modeling multiple scattering is necessary to accurately predict losses of radiation. Current efforts are close to modeling multiple scattering using HELEEOS on a high performance computer [8]. However, the computer power required is still intensive.

Absorption.

According to Petty [23], a restatement of Beer's Law is given in Equation 8. Beer's law governs the attenuation of photons as they pass through a slab of absorbing or scattering medium.

$$F = F_o e^{-\beta_a x} \tag{8}$$

where F_o is the incident flux of photons on a parcel of air and F is the flux that makes it through a portion of linear distance x. β_a is the absorption coefficient (in units of inverse length so that the argument of the exponent is unit-less) derived from the imaginary component of N by referencing Equation 4:

$$\frac{\omega}{c} Im\{N\} = \frac{\omega n_i}{c} = \frac{2\pi\nu n_i}{c} \tag{9}$$

where n_i is the magnitude of $Im\{N\}$ and ν is the frequency of the wave in Hertz. Therefore, β_a becomes:

$$\beta_a = \frac{4\pi\nu n_i}{c} = \frac{4\pi n_i}{\lambda} \tag{10}$$

By referencing Equation 8, it is apparent that the distance of β_a^{-1} is the distance

for the wave's fluence to be attenuated by a factor of $\frac{1}{e}$. Note that n_i depends on the permittivity and permeability of the propagation medium which is influenced by several parameters such as size of the absorbers, density, type of absorbers, and many other factors. Also, the presence of λ in Equation 10 shows an inverse wavelength dependence on the absorption coefficient.

It is also important to note that when atmospheric radiation is absorbed, an atom or molecule becomes excited. In turn, the excited molecule may relax back to its ground state and release a photon. Thus, there is a need to determine the quantum probabilities that a molecule will re-emit when excited with incident radiation.

Because these values of β_a are dependent on so many various factors, in order to calculate gaseous absorption, each atmospheric constituent and has been categorized for its specific effect at a certain wavelength into tabulated databases, the most common of which is HITRAN. This spectroscopic database lists various atmospheric atoms and molecules and the strength of their absorption coefficient in cm^{-1}. Radiative transfer models take these coefficients and discretize the atmosphere and sum the effects of each atmospheric layer and constituent to get a total path transmittance. This same methodology will apply to MMW radar propagation; by determining the absorbing constituents, a radiative transfer model can determine the strength of the beam after passing through a parcel of air.

Atmospheric Transmittance Calculations.

In order to determine the change in intensity of an EM wave, a general form of Beer's Law is invoked:

$$I_\lambda = I_{\lambda o} \exp\left[-\int_{s_1}^{s_2} \beta_e(s)\, ds\right] \tag{11}$$

Equation 11 calculates the final intensity of an incident EM radiation after passing

14

through a homogeneous parcel of air with an extinction cross section β_e where the path is defined by s_1 and s_2.

The value of the integral in Equation 11 is defined as the optical path (τ) which is analogous to optical depth/thickness when measured vertically.

$$\tau \equiv \int_{s_1}^{s_2} \beta_e(s) \, ds \tag{12}$$

When taking the exponent of Equation 12, the transmittance is calculated over a path s:

$$t \equiv e^{-\tau} \tag{13}$$

Transmittance is a number from zero to one where zero is an optically thick (or opaque) atmosphere and 1 is an optically thin (transparent) atmosphere. When discretizing the atmosphere into several layers, the total transmittance is the product of each layer's transmittance. The total optical depth is the sum of all optical depths [23].

Absorption in the MMW Regime.

In the millimeter wave regime, molecular absorption is primarily due to water and oxygen. Figure 5 depicts extinction as a function of frequency. The peaks at 22 GHz and 60 GHz are due to water and oxygen, respectively. The test frequencies for this research (35 and 94 GHz) are denoted with stars. Also in the MMW regime are peaks for oxygen at 120 GHz and water at 183 GHz. These successive peaks drive an overall upward trend as frequency increases. Therefore, lower frequencies are not as affected by this continuum absorption as the higher frequencies.
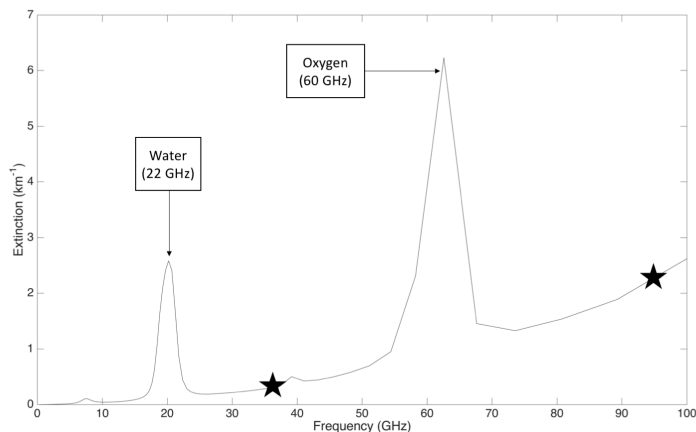
Figure 5. Extinction as a Function of Frequency for 0 - 100 GHz

Radar Range Equation.

To this point, the attenuation of an EM wave has been discussed according to atmospheric absorption and scattering. However, in radar applications, since the wave originates at a point (radar transmitter) and radiates out in a semi-spherical pattern, a significant amount of the attenuation is due to the power of the initial beam being spread over the area of the semi-sphere. This loss mechanism is called free space path loss. To illustrate free space path loss, consider a balloon being blown up. When deflated, the latex is very thick, but the length from the hole to tip of the balloon is shorter than when inflated. As you inflate the balloon, the distance increases at the expense of the latex being thinned out. Because of this effect, the strength of the energy as it travels out in a spherical pattern is proportional to $\frac{1}{4\pi R^2}$, where R is the distance between transmitter and signal detection location.

Because a radar signal must traverse both from the transmitter, to the target, then back to the receiver (assumed to be at the same location as the transmitter), the total strength back to the receiver is proportional to $\frac{1}{(4\pi)^2 R^4}$. Putting these concepts together, a general radar range Equation for a specific radar system is formed:

$$P_{rec} \cong \frac{P_{avg} G \sigma A_e t_{int}}{(4\pi)^2 R^4} \qquad (14)$$

where

$$P_{avg} = \text{Average Transmitted Power}$$

$$G = \text{Antenna Gain}$$

$$\sigma = \text{Radar Cross Section of Target}$$

$$A_e = \text{Antenna Area}$$

$$t_{\text{int}} = \text{Interrogation Time}$$

Note that this Equation does not account for atmospheric losses in the radar signal. This is because at traditional radar wavelengths, atmospheric attenuation is very low. However, as the wavelength shortens and begins to get on the scale of atmospheric phenomena (i.e. raindrops), attenuation becomes a factor. In order to account for atmospheric losses, a propagation factor, F is defined such that

$$F = \frac{|E|}{|E_o|} \qquad (15)$$

where E is the magnitude of the electric field when propagated through the atmosphere, and E_o is the magnitude of the electric field given by free space propagation such as in Equation 14. This method allows easy computation of the strength of the signal by combining all the effects computed from the total extinction from the atmospheric transmittance calculation sections. Because the atmosphere is not homogeneous in all directions, it is possible that the value of F changes dramatically depending on location in space. Accounting for this is the prime benefit of using a weather model based package such as HELEEOS to propagate the EM wave in three dimensional space [28].

17

2.2 Radiative Transfer Models

A radiative transfer model is any program that predicts the propagation of electromagnetic radiation in the atmosphere or free space. The Air Force Institute of Technology Center for Directed Energy (AFIT CDE) has developed extensive research and products to calculate the propagation of lasers in the atmosphere in order to support the ongoing DoD high energy laser research and development. In order to capture such effects, such as thermal blooming, optical turbulence, and extinction, programs such as LEEDR build an atmosphere from climatology or numerical weather model in both space and time. This allows for highly accurate determination of parameters that also will affect energy propagated in the RF frequencies. The atmosphere that LEEDR creates can also be ingested into HELEEOS which applies a laser propagation code through that atmosphere to determine irradiance and other laser measures of merit. Other models evaluated in this research include APM/AREPS and IMOM which are mission planning tools that evaluate the propagation of radar and communication systems. Figure 6 provides a comparison and relationship of the propagation models further explained below.
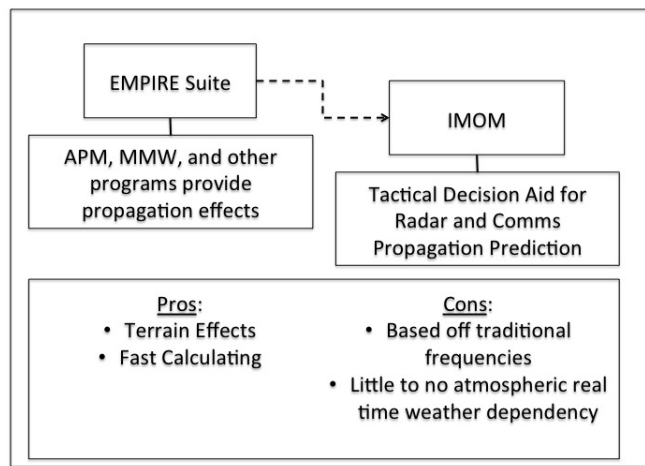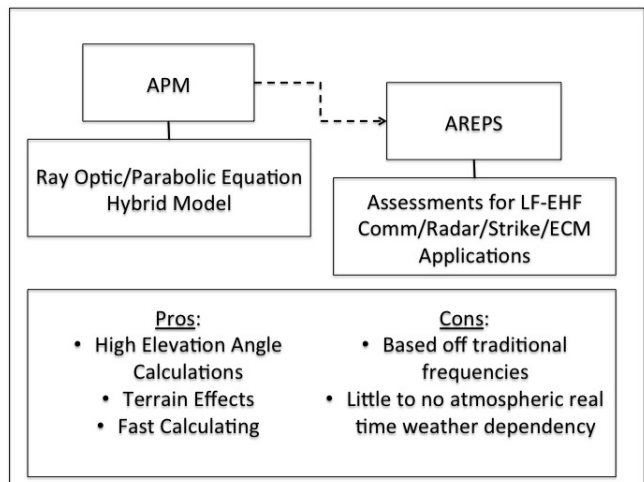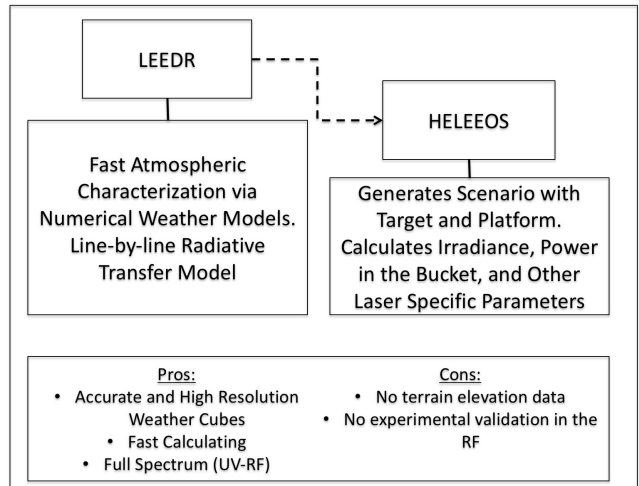
Figure 6. Comparison of Models Evaluated

LEEDR.

The AFIT CDE developed LEEDR in order to build realistic profiles of atmospheric effects which incorporate climatology or numerical weather prediction. The program runs in the MATLAB environment and allows the user to define a wavelength, atmosphere, and scenario geometry (slant angle and altitude). While initially created for high energy laser propagation for the Air Force's Airborne Laser System (ABL), it is capable of providing profiles for temperature, pressure, water vapor content, optical turbulence, and atmospheric particulates and hydrometeors and relate them for EM propagation from the UV to RF. The user can either choose a standard atmosphere, aerosol profile, and weather conditions; or, LEEDR can import data from a numerical weather prediction (NWP) model using NOAA's National Operational Model Archive and Distribution System (NOMADS) or climatology database (ExPERT) in order to provide actual weather conditions at a specific event time [9]. The atmosphere built by LEEDR is a three dimensional model of the atmosphere and takes into account the change in propagation due to vertical and horizontal (if using NWP) gradients in the atmosphere. The Graphical User Interface (GUI) for LEEDR is similar to the GUI for HELEEOS found in Figure 8 with the exception of the scenario setup.

Once LEEDR has built the atmosphere, the path transmittance, path extinction (km^{-1}), surface visibility (km), and slant path visibility (km) for the specific wavelength are calculated by using a line-by-line radiative transfer model. The ability to use a correlated-k method will also increase computation speed, if high spectral resolution is not necessary. Once LEEDR has calculated the atmosphere, it is able to generate a transmittance plot for the path of interest, as shown in Figure 7. This allows one to determine which portions of the spectrum are most opaque and which are transparent for the chosen atmospheric path and conditions [10].

20
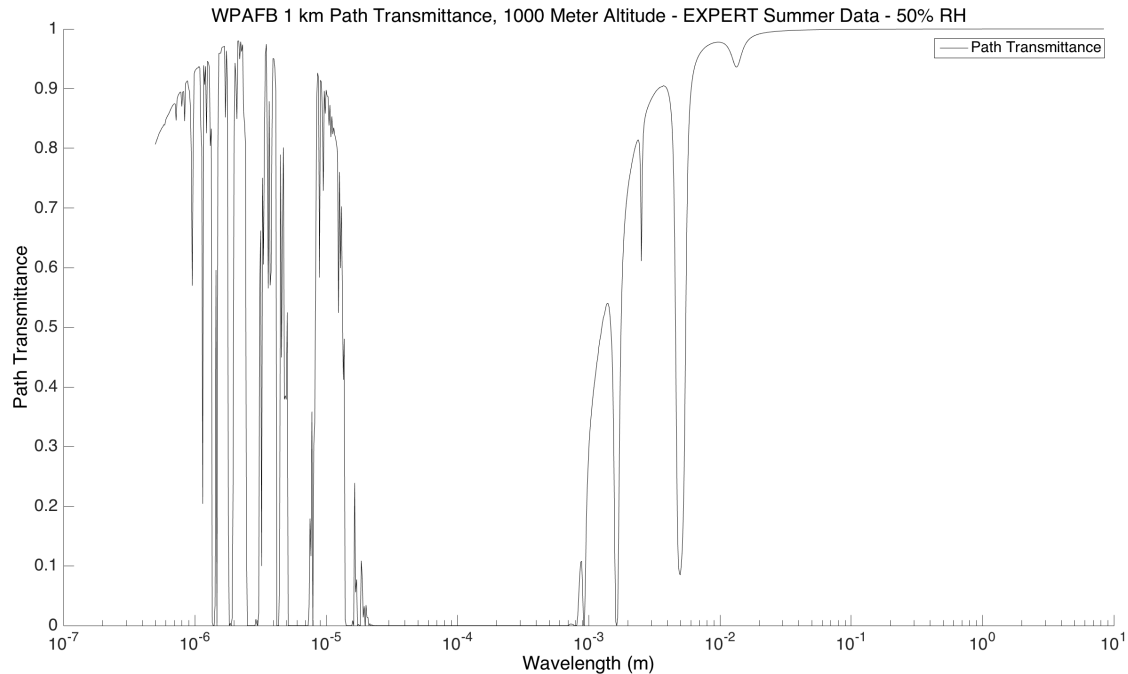
Figure 7. Example of path transmittance calculated by LEEDR for WPAFB at 12-15 Local Time on During Summer for a 1 km path at 1000 meters altitude.

A thorough knowledge of the LEEDR generated atmosphere is necessary in order to understand the assumptions and methods that LEEDR applies to generate the wavelength dependent absorption and scattering of the atmosphere. For molecular absorption, LEEDR considers the constituents and concentrations listed in Table 2. The absorption parameters are calculated using the HITRAN database and using a Lorentz line shape for pressure broadening at wavelengths for less than 1 millimeter. For wavelengths over 1 millimeter, the van Vleck-Weisskopf line shape is used [9].

Table 2. Molecular Absorbers Considered in LEEDR (Adapted from [9])

Absorber	Concentration
H_2O	Variable
CO_2	3.80×10^{-4}
O_3	Variable
N_2O	3.20×10^{-7}
CO	1.50×10^{-7}
CH_4	1.794×10^{-6}
O_2	.209
NO	2.99×10^{-10}
SO_2	2.93×10^{-10}
NO_2	2.99×10^{-11}
NH_3	5.03×10^{-11}
HNO_3	5.30×10^{-11}

For scattering, a number density must be assumed based off particle and droplet sizes. LEEDR uses a log-normal distribution to derive a normalized radius specific particle number density per unit volume as demonstrated in Equation 16 [9].

$$\frac{dN(r)}{d(\log r)} = \frac{N}{\sqrt{2\pi} \log(\sigma)} \exp\left(-\frac{(\log r - \log r_m)^2}{2(\log \sigma)}\right) \tag{16}$$

Taking this range of radii, LEEDR integrates over each radius (discretely) to determine a wavelength dependent extinction, scattering, and absorption coefficients for each particle. Using the Wiscombe Improved Mie Scattering algorithm [35], a total attenuation is calculated depending upon particles and atmospheric composition.

$$\sigma_{e,s,a}(\lambda) = \int\limits_{r1}^{r2} Q_{e,s,a}(m,\lambda,r)\pi r^2 \frac{dN(r)}{r\ln 10 d(\log r)}dr \approx \sum_{i=r_{min}}^{r_{max}} Q_{e,s,a}(m,\lambda,r)\pi r^2 \frac{dN_i}{r_i\ln 10 d(\log r_i)}\Delta r_i$$

$$(17)$$

These line-by-line and Mie Scattering calculations allow a first principles treatment of radiative transfer in a realistic LEEDR generated atmosphere. For more in-depth analysis and specific equations and assumptions that are included in the LEEDR transmittance calculations, the reader is directed to [9] and the LEEDR Equations and Principles Handbook published by the CDE [12].

HELEEOS.

HELEEOS builds on the functionality of LEEDR by creating a laser weapon-target scenario and determines probability of kill (P_k) along with other laser metrics for a given scenario. HELEEOS uses an wavelength dependent atmosphere built by LEEDR. Additionally, HELEEOS enables the user to specify a laser power, shape, and target type to determine laser operational parameters such as peak irradiance, power in the bucket, spot size, and other interesting measures of merit for laser performance. These fast-calculating values allow for on-the-fly operational assessments for effectiveness of laser propagation. HELEEOS has been well validated and useful in the UV to RF wavelengths. [11]. Figure 8 gives examples of the end user's GUI for running a HELEEOS simulation. While the GUI is acceptable for understanding general principles of operation for the program, as discussed in Chapter III, a script will be written which will set up the scenario and run the calculations and extract values of interest. Figure 8 walks through setting up a generic scenario beginning with location selection for climatology or NWP, selecting atmospheric constituent information, weather effects, laser and platform information, and finally scenario geometry.
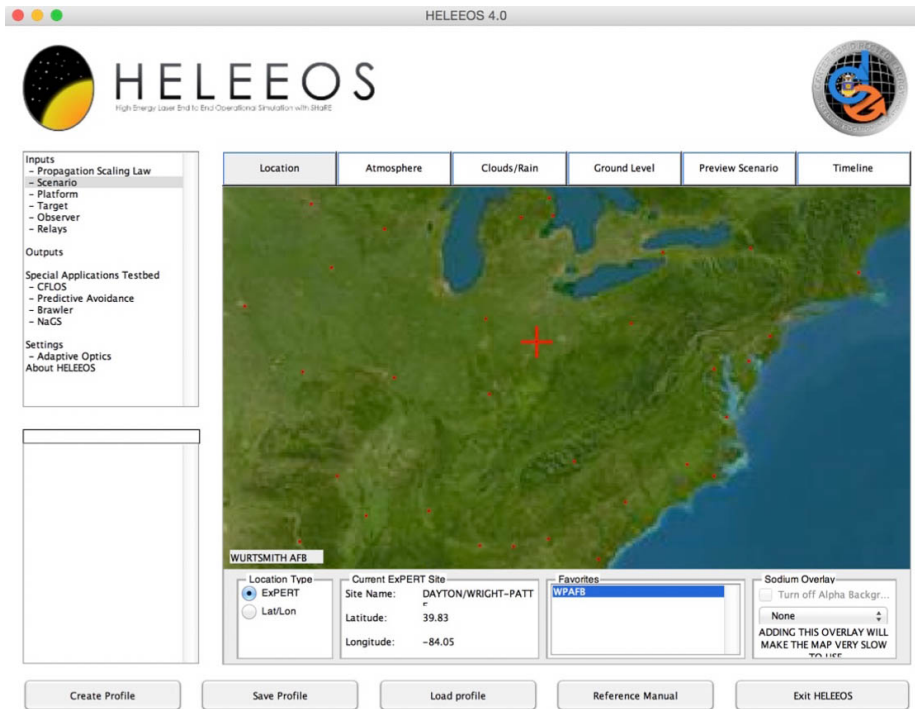
(a) Location Selection for ExPERT or NOMADS Data
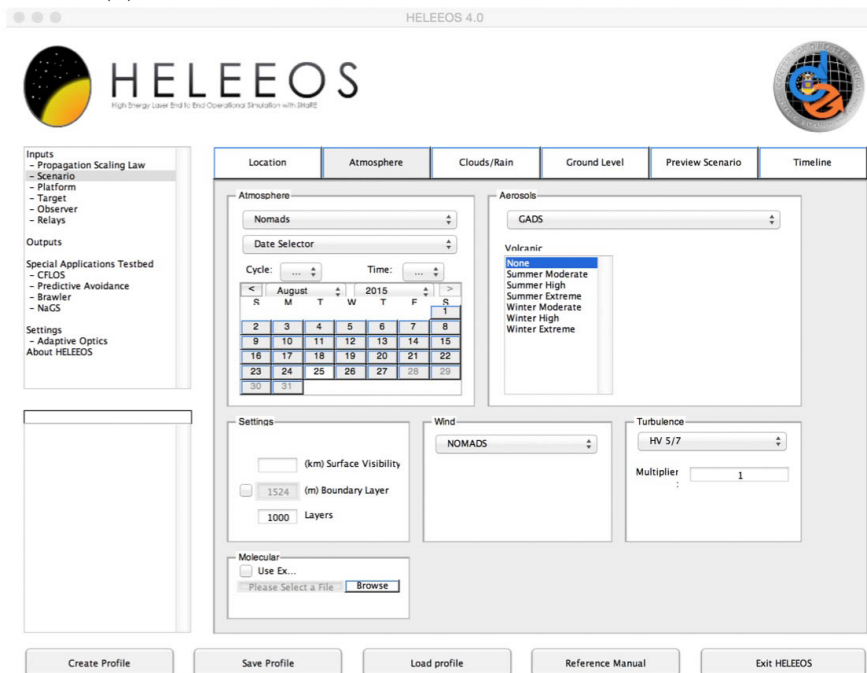
(b) Atmospheric Data Selection
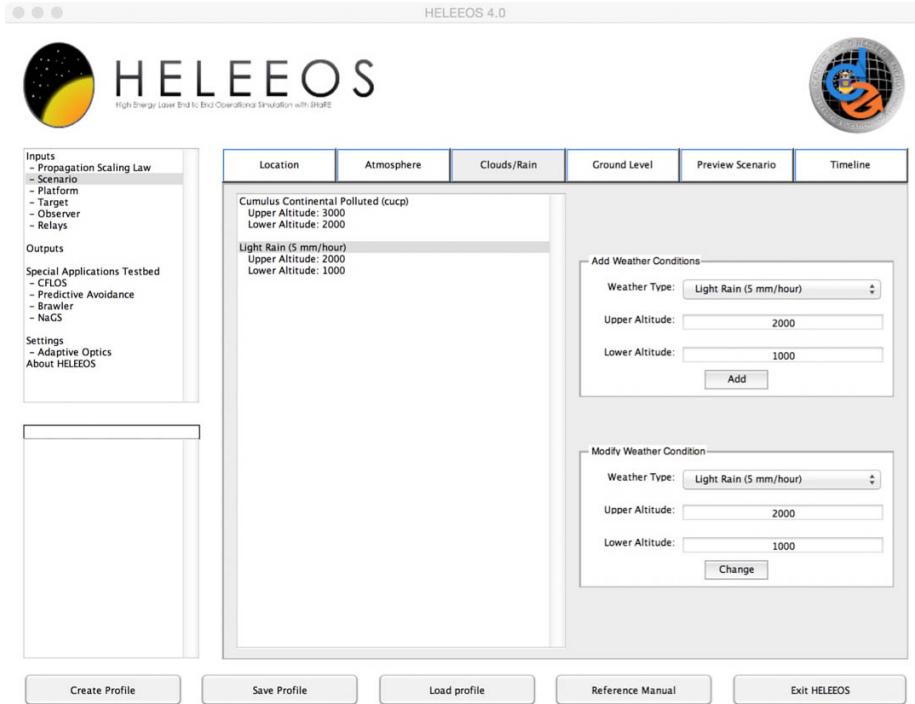
(c) Cloud and Rain Manual Selection
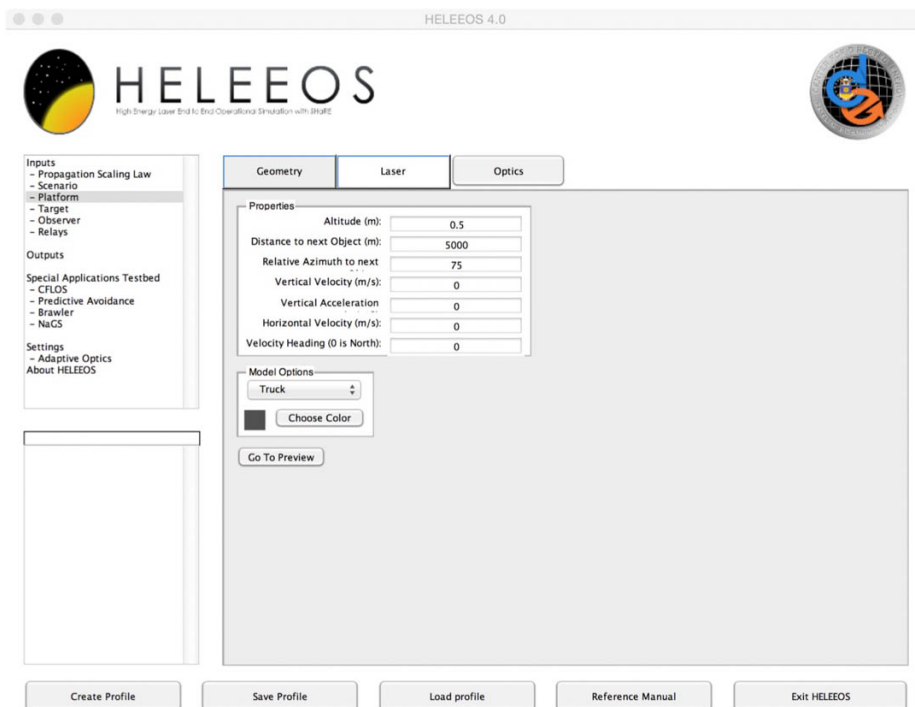
(d) Source Platform Information
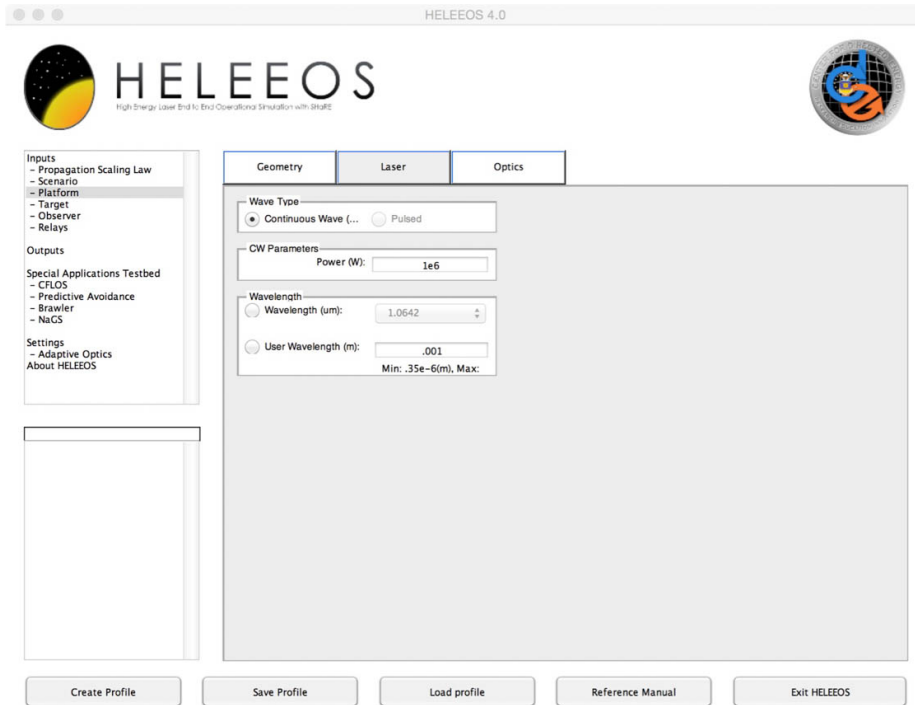
(e) Wavelength and Power Designation
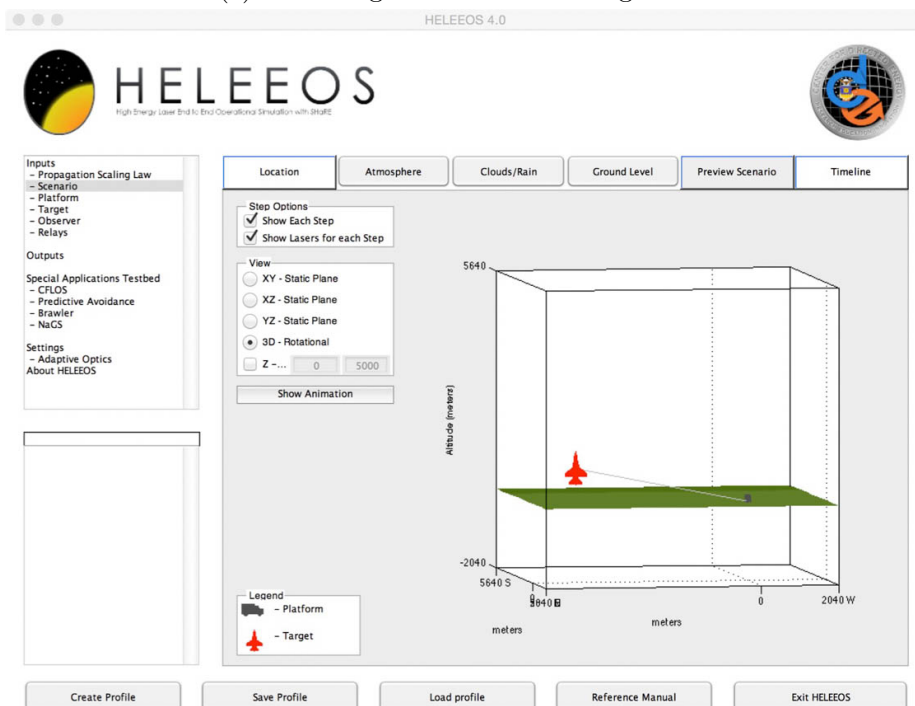
(f) Scenario Geometry Display

Figure 8. HELEEOS GUI Displays

Chapter III gives a description of how HELEEOS is used to provide a prediction of a radar pattern as it propagates in a real atmosphere. While traditional extinction makes it difficult to separate the absorption and scattering, HELEEOS treats the two phenomena separate and combines absorption and scattering to provide a total path extinction. Also, HELEEOS provides the scattering information which can, with further research, provide utility in determining off axis radar propagation that could either weaken the beam or allow a radar path more likely to be detected off the area of focus.

HELEEOS Assumptions.

HELEEOS uses the Scaling for High Energy Laser and Relay Engagement (SHaRE) [20] laser propagation and beam control toolbox for MATLAB. The wave optics code in this toolbox treats the EM radiation as a converging beam; this is unlike radar radiation which can be modeled as a diverging source. Our simulation methodology will circumvent this limitation by dividing the radar pattern into a large array of discrete laser like sources. Each angle, or fraction of the radar pattern will be treated as a laser beam. More on this methodology can be found in Chapter III.

It is also important to note that HELEEOS currently only has the ability to calculate single scatter radiation. This feature is implemented in LEEDR however, it has yet to be included in HELEEOS. Currently, there are plans to implement multi-scatter effects in the future. Implementing these calculations will greatly enhance the accuracy of beam propagation and provide a more thorough picture of where MMW energy is scattered to while propagation through the atmosphere. These calculations will greatly increase computation time, therefore, a simultaneous investigation into operating HELEEOS scripts on a high performance computer will make timely computations possible.

AREPS and APM.

The Space and Naval Warfare Systems Center (SPAWAR) developed the Advanced Propagation Model (APM), which is a hybrid ray-optic and parabolic equation model that constructs a fast, yet accurate model of EM propagation. By using a hybrid model, the APM can solve for high elevation angles where pure PE would not be used.

Furthermore, APM accounts for various sea and terrain paths using the Digital Terrain Elevation Data (DTED) database and also incorporates dielectric ground constants for finite conductivity and vertical polarization calculations. APM determines attenuation via oxygen, water vapor, interference, diffraction, tropospheric scatter, and ground waves. APM data have been validated to be very accurate in the 1.8 meter wavelength regimes; however, no millimeter wavelengths have been validated [16]. The atmosphere that AREPS incorporates is able to take an input of temperature, dew point, relative humidity, winds, and other atmospheric data and create a vertical atmosphere using the gridded data.

AREPS (Advanced Refractive Effects Prediction System)is the graphical user interface to APM. AREPS is an end user product that runs on Microsoft Windows operating systems and enables the user to create high quality graphic depictions of radar propagation scenarios. AREPS and APM provide assessments for LF to EHF communications, radar, strike and ECM, and other applications [22].

AREPS generates graphical plots of dB attenuation at various heights and ranges. The two types of plots that will be used for this research include propagation loss and plots. An example of propagation loss is given in Figure 9 and propagation factor is seen in Figure 10. The propagation factor is the ratio of the actual electric field strength with respect to the field strength in free space conditions such as in Equation 18. Using the propagation factor, propagation loss can then be defined

using Equation 19 where L_{fs} is the free space path loss due to the spherical spreading of the energy. Because propagation loss also accounts for free space path loss, that will provide the most similar comparison to HELEEOS. It is also important to note the difference using the factor of 20 that arose from converting from power to voltage. This difference will cause decibel attenuation values to not align between HELEEOS and AREPS. Correlating the two models is an area rich for future research. For this reason, a significant portion of the analysis will be qualitative comparisons between the two outputs.

$$F = \frac{E}{E_{fs}} \tag{18}$$

$$L = L_{fs} - 20 \log_{10}(F) \tag{19}$$
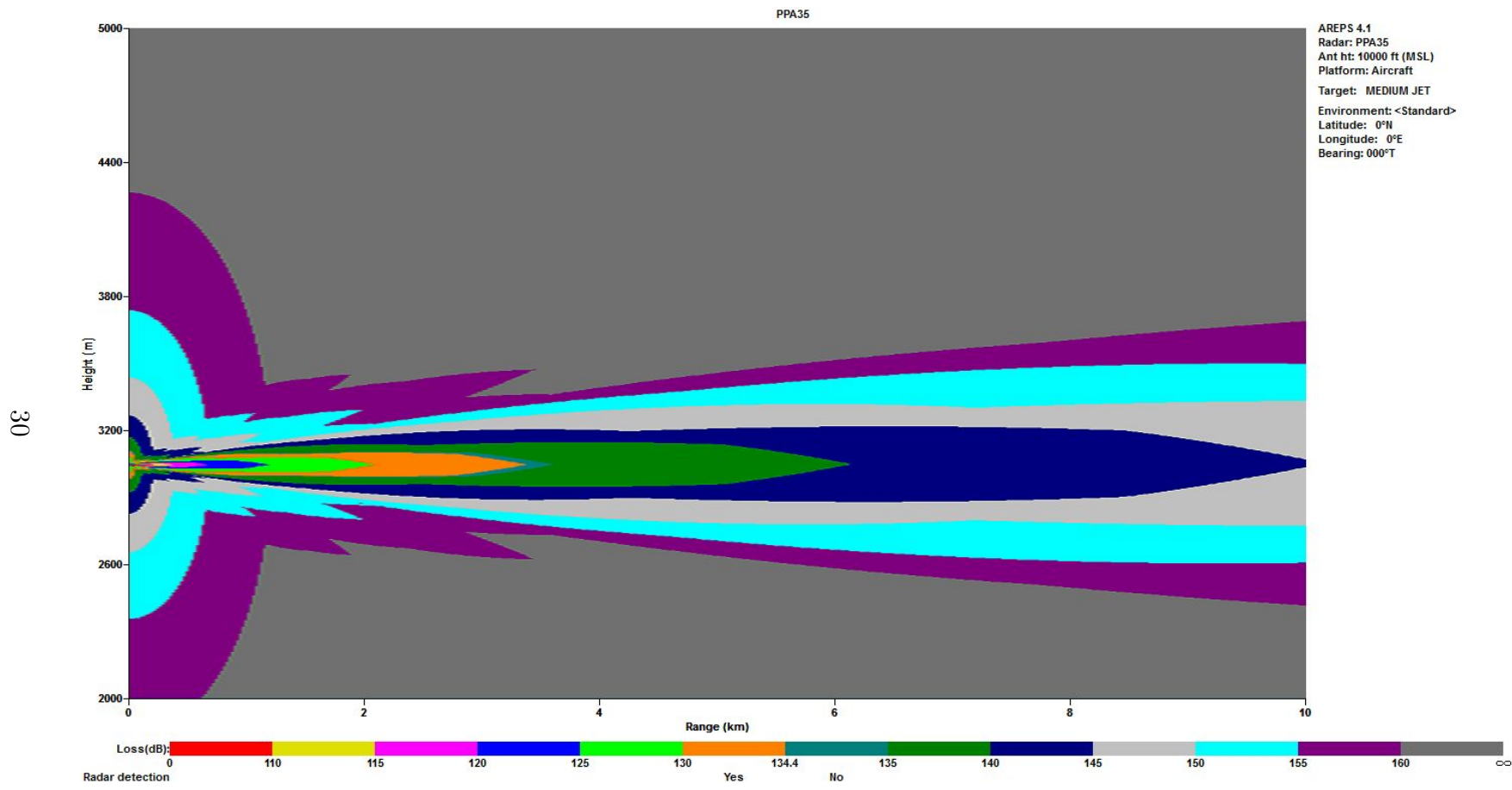
Figure 9. Example of AREPS Propagation Loss Plot

PPA35

AREPS 4.1
Radar: PPA35
Ant ht: 3048 ft (MSL)
Platform: Aircraft
Target: MEDIUM JET
Environment: <Standard>
Latitude: 0°N
Longitude: 0°E
Bearing: 000°T

Factor(dB):

Figure 10. Example of AREPS Propagation Factor Plot

IMOM.

Improved Many on Many (IMOM) is an end user computer simulation software that provides radar and communication propagation prediction. Originally developed as a tactical decision aid for radar threat detection, it has evolved into communications, broadcast, and even acoustic prediction with an extensive terrain effects package that also uses DTED [29] [18].

The limiting factor of IMOM and AREPS in the MMW regime is the inability to build a three dimensional atmosphere based off weather data. Figure 11 shows the part of the GUI that enables the user to select the atmosphere and limits the selection to a definition of humidity. In the MMW regime, there are many more effects to be concerned with in the atmosphere in order to correctly model a MMW pattern such as referenced in Table 1 and discussion on scattering and absorption provided in Chapter II.

IMOM will be used in conjunction with HELEEOS to provide a baseline and comparison of data in terms of MMW propagation. It will not be treated as a control because the atmospheric and weather models that are input into it are not as robust as the numerical weather data that is ingested into HELEEOS.

Parabolic Equations.

AREPS and IMOM both employ a technique called Parabolic Wave Equation (PWE) Modeling. PWE is different from HELEEOS and LEEDR which use a line-by-line radiative transfer code to determine atmospheric absorption. PWE solves the Helmholtz equation in a small angle, forward scattering approximation, PWE is able to determine propagation by including spherical-Earth diffraction, atmospheric refraction, and surface reflections. For a rigorous derivation and explanation of various PWE Equations, the reader is referred to Parabolic Equation Methods for Electro-
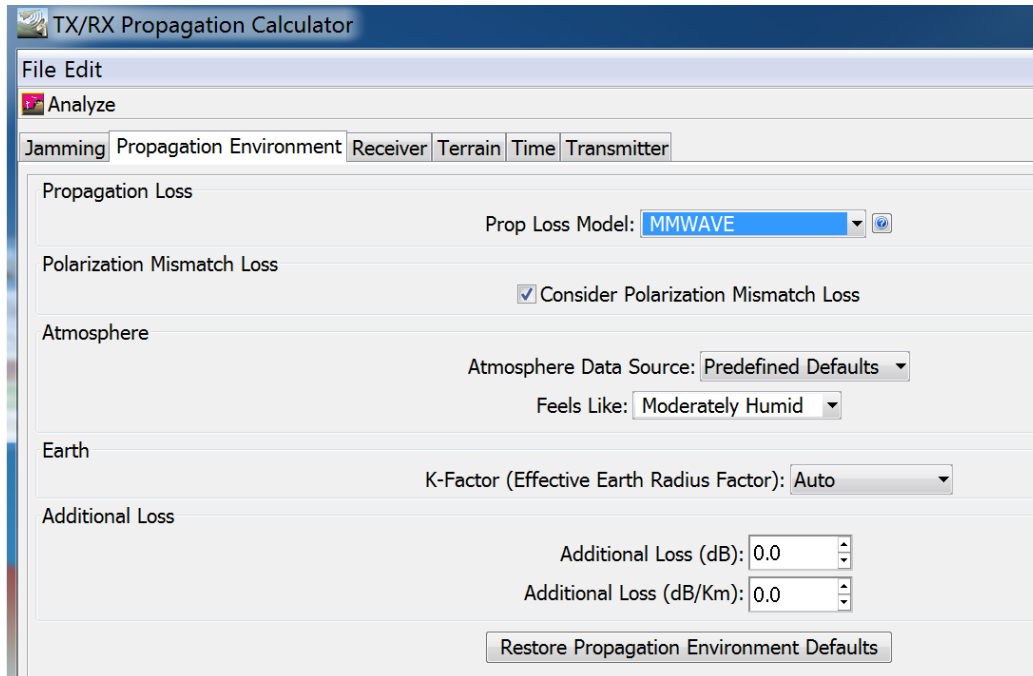
Figure 11. Defining an Atmosphere in IMOM

magnetic Wave Propagation by Mireille Levy [19]. More recent and advanced models have the capability to model impedance boundaries, rough surfaces, completed antenna patterns, irregular terrain, atmospheric absorption, and other scattering phenomena. PWE works because it uses the index of refraction of a parcel of the atmosphere to forward step in the direction of propagation and use numerical evaluation methods to solve the wave Equation. This method eliminates the need for separate approximations and algorithms for different geometries and frequency regimes. Also, PWE is better suited to handle certain radar specific phenomena such as ducting, where radiation gets trapped in atmospheric ducts due to a negative gradient in the index of refraction [26].

In order to implement a PWE calculation, an initial-value problem is defined at the antenna of interest and "marched" out in range and/or altitude. This produces a range-height grid of calculated values for each defined initial-condition. While running a PWE code is very efficient, it is still computationally demanding and difficult to

use in real-time operational scenarios. Two popular methods to solve PWE are the Fourier Split-Step (FSS) and the implicit finite difference (IFD) Equations. The FSS determines an approximate solution the PWE in the Fourier Transform domain and the IFD converts the PWE to a system of coupled differential Equations that uses matrix mathematics and linear algebra to solve the wave Equation. In general, the FSS is more stable, which encourages the use of larger step increments; however, the IFD is able to implement complicated boundaries easier than the FSS [6].

Understanding the contribution of PWE to radar modeling is important because PWE is able to solve the wave Equation and determine properties of a wave much quicker than the line-by-line radiative transfer methods employed by LEEDR and HELEEOS. Future iterations of LEEDR and HELEEOS could incorporate elements of PWE modeling in order to speed up calculations in regimes where accuracy would not be sacrificed. It is an alternative method and the underlying engine behind AREPS and IMOM's scheme of calculating radar propagation.

2.3   Atmospheric Effects in the MMW Regime

Weather Effects.

The standard dry atmosphere is approximately 78% N_2, 21% O_2, and 1% other, such as Ar, CO_2, and other trace gases Not included in the dry atmosphere is water vapor (between .001% - 5%), which can greatly affect atmospheric attenuation due to H_2O absorption lines. The strong dipole moment present in H_2O creates strong absorption features at 22, 183, and 323 GHz, which fall within the MMW spectrum. The effect of humidity on transmittance can be seen in Figure 12. As the location changes from a relatively dry Kandahar, Afghanistan to a more humid Libreville, Gambon in Africa, the path transmittance decreases under an effect deemed continuum absorption. For reference, the absolute humidity at Libreville is 13.47 g/m^3 and

34

at Kandahar, much less moisture is in the air, 6.63 g/m^3.

In addition to water vapor absorption, oxygen has resonance lines in the millimeter regime due to magnetic dipole transitions. At 60 and 118 GHz, O_2 has strong absorption features due to these effects. Because water vapor and oxygen are concentrated and of greatest density like most constituents at the lower altitudes of the atmosphere, altitude is crucial to consider when calculating attenuation in the MMW regime. Figure 13 demonstrates the differences in attenuation between 1000 meters and 10,000 meters on the exact same day and location. Also, at the higher altitudes, a phenomena known as pressure broadening is more dominant and causes the absorption lines to have increased width.
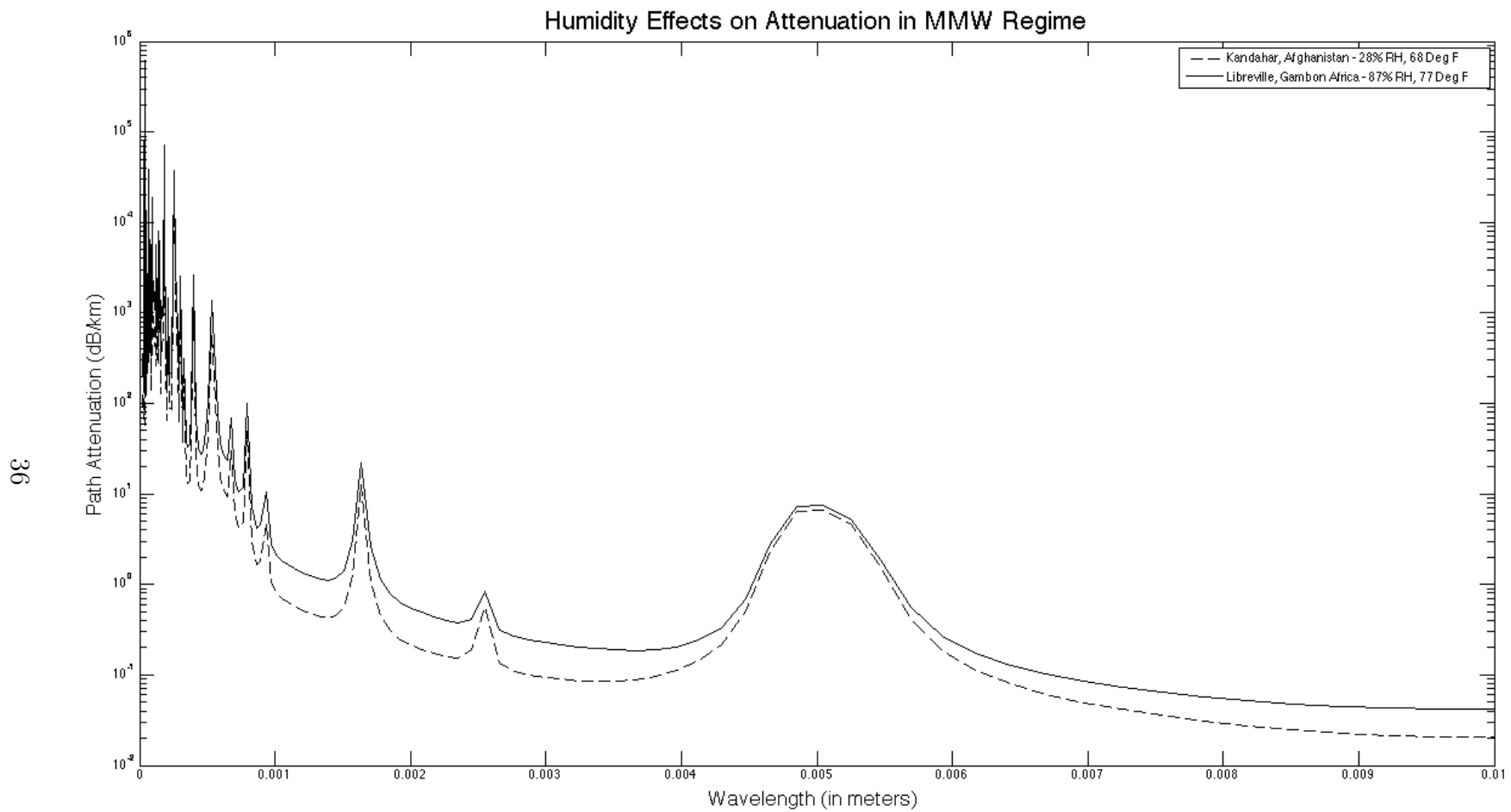
Figure 12. Comparison of path specific attenuation using LEEDR and the ExPERT database during Summer. Location 1 is Kandahar, Afghanistan with 28% relative humidity (absolute humidity = 6.63 g/m^3) at 1000 meters. Location 2 is the coastal town of Libreville, Gambon with 87% relative humidity, (absolute humidity = 13.46 g/m^3) at 1000 meters
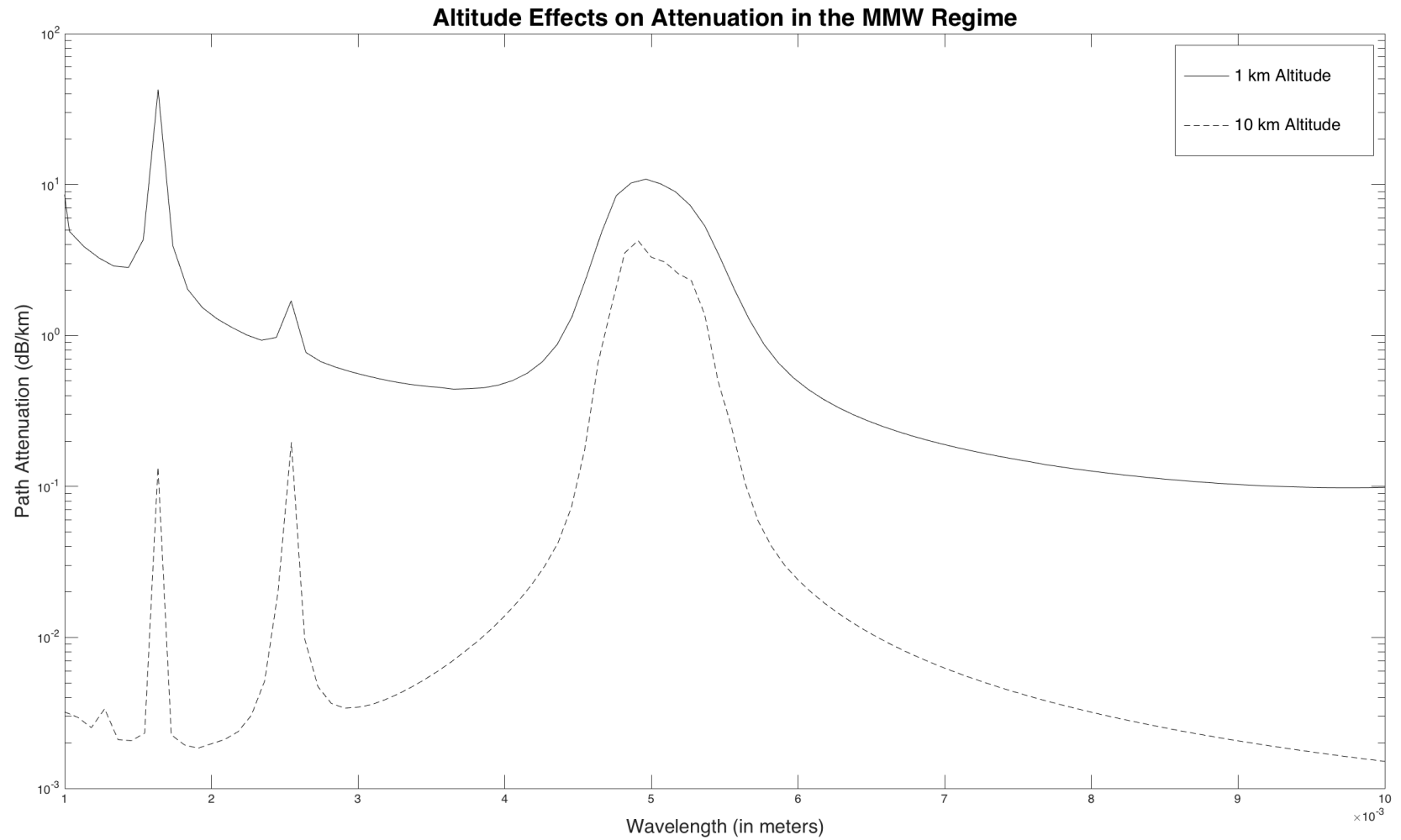
Figure 13. Comparison of path specific attenuation using LEEDR and the ExPERT database during Summer at WPAFB at 12-15 UTC. Attenuation was calculated at 1000 meters and 10,000 meters above ground level.

The water vapor and oxygen presence in the atmosphere is captured in density (pressure) and humidity (temperature and dew point) observations of the atmosphere. As the atmosphere is never in a standard condition, it is important to capture these variances from standard to account for the change in performance of a MMW radar beam in the real atmosphere.

In order to account for attenuation, Bean and Dutton [2], modified from Van Vleck [32], define three attenuation coefficients that quantify absorption due to oxygen in the atmosphere (α_1), attenuation due to water vapor at 40 GHz (α_2), and attenuation due to water vapor above 40 GHz (α_3). These coefficients are calculated at nonstandard temperature (T) (in ^oK), pressure (P) (in millibars) and density (ρ), (in g/m^3) from empirical observations using the Equations in Table 3 and line width values from Table 4.

Table 3. Calculation of Absorption Coefficients due to Oxygen and Water Vapor [2]

Absorption Coefficient [dB/km]	Intensity Calculation	$\Delta \nu_i$ Correction
α_1	$\frac{0.34}{\lambda^2} \left(\frac{P}{1013.25}\right) \left(\frac{293}{T}\right)^2$	$\Delta \nu_1 \left(\frac{P}{1013.25}\right) \left(\frac{293}{T}\right)^{3/4}$ and $\Delta \nu_2 \left(\frac{P}{1013.25}\right) \left(\frac{300}{T}\right)^{3/4}$
$\frac{\alpha_2}{\rho}$	$\frac{0.318}{\lambda^2} \left(\frac{293}{T}\right)^{5/2} \exp\left(-\frac{644}{T}\right)$	$\Delta \nu_3 \left(\frac{P}{1013.25}\right) \left(\frac{318}{T}\right)^{1/2} (1 + .0046\rho)$
$\frac{\alpha_3}{\rho}$	$\frac{0.05}{\lambda^2} \left(\frac{293}{T}\right)$	$\Delta \nu_4 \left(\frac{P}{1013.25}\right) \left(\frac{318}{T}\right)^{1/2} (1 + .0046\rho)$

Table 4. $\Delta \nu$ Values for Equations in Table 3 [2]

Line Width	Reference Temperature [^oK]	Value [$cm^{-1}atm^{-1}$]
$\Delta \nu_1$	293	0.018
$\Delta \nu_2$	300	0.49
$\Delta \nu_3$	318	0.87
$\Delta \nu_4$	318	0.87

By using these Equations, an attenuation coefficient (in dB/km) can be calculated from weather observations, and the oxygen and water vapor attenuation can be assigned a value which enhances the ability to predict attenuation of a signal of MMW radar.

Suspended Water Droplet Effects.

As water droplets grow in size to become clouds and fog, their scattering properties change as well (see Figure 3). Therefore, it is important to consider scattering due to fog and clouds, which are defined as droplets with radii less than $100\mu m$ and typically on the order of $10\mu m$. The latter places cloud droplets mostly in the Rayleigh scattering regime.

Densities of water in clouds are from 1 to 2.5 g/m^3; however, some instances of 4.0 g/m^3 have been reported. For clouds of ice, density is typically less than 0.5 g/m^3 and often can be found at less than 0.1 g/m^3. It is important to note that these figures assume a uniform distribution of droplets, which may or may not be true. However, at $\lambda > 5mm$, effects in attenuation due to inhomogeneities are negligible. Furthermore, due to the random nature of water droplets, it is highly unlikely to know for certain true water droplet distribution. Because of this, a uniform droplet distribution is generally assumed.

Gunn and East [15] created a method to determine the attenuation for a specific wavelength due to cloud droplets in Equation 20 where $\vec{k}$ is defined in Section 2.1 and λ is wavelength in meters.

$$\alpha_{clouds} = 0.4343 \frac{6\pi}{\lambda} \frac{\rho_{droplets}}{\rho_{atmosphere}} \text{Im}\left(\vec{k}\right) \tag{20}$$

Due to the sparsity of crystals and small size of ice particles in ice clouds, attenuation may be neglected for consideration of MMW propagation [2].

Turbulence Effects.

As wind, wind shear, and temperature gradients create inhomogeneities in the air, local fluctuations in the index of refraction and absorption coefficient occur and create what is referred to as optical turbulence. While previous models discussed have discounted turbulence as a prominent effect to MMW propagation, turbulence is a function built into HELEEOS and may have tactical implications when determined.

The metric used to determine the strength turbulence has on EM propagation is the index of refraction structure constant, C_n^2. Much research has been done on optical turbulence and an excellent reference for for a more in depth derivation and calculations of C_n^2 than performed in this thesis can be found in V.I. Tatarski's *Wave Propagation in a Turbulent Medium* [30].

In order to determine C_n^2 from observations, temperature values at two points are taken and used to calculate the temperature structure constant, C_T^2, where T is degrees in centigrade or Kelvin and r is measured in meters.

$$C_T^2(r) = \frac{[T(r_1) - T(r_2)]^2}{|r_2 - r_1|^{2/3}} \tag{21}$$

In order to get from temperature structure constant to index of refraction constant,

pressure in millibars is used (P).

$$C_n^2(r) = C_T^2(r) \left[79 \times 10^{-6} \frac{P(r)}{T(r)^2} \right]^2 \tag{22}$$

C_n^2 values on the order of $10^{-17} m^{-2/3}$ are considered weak turbulence and when the value reaches $10^{-13} m^{-2/3}$, the turbulence is considered strong. By quantifying turbulence values, a metric is created that allows for the distortion of EM radiation to be determined [14]. However, the current level of research does not fully understand the relationship between C_n^2 values in the optical versus MMW frequency bands. Therefore, future research should be focused on determining what C_n^2 values, if any, are significant in the MMW regime.

Refractive Effects.

A consequence of Equation 4 is refractive bending when radiation moves from medium with one index of refraction to medium with a different index of refraction. This phenomena is most noticeable in visible light; however, radar signals are affected as well. In order to describe this, a value for N must be determined from atmospheric observables.

Bohlander et. al, created an empirical fit for refractivity in the near-MMW regime [3]. For this regime, refractivity can be described as a sum of a constant N_o which accounts for contributions by lines at all frequencies (also referred to as continuum) and a dispersion term N_d which accounts for refraction due to water and oxygen lines in the region of interest. Unlike infrared and visible, the non dispersive term depends strongly on water vapor, not just barometric pressure and temperature. An empirical fit to index of refraction in the MMW regime is given in Equation 23

$$n = K_1 \frac{P_a}{T} Z_a^{-1} + K_2 \frac{e}{T} Z_w^{-1} + K_3 \frac{e}{T^2} Z_w^{-1} \tag{23}$$

where

$$K_1 = 7.760^{\circ K}/_{kPa}$$

$$K_2 = 7.15^{\circ K}/_{kPa}$$

$$K_3 = 3.750 \times 10^{4\,\circ K^2}/_{kPa}$$

$$e = \text{ Water Vapor Partial Pressure}$$

$$Z_a \& Z_w \approx 1 \text{ (Correction for nonideal relation between } \rho \text{ and } P)$$

$$T = \text{Atmospheric Pressure}$$

(24)

When outside of strong absorption lines, the dispersive term is negligible and total refractivity (N) is typically due to the value of $N_o = 350ppm$ [3]. By being able to assign a value to N, the bending of the radar beams can be determined as N changes along propagation path. LEEDR is able to capture this effect, however, the effect has yet to be implemented in HELEEOS at the time of this thesis. Current efforts are focusing on adding refractivity capabilities to HELEEOS which will enable extracting any bending of the radar beam as it propagates through an atmosphere.

Aerosols.

Aerosols are suspended in the atmosphere from man-made and natural sources. Typical sizes of the largest aerosols are on the order of $1\mu m$; most are much smaller. Due to these small sizes, and referencing Figure 3, aerosols have negligible scattering in the MMW regime. Therefore, for purposes of this research, aerosols are not anticipated to be significant contributers to MMW attenuation. This is demonstrated with LEEDR and using increasing scaling on aerosol concentration on a 94 GHz signal in an ExPERT atmosphere at Libreville. Table 5 shows attenuation using these scaling factors. There is no difference at all between the various aerosol concentration factors showing it is safe to neglect aerosol effects in the MMW regime.

42

Table 5. Evaluation of Aerosol Concentration Effects on Path Specific Attenaution

Aerosol Concentration Scaling Factor	Insoluble (Parts/cm^3)	Soot (Parts/cm^3)	Water Soluble (Parts/cm^3)	Path Specific Attenuation (dB/km)
1	0.003740508	17.53191026	101.0169956	0.646643734
5	0.018702539	87.65955128	505.0849779	0.646643734
50	0.187025389	876.5955128	5050.849779	0.646643734
500	1.870253889	8765.955128	50508.49779	0.646643734

Precipitation Effects.

Rain

Rain droplets are on the same size as MMW wavelengths which implies approaching Mie Scattering. In order to account for attenuation due to a specific rain rate, Crane and Blood developed the following Equation to determine attenuation, A, in dB. Originally, these Equations were developed for space link attenuation in microwave frequencies, but the relationship still provides appropriate attenuation data for radar operating in the same regime.

$$A = \frac{\alpha R_p^{\beta}}{\cos \theta} \left[\frac{e^{u\beta d} - 1}{u\beta} - \frac{b^{\beta} e^{c\beta d}}{c\beta} + \frac{b^{\beta} e^{c\beta D}}{c\beta} \right] \tag{25}$$

where

$A =$ Total Path Attenuation due to Rain (dB)

$\alpha, \beta =$ Parameters from Figure Relating Attenuation to Frequency

$R_p =$ Rain Rate in mm/hr

$\theta =$ Elevation Angle of Path $(\geqslant 10^o)$

$D =$ Horizontal Path Distance Through Rain Volume $\tag{26}$

$u = \dfrac{\ln \left(b e^{cd} \right)}{d}$

$b = 2.3 R_p^{-0.17}$

$c = 0.026 - 0.03 \ln R_p$

$d = 3.8 - 0.6 \ln R_p$

α and β values can be determined from the graph in Figure 14.
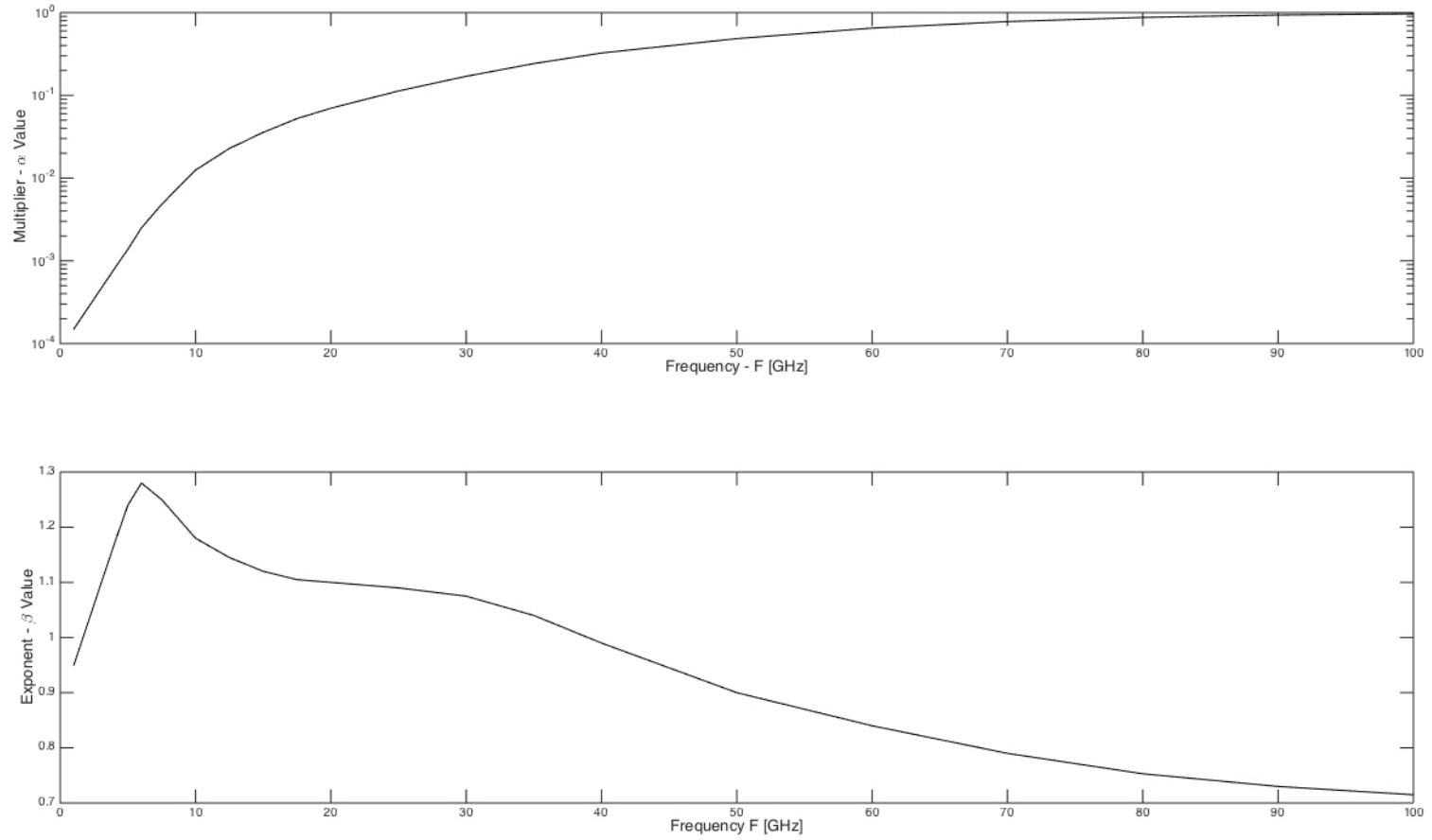
Figure 14. α and β Values from Equation 25

If $D < d$:

$$A = \frac{\alpha R_p^{\beta}}{\cos \theta} \left[\frac{e^{u\beta D} - 1}{u\beta} \right] \tag{27}$$

If $D = 0$ and $\theta = 90^o$

$$A = (\delta H) \left[\alpha R_p^{\beta} \right] \tag{28}$$

where δH is the path height through the rain area. These Equations provide excellent fitting with measurements in the 1 GHz - 100 GHz range and allow for calculation of attenuation due to rain [4].

The effect of various rain rates are demonstrated in Figure 15. Note that as rain rate increases, a nonlinear response to path attenuation arises and the shape of the attenuation versus wavelength curve changes slightly. These effects are vital to capture when propagating radar in the MMW regime.

Snow

Many assumptions must be made when determining absorption from snow. This is because snow can assume a wide variety of shapes, sizes, types (i.e. wet or dry), and orientations. A proposed method from Nicholas Currie of determining attenuation due to snow is found in Equation 29.

$$\alpha = 0.00349 \frac{R^{1.6}}{\lambda^4} + 0.00224 \frac{R}{\lambda} \tag{29}$$

where R is the snowfall rate in millimeters of water per hour. This Equation clearly has a lot of inherent assumptions; however, in the MMW regime, this Equation has been validated against experiment [5].
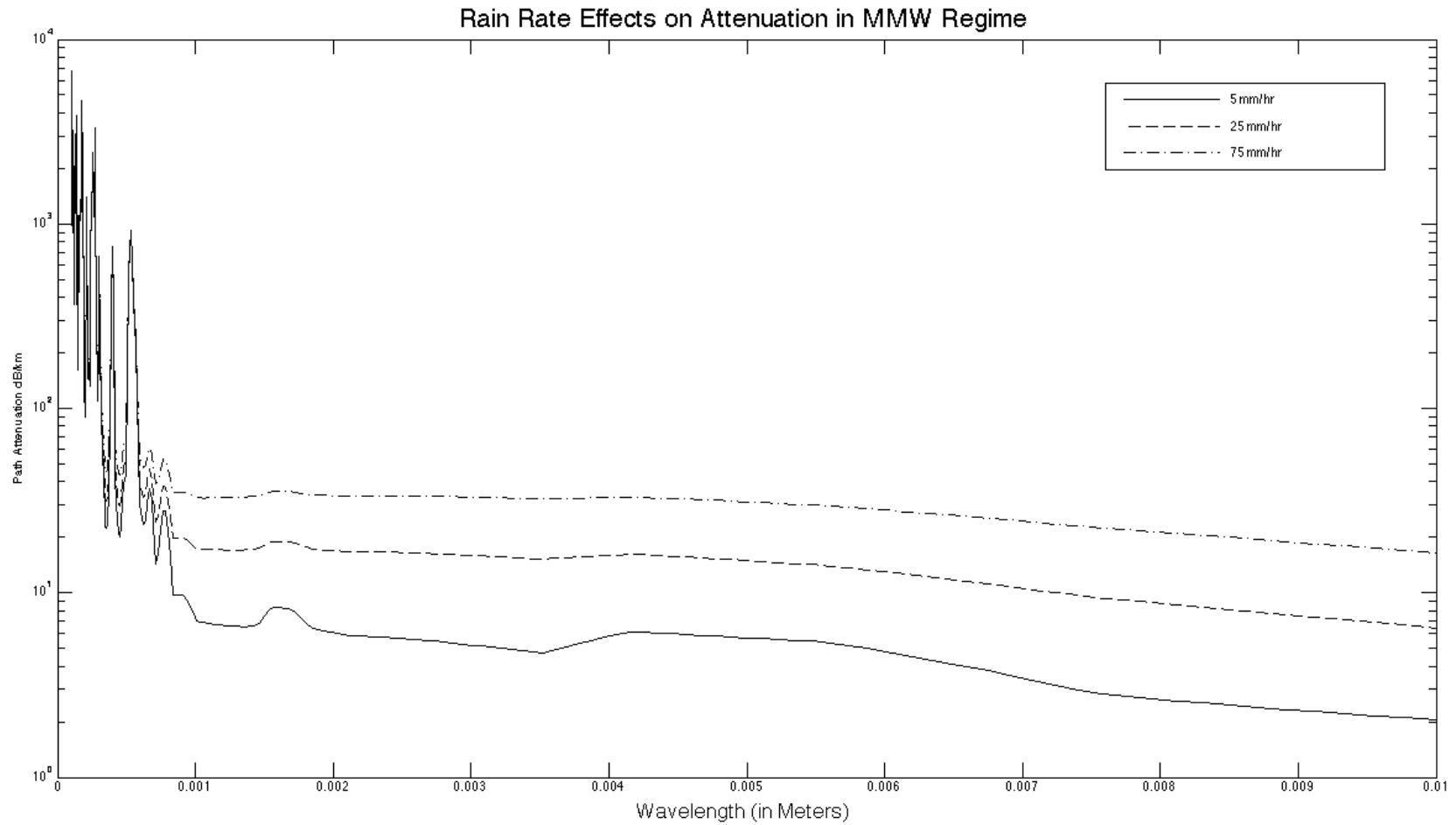
Figure 15. LEEDR generated attenuation at 2500 meters in 5, 25, and 75 mm/hr rain rate. Note differences in shape and values in the MMW regime. Simulation was run in the 1976 Standard Atmosphere.

Ice Precipitation

In the section on suspended water droplets, it was determined that due to the small size and sparsity of ice, the affect on radar attenuation is negligible.

Previous Measurements of MMW Propagation.

As mentioned in Section 1.1, MMW radar systems are expensive to test. Furthermore, the classified nature of many military systems results in data not being published. Because of these limitations, it is difficult to get actual data for MMW propagation in real atmospheric conditions. A report was found from the Ballistic Research Laboratory (BRL) in 1983 [33]. This thorough analysis provided measurements of attenuation due to water vapor, fog, smoke and dust, rain, and snow. Unfortunately, not enough is known about their specific radar patterns, powers, and atmospheric conditions to enable an accurate correlation between HELEEOS and experimental radar test measurements. While providing correlated results is outside the scope of this research, future research will require a controlled experimental scenario with well known atmospheric and radar pattern information. Once these data are provided, HELEEOS dB loss with respect to reference irradiance can be correlated with actual experimental radar measurements to provide a useful tool for analyzing MMW propagation.

III. Research Methodology

3.1 General Methodology

The principal goal of this research is a proof of concept that HELEEOS can be used to show a 3-D MMW radar pattern propagate in the atmosphere. It is important to note that this research will only be focusing on the far field pattern of the MMW radar. For purposes of this thesis, the far field is defined as the region in which Fraunhofer diffraction is dominant. The crossover radius is given by Equation 30, where D is the largest dimension of the antenna [21]. By capturing atmospheric effects with climatology or numerical weather models, HELEEOS should prove a valuable tool for modeling MMW radar patterns by returning to first principles of radiative transfer.

$$R_f = \frac{2D^2}{\lambda} \tag{30}$$

Because HELEEOS was designed for laser propagation modeling, it does not have the capability to propagate a radar pattern (see Figures 16 and 17), which is characterized by a main lobe in the middle and smaller sidelobes off to the sides in all directions. These sidelobes are a result of diffraction of the antenna and are important to capture because the side lobes still represent energy which could cause another receiver to pick up the energy. Nonetheless, this research will assess and evaluate HELEEOS' capability to discern MMW pattern propagation through an inhomogeneous atmosphere.

In order to account for the various lobes and complex radar patterns in HELEEOS, each degree of directionality will be treated as a "laser source" at the appropriate wavelength and power of the lobe. Then the HELEEOS script will be run over the pattern, sweeping out range intervals and determining the strength of the signal at each range. By repeating this method across all angles, a picture can be built of the
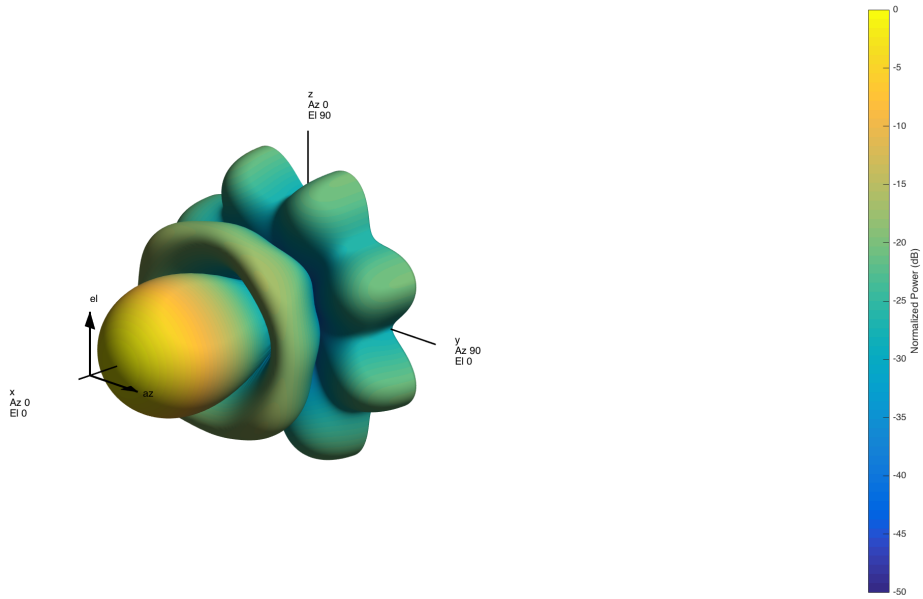
Figure 16. Simple sample radar antenna pattern in 3-D. Plot is normalized so that 0 dB is 100% of available power is emitted in the given azimuth and elevation angle.
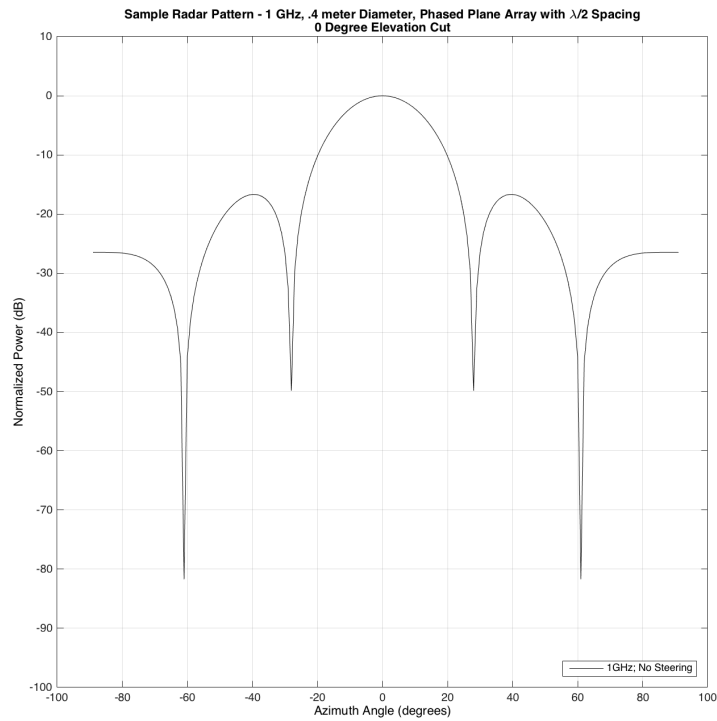
Figure 17. Simple sample radar antenna pattern in 2-D (0 Degree Elevation). Plot is normalized so that 0 dB is 100% of available power is emitted in the given azimuth angle.

strength of the various lobes at each angle, thereby creating the MMW pattern in space. Resolution of the model can be enhanced by creating finer angular resolution in the radar pattern. Figure 18 shows a two dimensional representation of this method where the each line is associated with a specific power and angle off boresight. The stars are points where HELEEOS will calculate the power received and path transmittance. This two dimensional figure will sweep around 360 degrees of azimuth to build a three dimensional representation of the radar pattern.
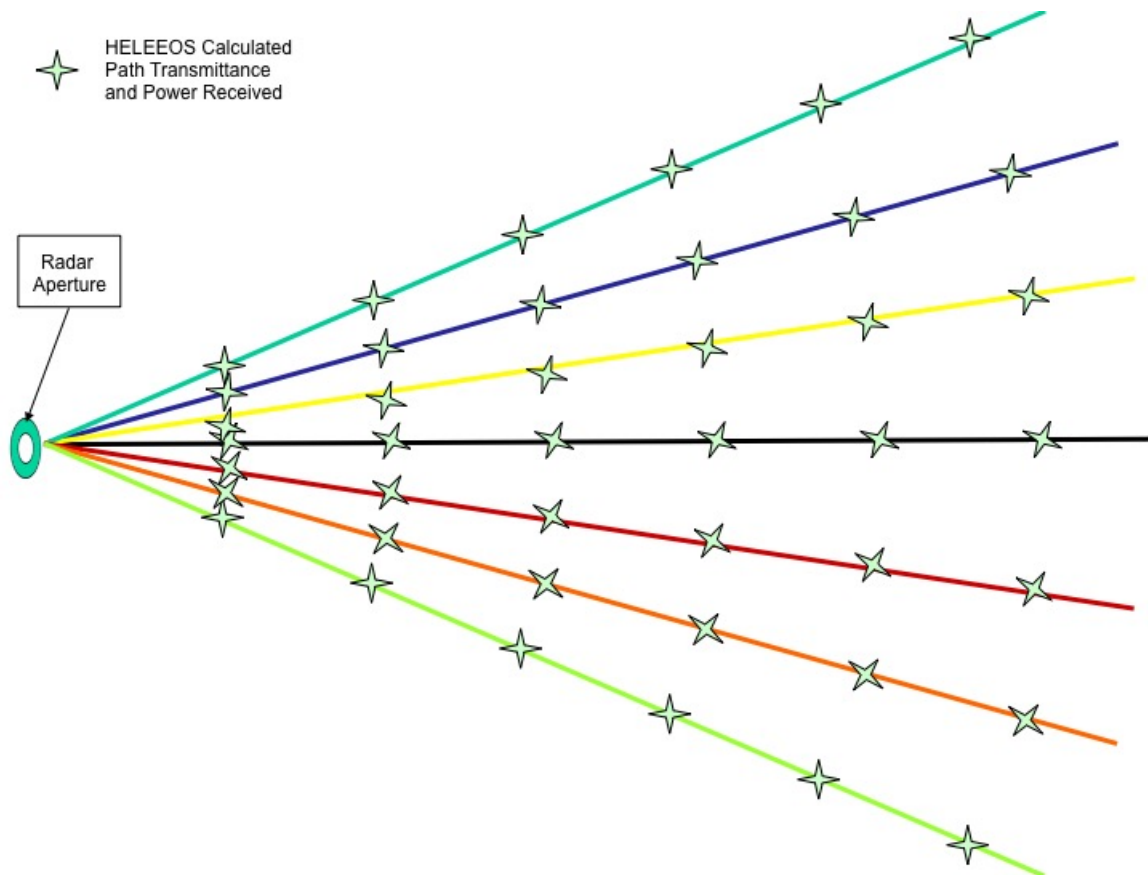
Figure 18. Two Dimensional Figure Depicting Calculation of Three Dimensional Radar Pattern

The traditional radar range Equation (Equation 14) has a $1/r^4$ proportionality to account for the loss of power as the main lobe spreads out in a spherical pattern on the outbound and return legs. The $1/r^2$ dependence for this research is accounted for in

51

the wave propagation code that HELEEOS applies to a beam. The fall off of power is proportional to $1/r^2$ and therefore that factor from the radar range equation is present in this analysis combined with other atmospheric effects. The gridding of the points is significant, as is spot size. It is possible that depending upon the spot size, there is a possibility that areas (especially close to the transmitter) could potentially overlap and wash out some of the resolution of the beam. As radar patterns get more complex and higher fidelity is demanded, future research should be done to ensure the pattern is being reproduced faithfully in the far field.

Refractive Bending.

Currently, a key limitation of HELEEOS is its inability to ingest refractive bending from LEEDR. In order to assess the significance of refraction, LEEDR was used to calculate refractive bending at 35 and 94 GHz, in atmospheric profiles of interest (see Section 3.7). These results are displayed in Table 6. Data shows, that even for very high humidity conditions, maximum refractivity accounts for well under 1° error over 10 km. Furthermore, little difference in the refractive displacement is calculated between the various scenarios. Because of these facts, refractivity can safely be neglected for purposes of this research. However, for more exact calculations, or perhaps a different wavelength, this error will need to be captured. At current program limitations, LEEDR would have to separately run the calculation to get path refractivity to provide for the bent path. This link between LEEDR and HELEEOS has yet to be implemented. Being able to research the effect of refractive bending will greatly enhance the understanding of ducting by the radar in the MMW regime. Ducting and trapping occurs when a radar beam is guided with the curvature of the earth and experiences less attenuation than had the ducts not been present at all. These effects could be addressed with future research in the MMW regime using

HELEEOS and LEEDR as tools to characterize the atmosphere and propagation of the shorter wavelengths.

Turbulence.

HELEEOS models turbulence essentially as a loss factor due to beam spreading and scattering. Crane and Blood qualify this source of attenuation to only be a loss of 1-2 dB per kilometer in the microwave frequencies, relatively small considering other attenuation mechanisms at play [4] [8]. While the discussion and development of C_n^2 was included in Section 2.3, due to time constraints, this research was unable to compare turbulence effects on patterns generated in HELEEOS. This is an area ripe for further research in the future, especially in the atmosphere near the boundary layer where there is an abrupt change in the characteristics of air.

Atmospheres Used.

This research will assess two generic radar array patterns as impacted by various atmospheres and weather conditions and show the effects that HELEEOS is able to highlight. The utility of using climatology and ingesting numerical weather model data will be shown by comparing patterns to standard and vacuum atmospheres. A flowchart of this methodology is shown in Figure 19. Various weather conditions include light (5 mm/hr), heavy (25 mm/hr), and extreme (75 mm/hr) rain. Furthermore the characteristics of fog and ice fog will be evaluated. Cloud effects will be investigated using clean continental cumulus clouds as these are the relatively simple clouds and found in most climates. LEEDR has the capability to model other types of clouds, and future research may address the effects that various cloud type have on MMW propagation.

Table 6. LEEDR Generated Path Refraction Comparison for 35 and 94 GHz

| Atmosphere	Vertical Path Displacement (in meters) over 10 km	Original Zenith (deg)	Corrected Zenith (deg)	Angular Correction Needed (deg)
		35 GHz		
Standard Tropical	0.594305	90.0045	90.000008139	0.004491862
ExPERT (Panama City)	0.594351	90.0045	90.000013897	0.004486103
Cumulus Clean Continental Cloud	0.594445	90.0045	90.000011248	0.004488752
		94 GHz		
Standard Tropical	0.594212	90.0045	90.000008142	0.004491858
ExPERT (Panama City)	0.594296	90.0045	90.000013898	0.004486102
Cumulus Clean Continental Cloud	0.594351	90.0045	90.000011249	0.004488751
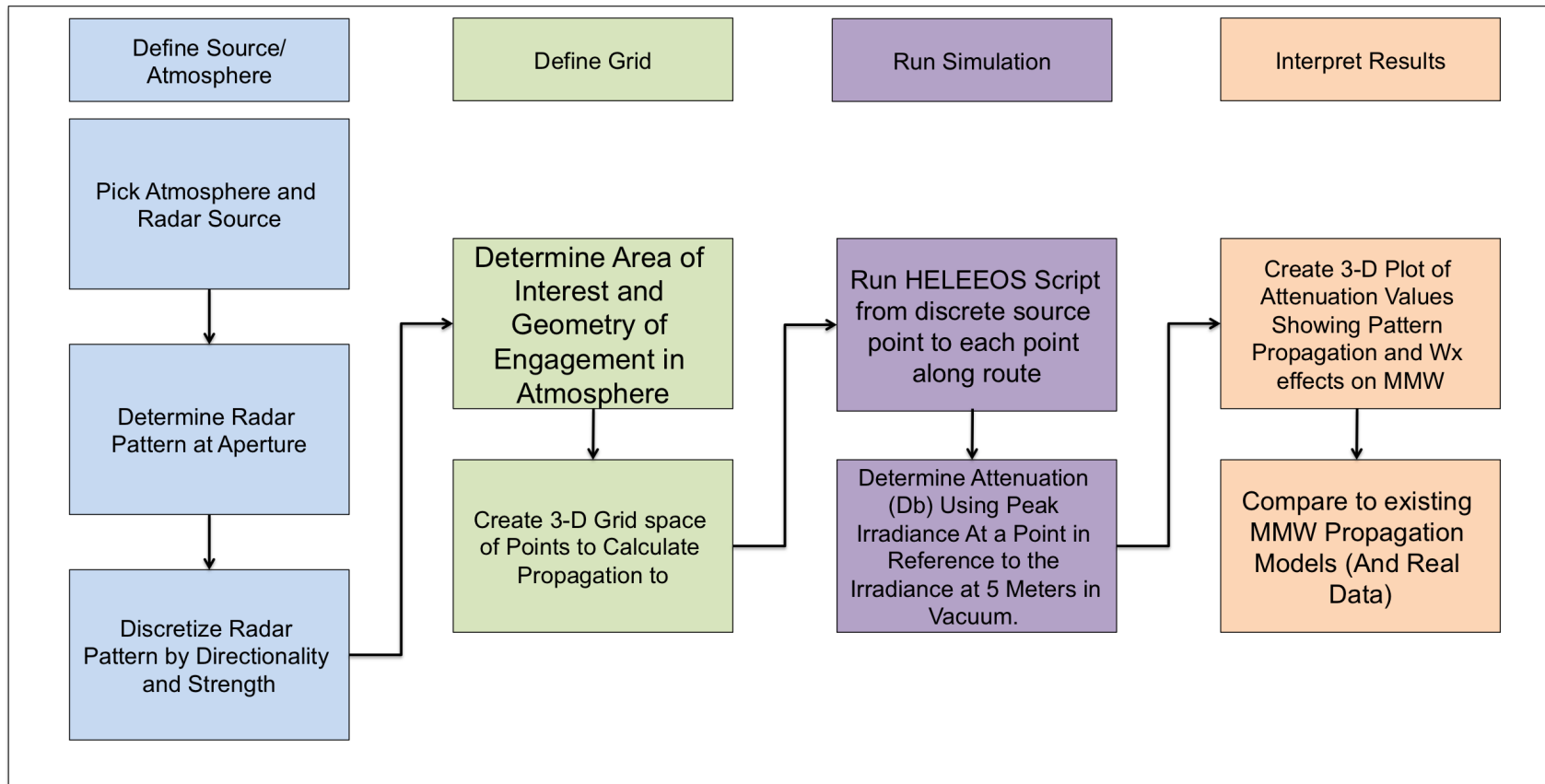
Figure 19. Flowchart detailing the method used to determine how HELEEOS can be used to model MMW radar propagation.

Table 7. Summary of Test Engagement Scenarios

Radar Array	Frequency (GHz)	Platform Altitude (meters)	Look Angle (degrees)	Atmosphere Type	Weather Type	Weather Low Alt (meters)	Weather High Alt (meters)
PPA	35	5	45	U.S. 1976 Standard			
PPA	35	300	0	U.S. 1976 Standard			
PPA	94	300	0	U.S. 1976 Standard			
PPA	35	300	0	Standard - Tropical			
PPA	94	300	0	Standard - Tropical			
PPA	35	3048	0	U.S. 1976 Standard			
PPA	35	3048	0	Standard - Tropical			
PPA	94	3048	0	Standard - Tropical			
PPA	35	12192	0	Standard - Tropical			
ULA	94	1524	-45	U.S. 1976 Standard			
PPA	35	5	45	ExPERT			
PPA	94	5	45	ExPERT			
PPA	35	300	0	ExPERT			
PPA	94	300	0	ExPERT			
ULA	94	1524	-45	ExPERT			
PPA	35	5	45	NWP Atmosphere	Fog	0	300
PPA	35	5	45	NWP Atmosphere			
PPA	35	5	45	NWP Atmosphere	Ice Fog	0	300
PPA	35	3048	0	NWP Atmosphere	Light Rain (5 mm/hour)	2500	3500
PPA	94	3048	0	NWP Atmosphere	Light Rain (5 mm/hour)	2500	3500
PPA	35	3048	0	NWP Atmosphere	Heavy Rain (25 mm/hour)	2500	3500
PPA	94	3048	0	NWP Atmosphere	Heavy Rain (25 mm/hour)	2500	3500
PPA	35	3048	0	NWP Atmosphere	Extreme Rain (75 mm/hour)	2500	3500
PPA	94	3048	0	NWP Atmosphere	Extreme Rain (75 mm/hour)	2500	3500
PPA	35	3048	0	NWP Atmosphere	Cumulus Continental Clean (cucc)	2500	3500
PPA	94	3048	-45	NWP Atmosphere	Cumulus Continental Clean (cucc)	1500	2500
PPA	35	3048	0	NWP Atmosphere			
ULA	94	1524	-45	NWP Atmosphere			
ULA	35	3048	0	NWP Atmosphere	Cumulus Continental Clean (cucc)	1500	2500

3.2   Summary of Test Conditions

Table 7 shows a list of engagements used to thoroughly test all conditions. A variety of geometries are used that simulate air-to-air, ground-to-air, and air-to-ground scenarios.

3.3   Coding Considerations

Due to the fact that HELEEOS is a laser propagation code running on MAT-LAB (which operates single threaded by default), fully simulating a radar pattern as depicted in Figure 18 can become very computationally intensive. Presuming 1° sampling for source simulation, one could expect 180 azimuth and 180 elevation values, effectively creating 32,400 "laser beams" that must be calculated at each range point. Each data point (i.e. each azimuth, zenith, and range point) can take up to one second for HELEEOS to calculate depending upon complexity of the atmosphere. Adding suspended droplets and other weather conditions can further increase computation time as HELEEOS runs a Mie code. Several efforts described below enabled more efficient computing without significant loss of accuracy and scope of coverage for the pattern.

First, in order to capture only the most pertinent information, only the 20 degrees off boresight (0 degree azimuth and elevation) were sampled. As can be seen in Figures 26a, 26c, 27a, and 27c, values outside of 20° are at -40 dB and below, effectively undetectable in most scenarios. Therefore, the data generated only includes a pyramid of 40 degrees in the vertical and horizontal directions.

Second, finding a balance between resolution of range points and computation time was crucial. The scenarios tested calculated from 5 meters from the aperture in 500 meter steps out to 10,005 meters. The maximum of 10 kilometers was chosen because with current technology, this is approximately the maximum range that a MMW

radar could expect to transmit at lower altitudes with higher amounts of water vapor present. These point spacings provided a grid that allowed the atmospheric effects to be seen without having to run the HELEEOS code too many times, preventing acceptable computation time.

Third, thresholds were set in the MATLAB code that would stop calculating for a given range once power was below a certain value. The code would then step to the next direction to calculate. If a given direction emitted a power that was below the threshold, the elevation and azimuth was skipped altogether. This greatly decreases computation time as the computer was not attempting to calculate minuscule values that would not be detectable by current radar receiver technology.

MATLAB does have a parallel computing toolbox and it would be greatly beneficial to run these functions using a multi-threading capable machine, or even a high performance computer. However, one of the conditions of parallelized code in MATLAB is the inability to put conditional statements inside the loop. Therefore, it would actually take longer to parallelize the code (due to the third consideration above) because the code would be forced to calculate all ranges. Some attempts were made to load the script to the high performance computer; however, limited research schedule prevented those codes from being run.

3.4   HELEEOS Output Variables

For every engagement calculated, HELEEOS has many outputs that help end users characterize the quality and power of a laser beam. Of interest to this research is Power in the Bucket (PIB) and irradiance.

Power in the bucket is measured in units of Watts and is dependent upon "bucket size", which is simply a measurement of power that is deposited in a "bucket", which is a standardized area on a target that is known to be vulnerable. In HELEEOS, the

standard bucket size is a 5 cm diameter and is defined by a 1000 x 1000 matrix of points. PIB values have been known to break down and decrease in accuracy when the laser spot size approaches the dimensions of the bucket [17]. These are important considerations when evaluating radar propagation using PIB from a MMW radar source. Nonetheless, the script is written so that PIB will be output to determine if it is an acceptable form of measuring radar power.

The more direct measurement of radar power on target is irradiance. Irradiance is measured in watts per meter squared and is simply the flux of energy per unit area. Irradiance differs from radiance in that radiance has a dependence upon solid angle, therefore radiance values are conserved with distance; irradiance drops off with the square of distance from a source. This makes irradiance ideal to measure radar energy as the R^2 factor is inherently accounted for.

The issue with using irradiance in HELEEOS is the fact that the output variable is peak irradiance which looks at the laser spot and calculated the average over all time steps of the peak value. In order to determine if peak irradiance varies from the irradiance that is present over most of the target, several runs were done using the GUI of HELEEOS at 2500, 5000, 7500, and 10000 meters. These runs were done at 35 and 94 GHz in a standard atmosphere at 3048 meters and the results can be seen in Figure 20. The far field spot was displayed, and by using the color bar values, the difference between irradiance at the center and outer portions were determined to be very small (on the order of at least .1 watts/m^2). Therefore, for MMW radar, it can be assumed that the peak irradiance is a realistic value to use and can represent far field radar power. For further reference, Figures 22 and 23 represent the entire spot distribution. The 94 GHz is still more focused than the 35 GHz, however they both subtend a large spot at 5000 meters. Similar spreads are found throughout the full ranges this research is investigating.
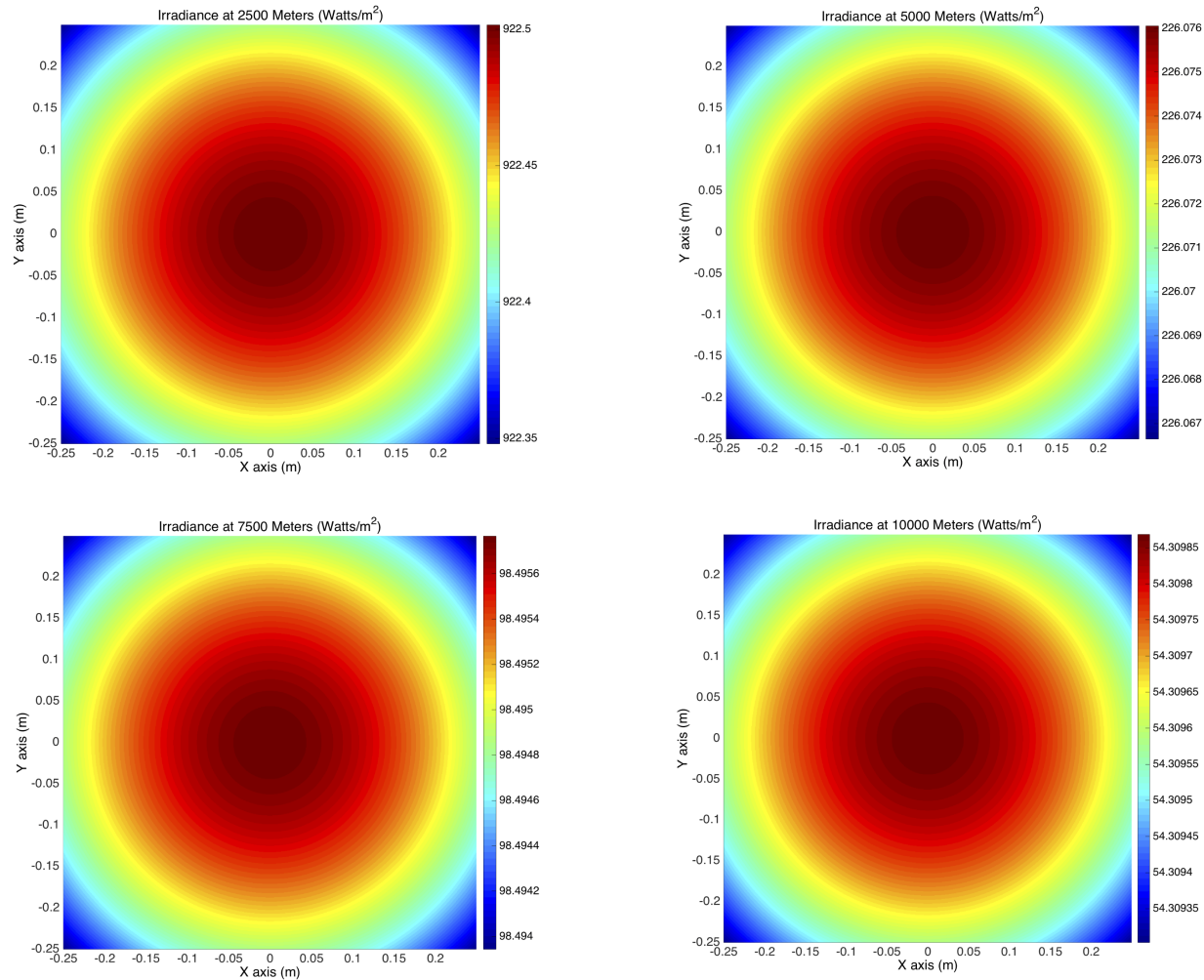
Figure 20. 35 GHz Irradiance Spot Distribution at various ranges from transmitter. Note the spread on the color bar is very small between radius = 0 and radius = .25 meters. This shows the spot is very large and homogeneous Therefore, irradiance is fairly constant and not focused like a laser beam.
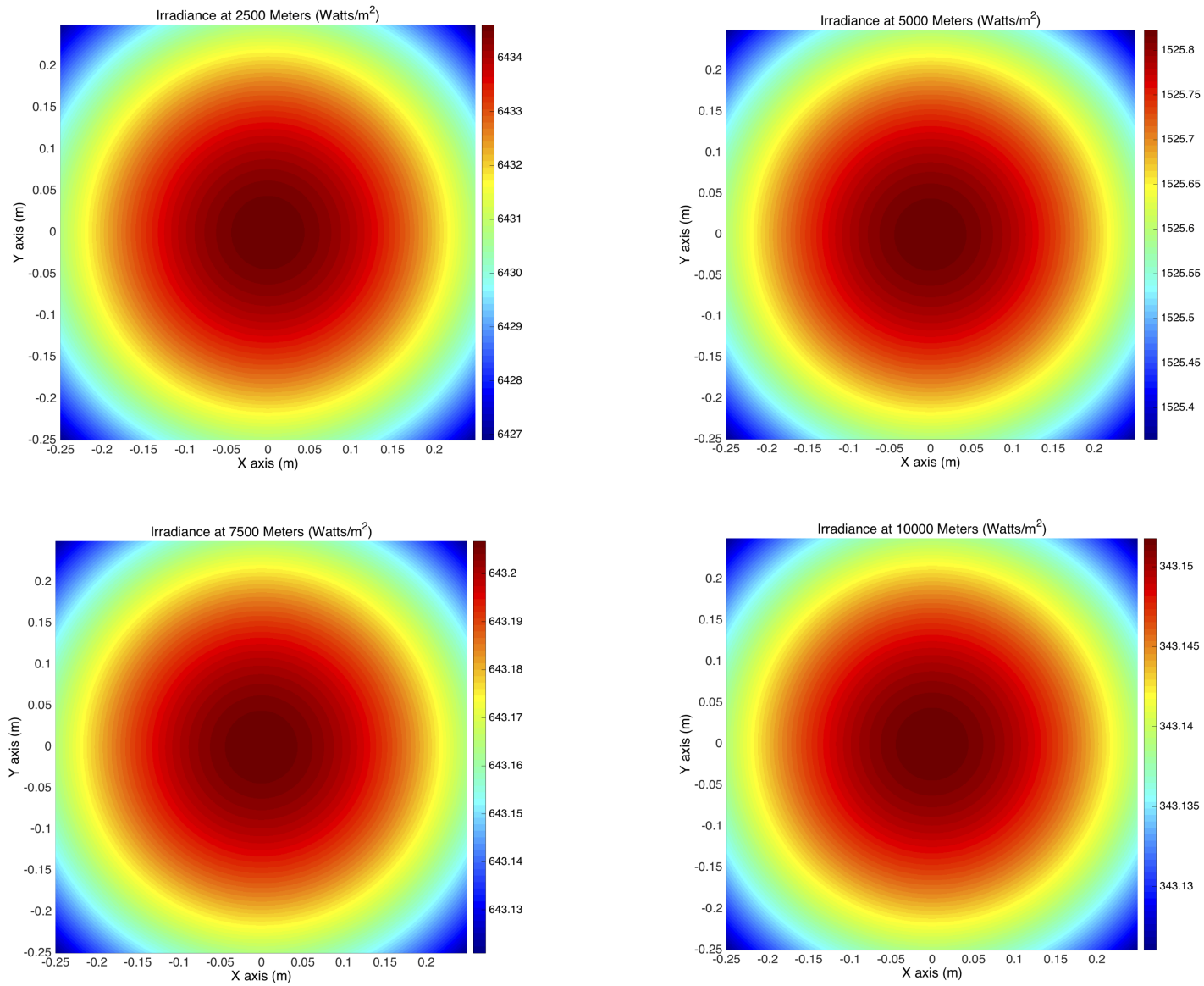
Figure 21. 94 GHz Irradiance Spot Distribution at various ranges from transmitter. Like 35 GHz in Figure 20, the spread on the color bar is very small between radius = 0 and radius = .25 meters.
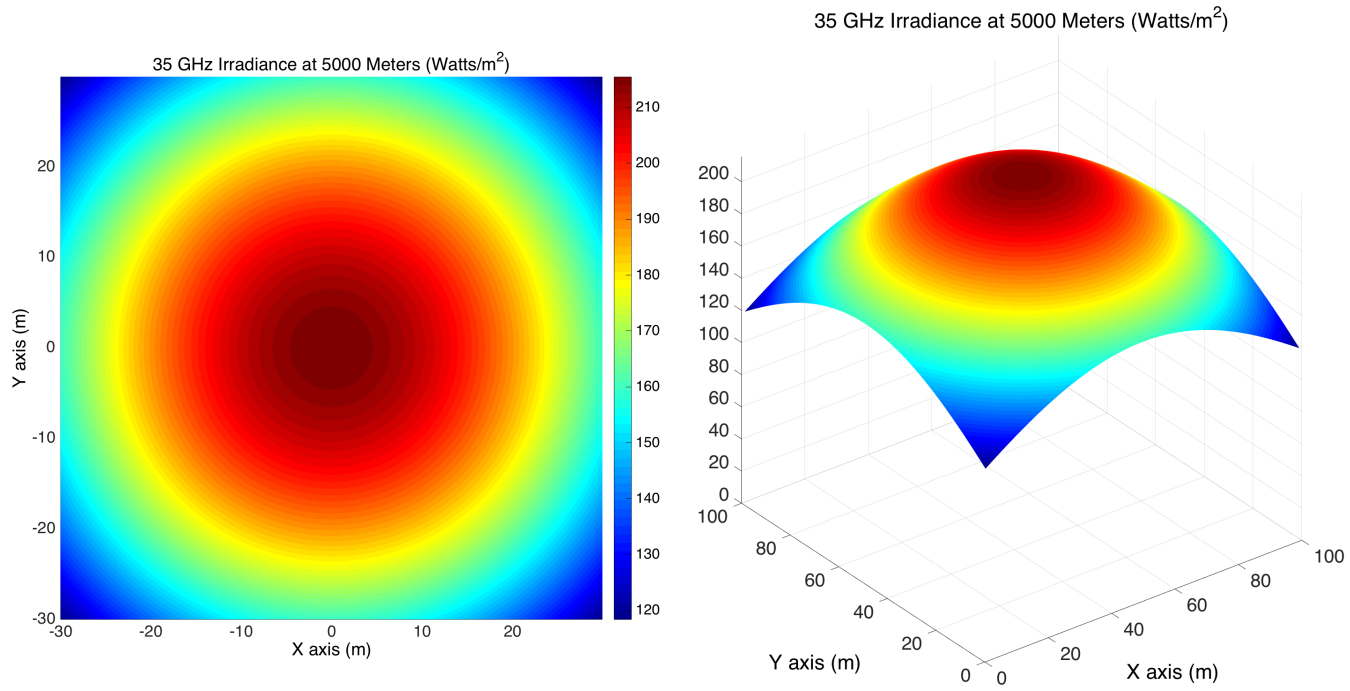
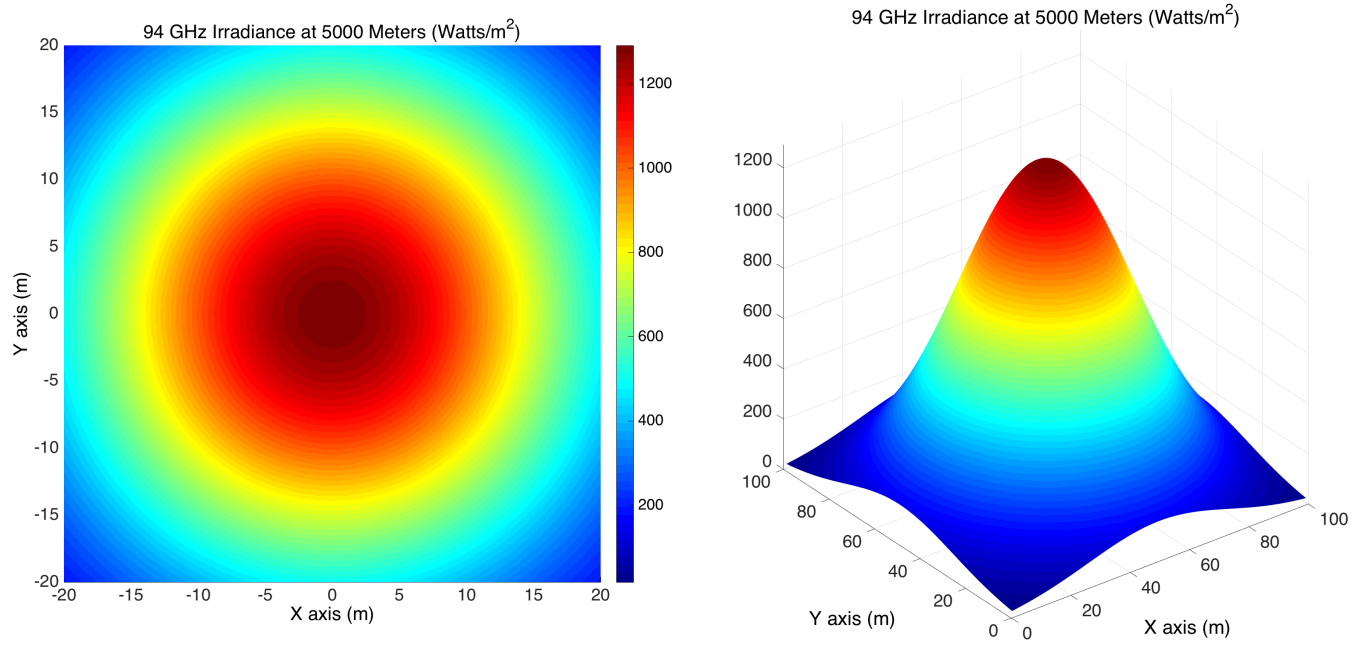Figure 22. 35 GHz Spot Distribution at 5000 Meters. Note the x and y axes

Figure 23. 94 GHz Spot Distribution at 5000 Meters. Note the x and y axes

Because irradiance is a representation of actual power received at a target after all diffraction and atmospheric effect are accounted for, the irradiance will be the primary metric used to determine the power from the radar receiver that is present at a given point. PIB values were collected and analyzed, and the results were quite similar to irradiance, however no results shown will display the PIB plotted values.

3.5   Method of Interpreting Outputs

In order to get from raw irradiance or PIB values to generating a pattern as it propagates in space, several post calculation processing treatments will occur. First, the data will be stored in a .mat format which includes the following values:

- Vector of all the azimuth values in degrees

    - Note: azimuth and elevation have been placed in a meshgrid format.

- Vector of all elevation values in degrees

- Peak irradiance from all effects

- PIB from all effects

- Powers vector that specifies the power emitted in each azimuth/elevation coordinate from the aperture. This is the power tied to each "laser" source.

- Target altitude matrix - describes the height of the query point after performing trigonometry for specific angle and range.

    - Defining this avoids having to redo the trigonometry calculations based off sensor look angle and elevation and azimuth values.

- Transmissivity vector of the fraction of power transmitted to each point

Once these values have been imported, there are several possible ways to look at the PIB or irradiance values:

- Plot the raw irradiance or PIB values

- Plot the irradiance or PIB values in dB attenuation as a ratio to:

    - The power transmitted in that particular elevation/azimuth coordinate at the aperture

    - The power that would have been present at that point if the pattern propagated in a vacuum

    - The maximum power transmitted in any direction from the aperture

    - The PIB or irradiance received at a specific range

        – In the particular elevation/azimuth coordinate

        – In the maximum power coordinate

        – Fraunhofer diffraction region could be driving factor to specific range chosen

Ultimately, the method chosen to provide the best scientific look at attenuation is the decibel loss with the reference power being vacuum irradiance at the crossover from Fresnel to Fraunhofer diffraction region. This allows the removal of actual power values to look at ratios using the decibel relationship described in detail in the next section.

Conversion to Decibel Attenuation.

In order to evaluate HELEEOS, IMOM and AREPS models will evaluate radar strengths in various atmospheres and report MMW radar strength at various points in the atmosphere and this will be compared with HELEEOS' calculations. It is

important to note these programs give outputs in decibel (dB) which is simply a ratio of power transmitted at antenna to the power received at another point. Equation 31 gives the value in decibels in reference to a reference power (P_o) and a received power (P). The section below, Determining Reference Irradiance, develops the reference power used and the reasoning for selecting it.

$$L = 10log_{10}\left(\frac{P}{P_o}\right) \tag{31}$$

Because the reference power used to calculate decibel loss in HELEEOS is different from reference powers used in traditional radar measurements and models, such as AREPS and IMOM, a direct comparison is difficult. The signal attenuation values are much higher in AREPS and IMOM than they are in HELEEOS. This is because the ratio used to calculate the decibel loss is based on a different reference power in HELEEOS than in typical radar modeling and testing. HELEEOS is calculating an irradiance value (in watts per square meter)for a "laser" at each point in an atmosphere and post processing will compare the calculated irradiance with a reference irradiance in order to calculate a decibel loss. This is the reason that future correlation studies against actual MMW data will allow a scaling to develop between irradiance and dB radar loss. Despite the fact that this research uses a different reference power for determining the power ratio for dB loss, the dB values will still be correlated and a more negative dB will equate to stronger attenuation of a signal.

Determining Reference Irradiance.

Because this research attempts to characterize the far field radiation pattern, it is important that our reference irradiance is in the Fraunhofer region defined in Equation 30. For the 35 GHz signal the crossover occurs at 58.3 meters and at 156.6 meters for 94 GHz. Figure 24 shows the irradiance values at a point for 35 and 94 GHz and also a $1/r^2$ reference line to show the irradiance falling off as expected. Nothing significant occurs with the irradiance crossing into the Fraunhofer Diffraction Region, however, using lower irradiance values than those found closer to the aperture creates higher contrast in the attenuation plots.

It is important to note that attenuation values, when expressed in dB, will not necessarily convert directly to dB attenuation from a radar transmitter. Because the reference power used in calculating the decibel losses are different in this research compared to typical radar calculations, the dB loss values will be correlated, but not exact. Therefore, future research should be focused on correlating HELEEOS dB outputs with raw values measured by a radar receiver. Some data has been collected at MMW frequencies in weather conditions [33], however much additional research needs to be done to fully understand the current effect of weather on the MMW radar bands.

Once the values for power or attenuation have been calculated, the coordinates are switched from spherical to Cartesian and MATLAB Scatter3 plot is used to plot the values in three dimensional space, allowing easy interpretation of atmospheric effects and the propagation of the radar pattern.
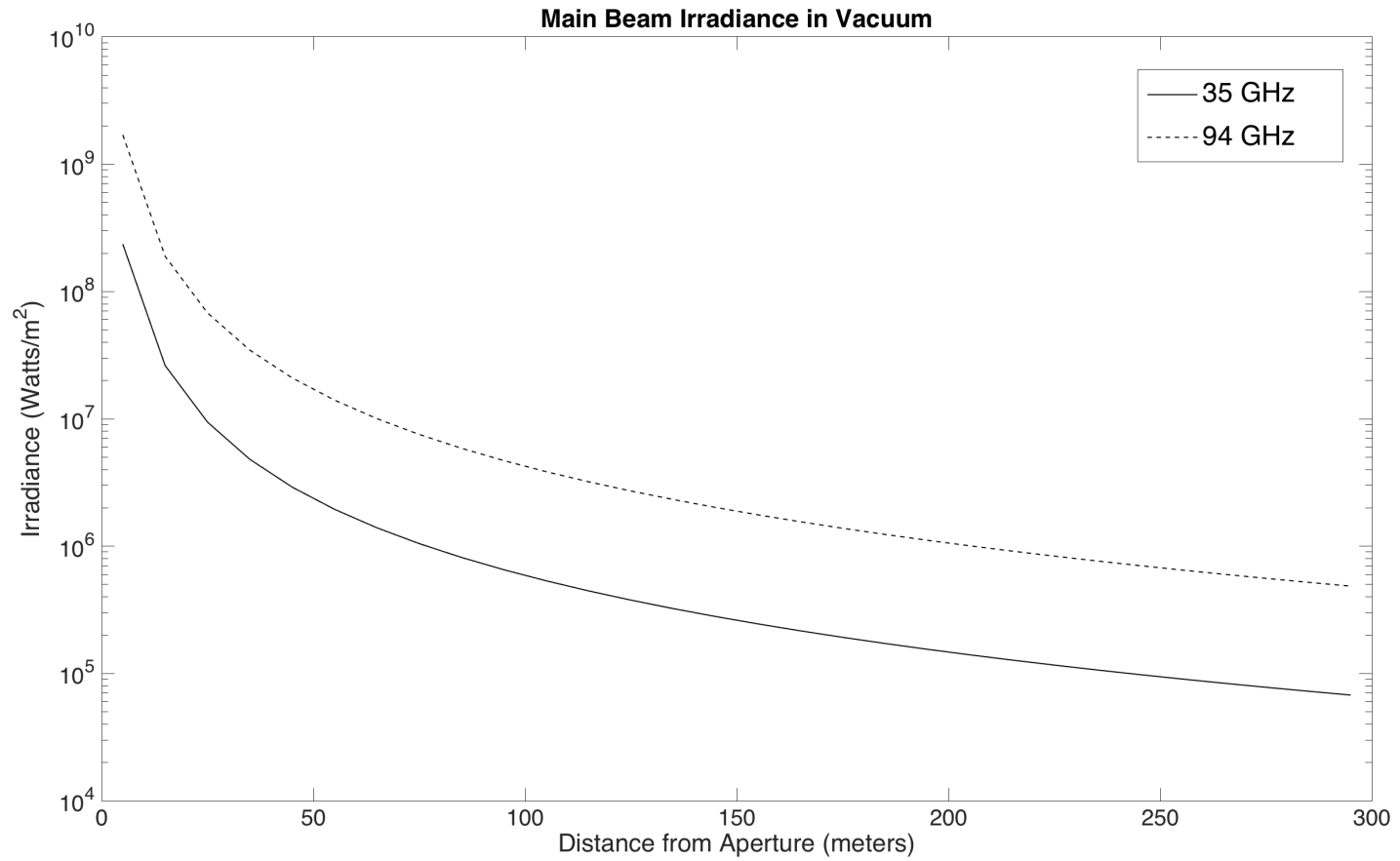
Figure 24. Main Beam Irradiance in Vacuum for 35 and 94 GHz

3.6 Radar Frequencies, Power, and Patterns Evaluated

Radar Frequencies.

Because this research focuses on the MMW regime, frequencies chosen will be pertinent to applications in the MMW regime such as active denial systems, communication links, and microwave satellite sensors. As much utility in MMW radar systems are at the lower end of the MMW regime, frequencies tested will be 35 GHz and 94 GHz, which coincide with relative windows in the atmosphere.

Power.

Transmitters in the MMW regime are typically gyrotrons. These generate power in a way that avoids typical heat increases seen in traditional microwave power tubes at higher frequencies. An example of a gyrotron power generator is the Navy's VGB-8194 *Warloc*, which is capable of producing 100 kW maximum power at 94.2 GHz ± 700 MHz [27]. The HELEEOS simulation will be set up with the transmitter power at 100 kW and losses will be reported in dB, as calculated by Equation 31. By reporting attenuation in dB, the actual power at the source will be irrelevant as the calculated values will simply be a ratio between source power and propagated power. To determine the power in a specific direction of the antenna, the total power provided by the transmitter will be divided over the area of the array. This will allow for a conversion between power per unit area. The 0 dB value corresponds to 100 percent of available power in that specific direction.

Radar Patterns.

Radar patterns are based off the following generic antennae, geometries, and dimensions:

- Phased Plane Array (PPA) - Figure 25a

    Circular Planar, Rectangular Lattice

    0.1 Meter Radius

    $\frac{\lambda}{2}$ Element Spacing

    Back Baffled

    No Taper or Steering

- Uniform Linear Array (ULA) - Figure 25b

    0.2 Meters Long

    100 Elements

    Back Baffled

    No Taper or Steering

Radiation patterns for 35 and 94 GHz were generated for the ULA and PPA with MATLAB's Sensor Array Toolbox found in version R2015a. Details for generating and exporting the radar pattern data can be found in Appendix B. Two and three dimensional representations of each pattern are displayed in Figures 26 and 27. The patterns are normalized such that 0 dB is considered 100 % of the radar's power being directed in that given direction.
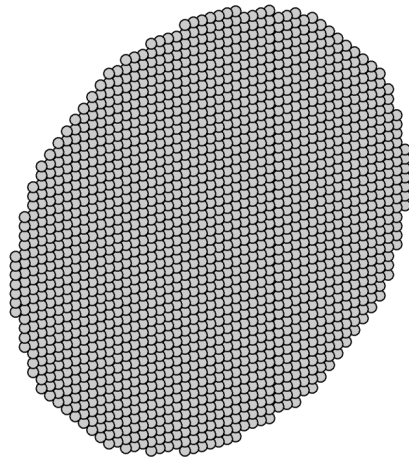
(a) Phased Plane Array Geometry
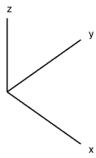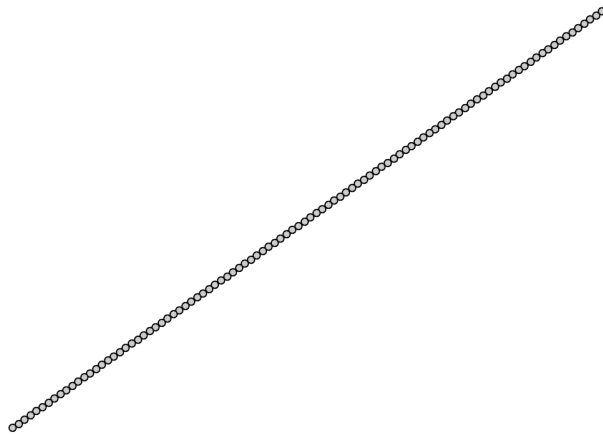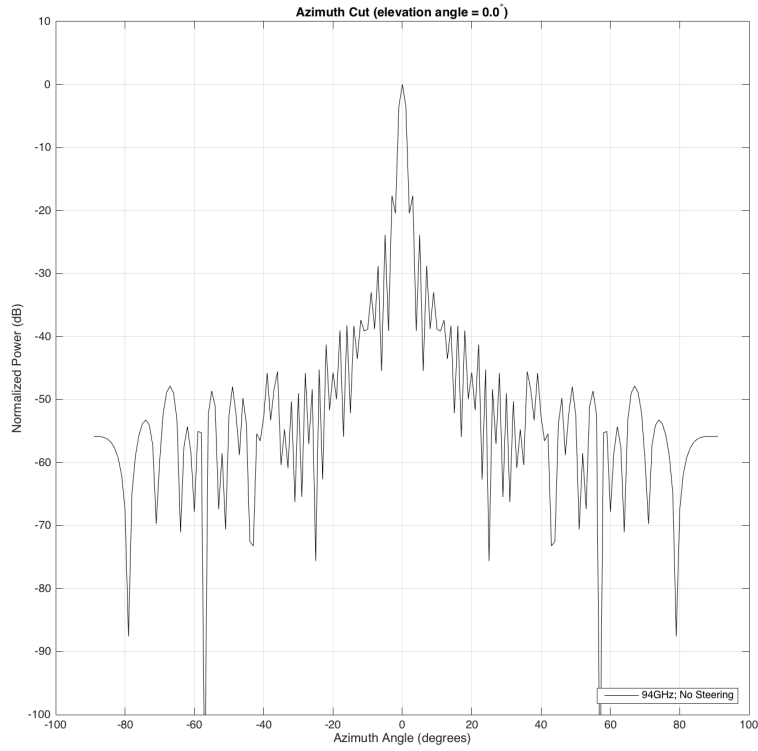

(b) Uniform Linear Array Geometry

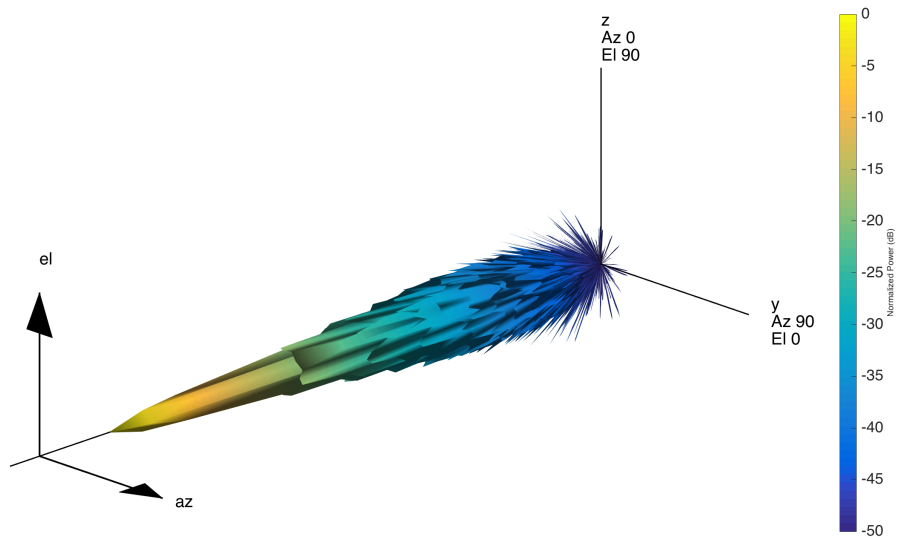Figure 25. Test Radar Geometries
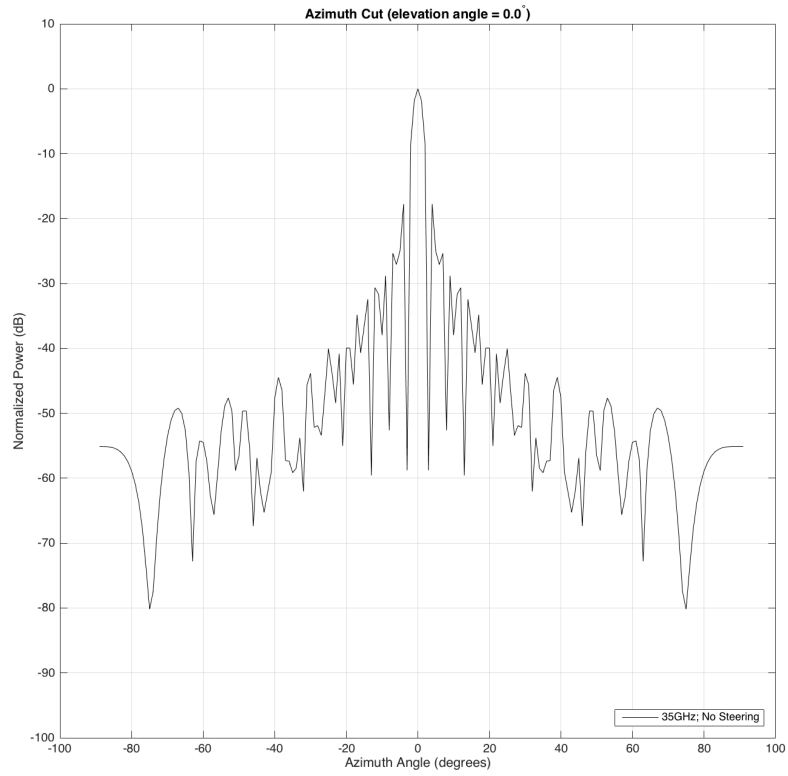
(a) PPA 35 GHz Two Dimensional Representation of Pattern (Zero Elevation Line)
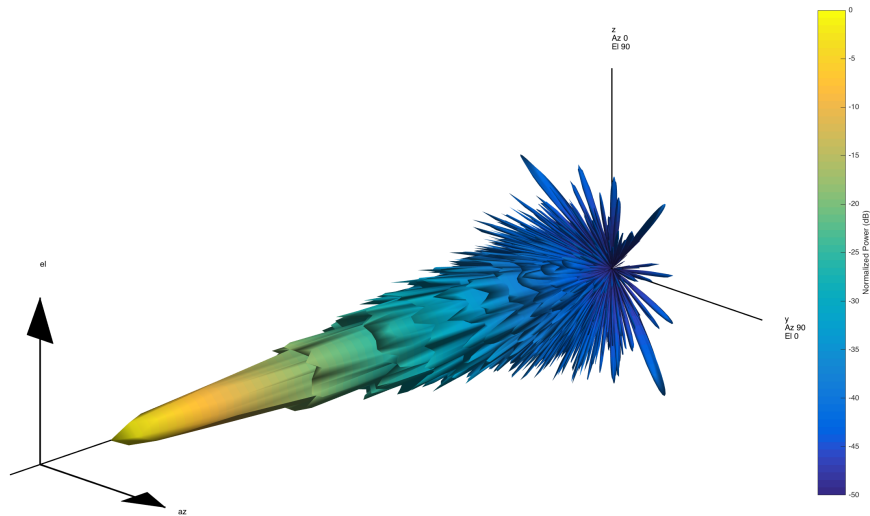
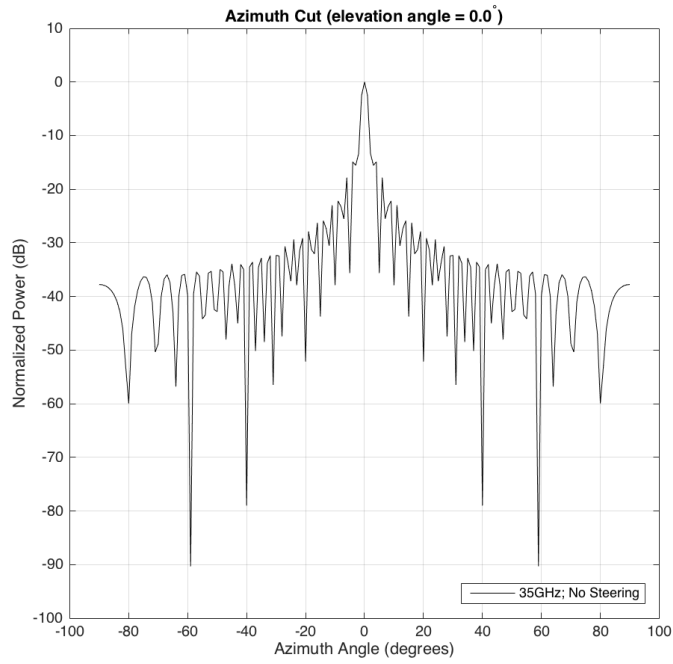(b) PPA 35 GHz Three Dimensional Representation of Pattern

(c) PPA 94 GHz Two Dimensional Representation of Pattern (Zero Elevation Line)
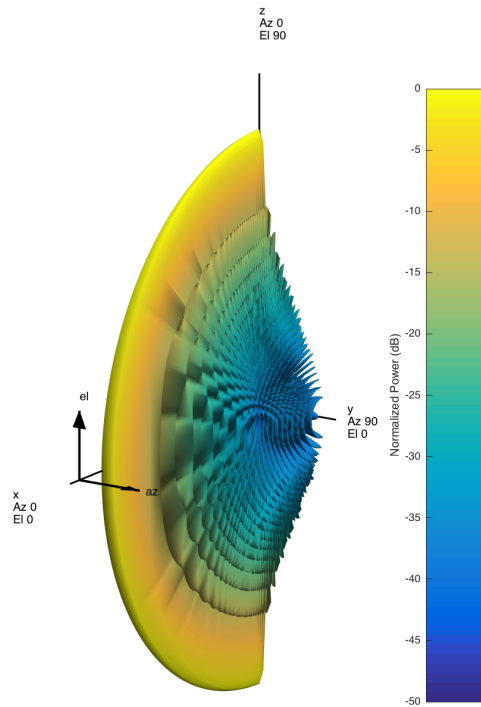

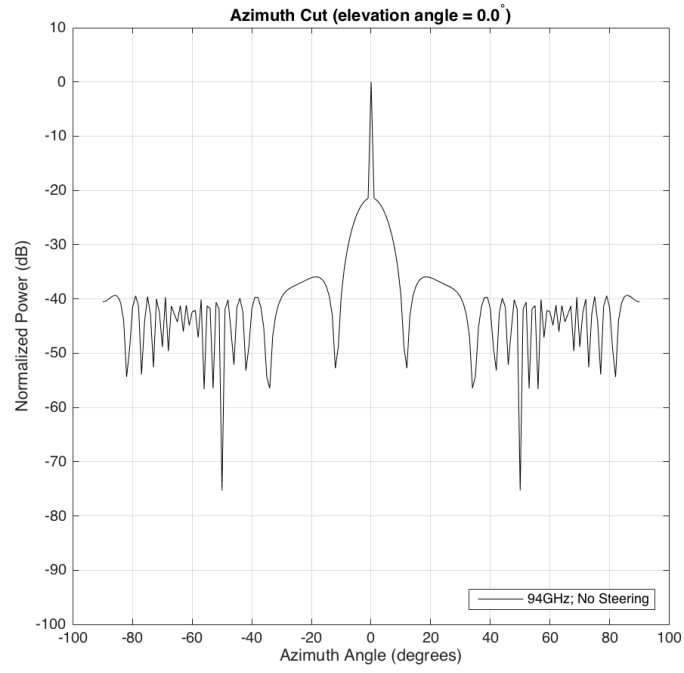(d) PPA 94 GHz Three Dimensional Representation of Pattern
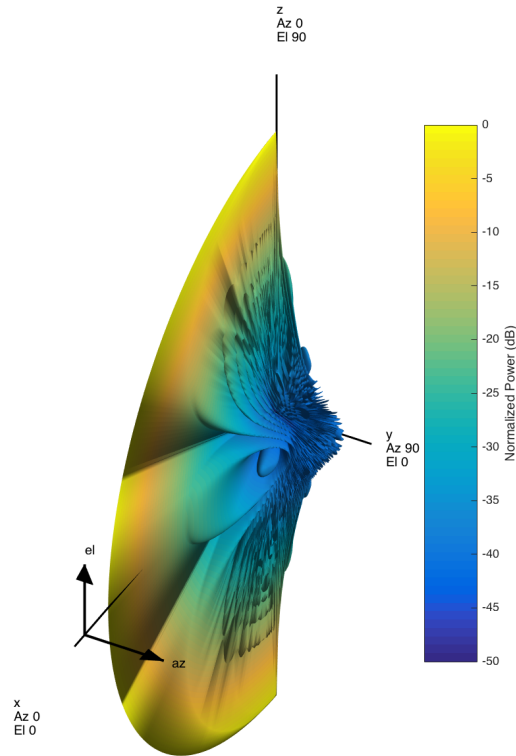
Figure 26. Phased Plane Array 35 and 94 GHz Patterns

(a) ULA 35 GHz Two Dimensional Representation of Pattern (Zero Elevation Line)

(b) ULA 35 GHz Three Dimensional Representation of Pattern

(c) ULA 94 GHz Two Dimensional Representation of Pattern (Zero Elevation Line)

(d) ULA 94 GHz Three Dimensional Representation of Pattern

Figure 27. Uniform Linear Array 35 and 94 GHz Patterns

3.7 Atmospheric Conditions Evaluated

All tests will initially be done in a 1976 U.S. Standard Atmosphere. The purpose of this is to provide a baseline that traditional models such as AREPS and IMOM usually assume. Then, by comparing non-standard atmospheres, effects that are currently not accounted for can be shown in comparison to the Standard Atmosphere. The tests will be performed in an air-to-air configuration at 3048 meters (10,000 feet) and 12,192 meters (40,000 feet). Furthermore an air-to-surface from 1524 meters (5000 feet) and surface-to-air scenario will be simulated. Also, due to the fact that the ExPERT atmosphere reverts to standard above the boundary layer, some ExPERT air-to-air scenarios will occur at 500 meters (1640 feet). Various atmospheric effects that will be considered are as follows. A more detailed listing of specific engagements is given in Section 3.2

- U.S. 1976 Standard Atmosphere

  - Moist, and Tropical

- Nonstandard Temperature Lapse - i.e. ExPERT and NOMADS Data Ingested

  - All ExPERT information is for Panama City, Panama (due to the high humidity) at during summer using 50th percentile relative humidity from 1200-1500 Local.

  - All NWP data is from Panama City, Panama using the Global Forecast System (GFS) 0600 model cycle forecasting for 1200 Zulu (1700 Local Time).

- Rain

  - 5 mm/hr

  - 25 mm/hr

  - 75 mm/hr

- Clouds

- Fog

- Ice Fog - simulates hail with a 1-3 mm size discrimination

Types of Humidity.

A quality discussion of the various measurements of humidity can be found in Ahrens [1]. Humidity can be measured in absolute humidity, specific humidity, and relative humidity. Absolute humidity is the ratio of mass of water to the volume of the air parcel as defined in Equation 32. Absolute humidity is a measurement that takes into account of the volume of parcel of air and typical units are grams per meter cubed.

$$\text{Absolute Humidity} = \frac{\text{Mass of Water Vapor}}{\textbf{Volume of Air}} \tag{32}$$

Specific humidity is the mass of water vapor to the total mass of air as shown in Equation 33. This does not have a volume dependency and units are typically given in grams of water vapor per kilograms of air. This specific humidity remains constant as long as the moisture content of a parcel of air remains constant.

$$\text{Specific Humidity} = \frac{\text{Mass of Water Vapor}}{\textbf{Total Mass of Air}} \tag{33}$$

Finally, relative humidity is the ratio of the amount of water vapor in the air with respect to the total amount that parcel could hold as defined in Equation 34. Relative humidity is the most common reported measurement of humidity but not the best measurement of how well an EM signal will propagate through it.

$$\text{Relative Humidity} = \frac{\text{Amount of Water Vapor in Air}}{\text{Amount of Water Vapor Air } \textbf{Can} \text{ Hold}} \tag{34}$$

As EM radiation is attenuated by the actual amount of water in the parcel of air, absolute humidity is the strongest indicator of water vapor for propagation calculations. Meteorologists often report relative humidity, and it is loosely related to amount of water vapor present. The dew point temperature is a proxy for absolute humidity in that the higher amount of water in a parcel of air, the higher its dew point. Therefore, the best way to correlate humidity effects with radar attenuation will be to consider dew point as that is the most widely reported and recorded variable that is tied to amount of moisture in a volume of air as the EM radiation passes through.

IV. Results

HELEEOS' performance can be assessed for multiple scenarios: vacuum propagation, standard, ExPERT, and Numerical Weather Prediction (NWP) generated atmospheres, and additionally weather (fog, rain clouds) effects. In turn, performance can be evaluated relative to 3-D radar propagation and attenuation throughout the pattern. The following sections demonstrate how HELEEOS was able to replicate these various effects. Finally, these plots are qualitatively compared to AREPS and IMOM evaluations of similar scenarios to ensure that HELEEOS accurately propagated the pattern and gave realistic results.

4.1 Propagation in Vacuum

In order to ensure that the MATLAB script and HELEEOS were accurately portraying the radar patterns, a vacuum free space propagation was calculated. This script ran at each azimuth and elevation angle from 5 to 10,000 meters in 500 meter increments. In addition to providing a check on the pattern, this allowed comparison between Power in the Bucket (PIB) and irradiance and determine if the two variables were giving similar propagation patterns.

The method of analyzing the data that produced the best results was using a decibel attenuation between the irradiance or PIB at specific azimuth, elevation, and range point with respect to the boresight data point the crossover to Fraunhofer Diffraction as discussed on Page 67. This provided the most realistic re-creation of the pattern and made the most scientific sense by comparing like values without having to scale between raw emitted power and irradiance or PIB.

PPA Antennas.

Figures 28 and 29 demonstrate that indeed, HELEEOS was able to replicate the radar pattern in a vacuum and qualitatively, the pattern appears to be representative of how the source pattern would propagate in three dimensional space. Because of the larger wavelength and the SHARE toolbox propagating the beam, note that large portions of the beam were below threshold values of 1 watt per meter squared with only $1/r^2$ drop off and diffraction.

Because these runs occurred in vacuum, there are no interesting atmospheric effects such as non-uniform attenuation. Note that there is attenuation as high as -11 dB in some areas, indicating that a MMW antenna concentrates energy in a very narrow main lobe as these swaths are only 20 degrees off boresight. Note that the 94 GHz is more narrow than the 35 GHz. However, there are still sidelobes that are present and could be detected by a sensor not aligned with boresight.
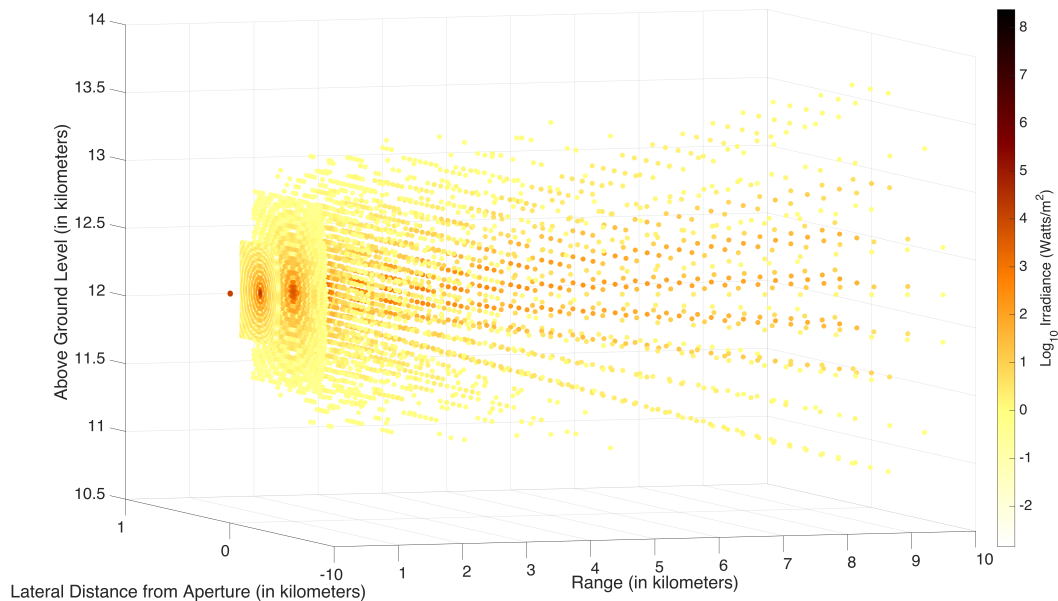
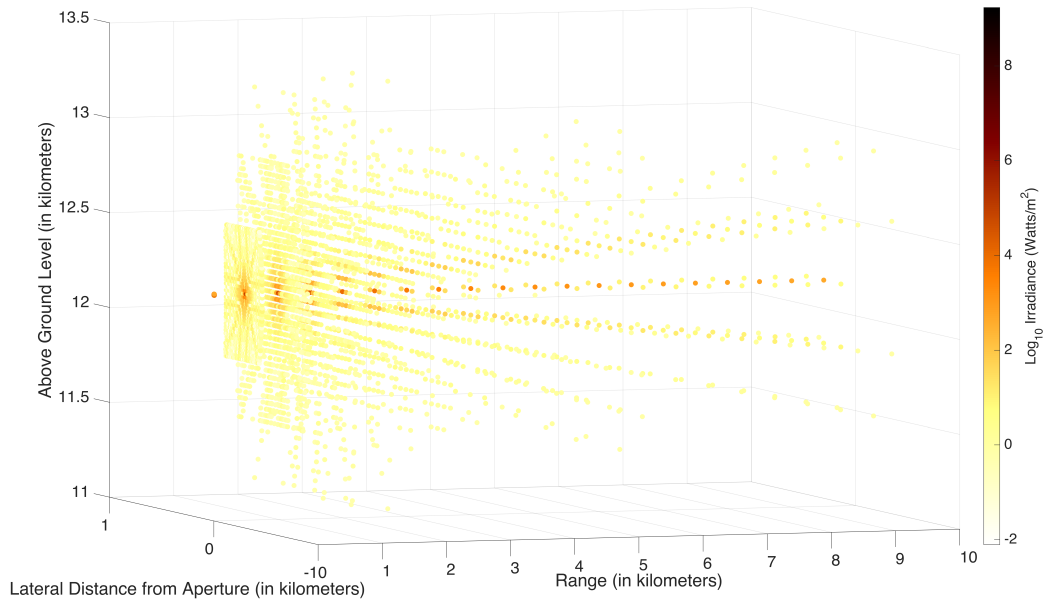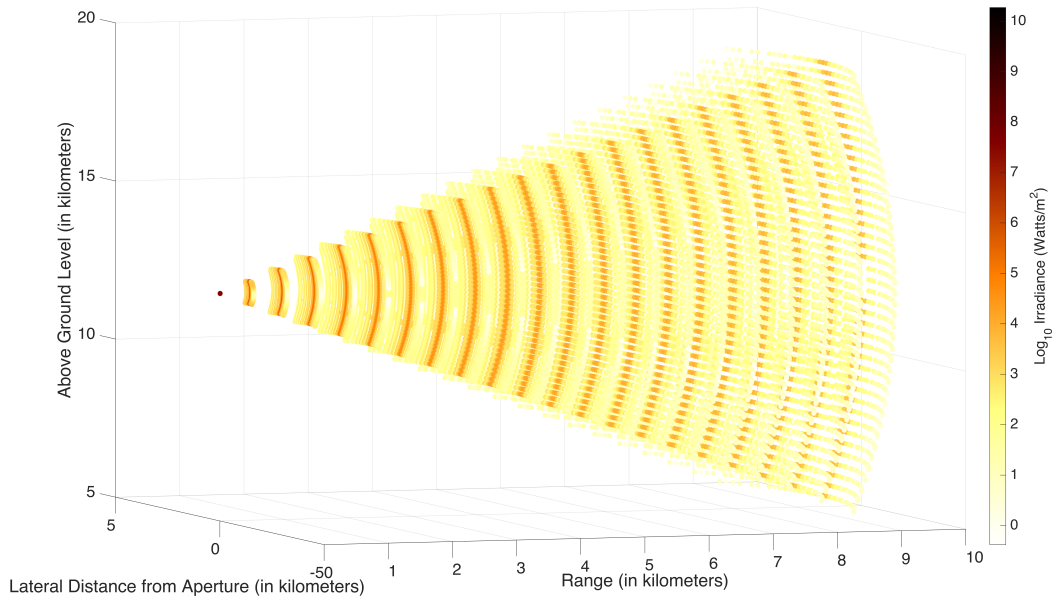Figure 28. HELEEOS Generated Irradiance Values of a PPA 35 GHz in a vacuum.

Figure 29. HELEEOS Generated Irradiance Values of a PPA 94 GHz in a vacuum.

ULA Antennas.

The ULA patterns can also be plotted in vacuum as shown in Figures 30 and 31. The higher frequency effect is more apparent in the ULA patterns as the main lobe is much more pointed and there is some interference patterns present in the 94 GHz pattern. Similar attenuation is shown with distance as found in the PPA patterns. Note the script stopped calculating many areas on the PPA antennas where the ULA patterns would run at each 500 meter step out to the maximum of 10 kilometers. This shows the high directivity of the PPA patterns with respect to the ULA antennas.

Figure 30. HELEEOS Generated Irradiance Values of a ULA 35 GHz in a vacuum.
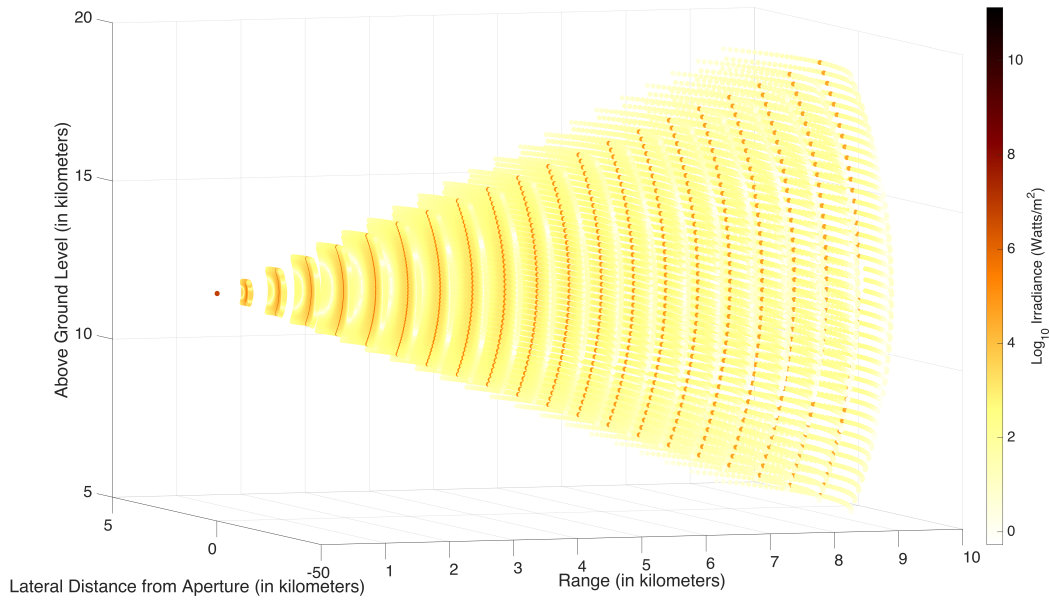

Figure 31. HELEEOS Generated Irradiance Values of a ULA 94 GHz in a vacuum.

4.2 Standard Atmosphere

Several engagements were modeled in an atmosphere using standard temperature, pressure, and humidity values from the U.S. 1976 Standard Atmosphere. No weather effects were included. Even less water vapor at higher altitudes, the oxygen absorption contributes to an appreciable amount of extinction from the 60 GHz resonance band. Figure 32 shows attenuation of the pattern. However, under 5 km range, there is a significant amount of energy still spreading into the sidelobes of the radar pattern.

Figures 32 and 33 show a standard atmosphere pattern at 3048 meters (approximately 3 km). At this altitude, there is little moisture compared to lower altitudes. There are very slight differences, highlighted with the green circle, in the far field pattern. These patterns looked very similar to higher altitudes and had similar attenuation. Because of these lack of differences, a standard atmosphere may be a good approximation for MMW patterns above 3048 meters. This is also supported by the fact that pressure broadening of spectral absorption lines is more dominant at lower altitudes (due to higher pressures). Therefore, the higher altitude limits the effects of pressure broadening. This assertion is supported further by the fact that the pattern only slightly changes at 12,192 meters in a tropical standard atmosphere.
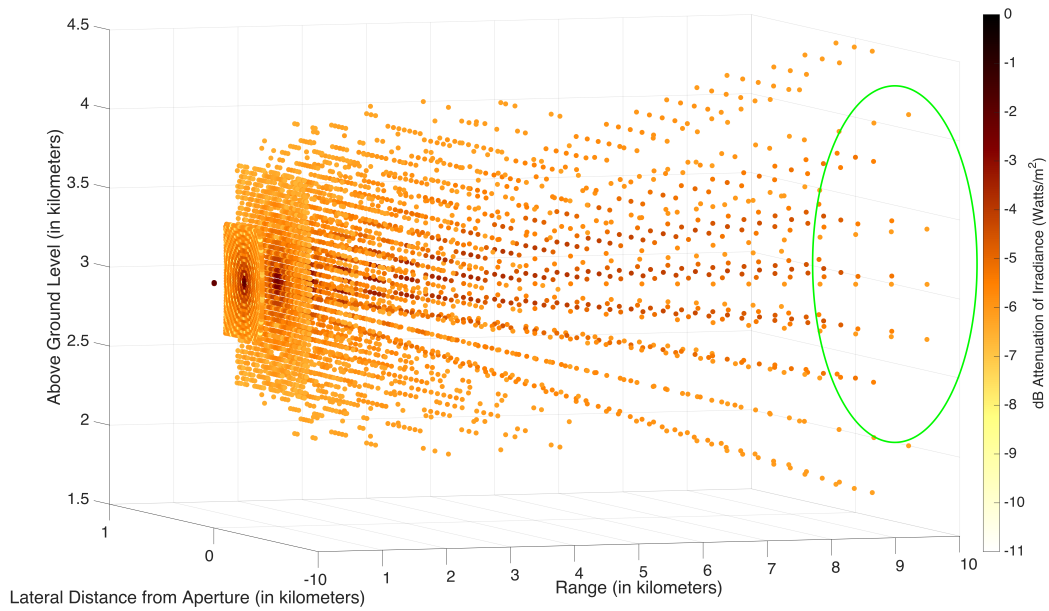
Figure 32. 35 GHz PPA aperture propagating in U.S. 1976 Standard Atmosphere at 3048 meters above the ground.
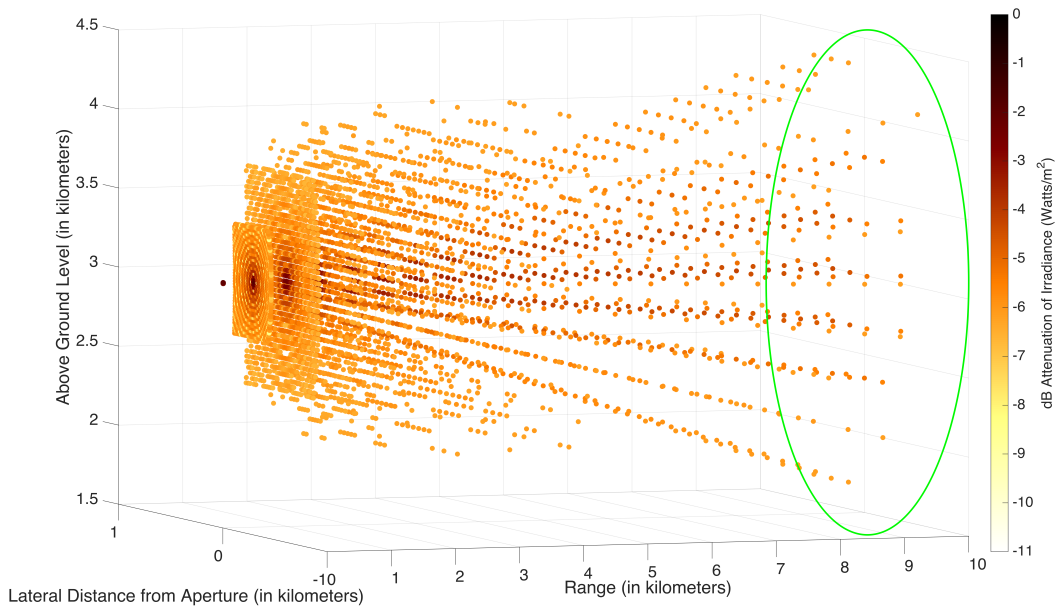

Figure 33. PPA 35 GHz at 3048 meters in Standard Tropical Atmosphere.

Figure 34 demonstrates a surface-to-air scenario in the same standard atmosphere.

84

This demonstrates more attenuation at lower altitudes (note the change in the color bar scale); however, similar ranges are seen still. In certain scenarios near the surface, the higher amounts of water vapor in the standard atmosphere created interesting phenomena. The boundary layer represents the transition between turbulent flow near the surface and more laminar flow at higher altitudes, and serves as a trap for more moist air. The standard atmospheres only serve to roughly approximate the lowest 1500 meters of the boundary layer. Even so, this creates a situation where on top of the rough boundary layer, radar propagated more freely than regimes within the rough boundary layer. It also created a situation where attenuation was greater in the lowest part of the simulated atmosphere.
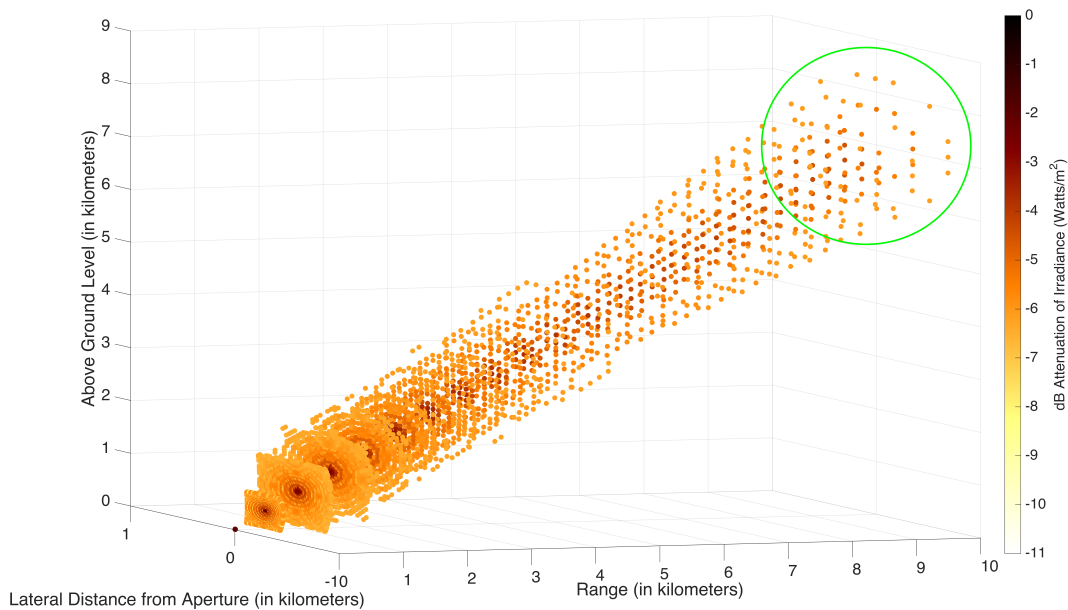

Figure 34. PPA 35 GHz Surface to Air in Standard Atmosphere

By implementing a standard tropical atmosphere, the previous figures are little affected; however, a slight amount of additional attenuation is measured when looking at individual data values. It is uncommon for there to not be significant moisture levels at lower altitudes. Therefore, the weather effects in Section 4.6 will show the

importance of capturing these effects.

Identical analysis was done on the PPA 94 GHz and ULA 35 and 94 GHz patterns and the results were similar. The higher frequencies had more pointed structure (as seen in Figure 35), yet similar attenuation values at altitude.
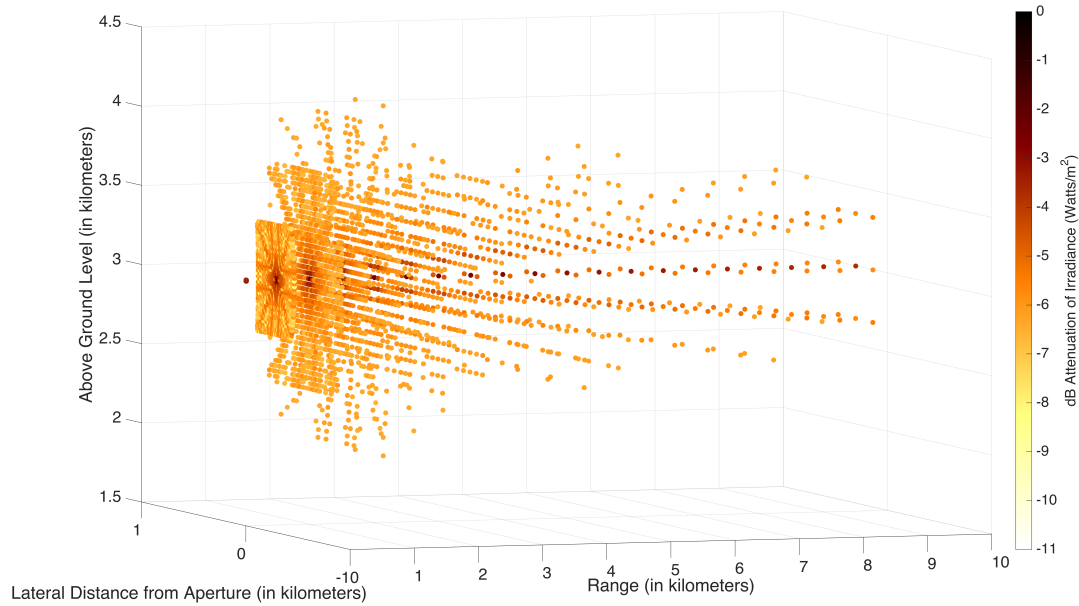

Figure 35. PPA 94 GHz at 3048 meters in Standard Tropical Atmosphere. Note the more pointed structure to the pattern yet similar attenuation to the 35 GHz pattern

4.3 ExPERT Atmosphere

There are many effects at lower altitudes that may be overlooked if only using a standard atmosphere, which represents conditions which are never replicated in direct observation. HELEEOS is able to capture these effects, such as a realistic boundary layer characterization, and show the impacts on attenuation. An ExPERT atmosphere only is advantageous within the boundary layer. Above the boundary layer, ExPERT returns to a standard atmosphere based on the latitude of the site, tropical standard for Panama City, Panama. One limitation of the ExPERT atmosphere is that the ExPERT atmosphere reverts to a standard atmosphere above the boundary

layer. As LEEDR defined the PBL at 500 meters for the scenarios ran, no results for above 500 meters will be shown because they would be identical to propagation in a standard tropical atmosphere.

At frequencies where refraction is important, future versions of HELEEOS may (with the help of LEEDR) show bending of lobes that travel through more refractive portions of atmosphere. A key limitation of this method is the refractive bending is ignored for reasons discussed in Subsection 3.1. The ExPERT atmosphere incorporates nonstandard (hence realistic) moisture and temperature gradients within the boundary layer Naturally, combining ExPERT with actual weather phenomena increases accuracy even further. Using an ExPERT atmosphere allows for calculations in diverse climates without having access to numerical weather data. ExPERT calculations provide increased accuracy over standard atmospheres without the increased computation time and data that is required for NWP generated atmospheres.

The vertical profile for the ExPERT atmosphere that was generated for these calculations in HELEEOS is shown in Figure 36. The high dew point values are indicative of a high absolute humidity, thus an increased amount of water vapor present in the atmosphere for this particular scenario which will contribute to increased molecular absorption.
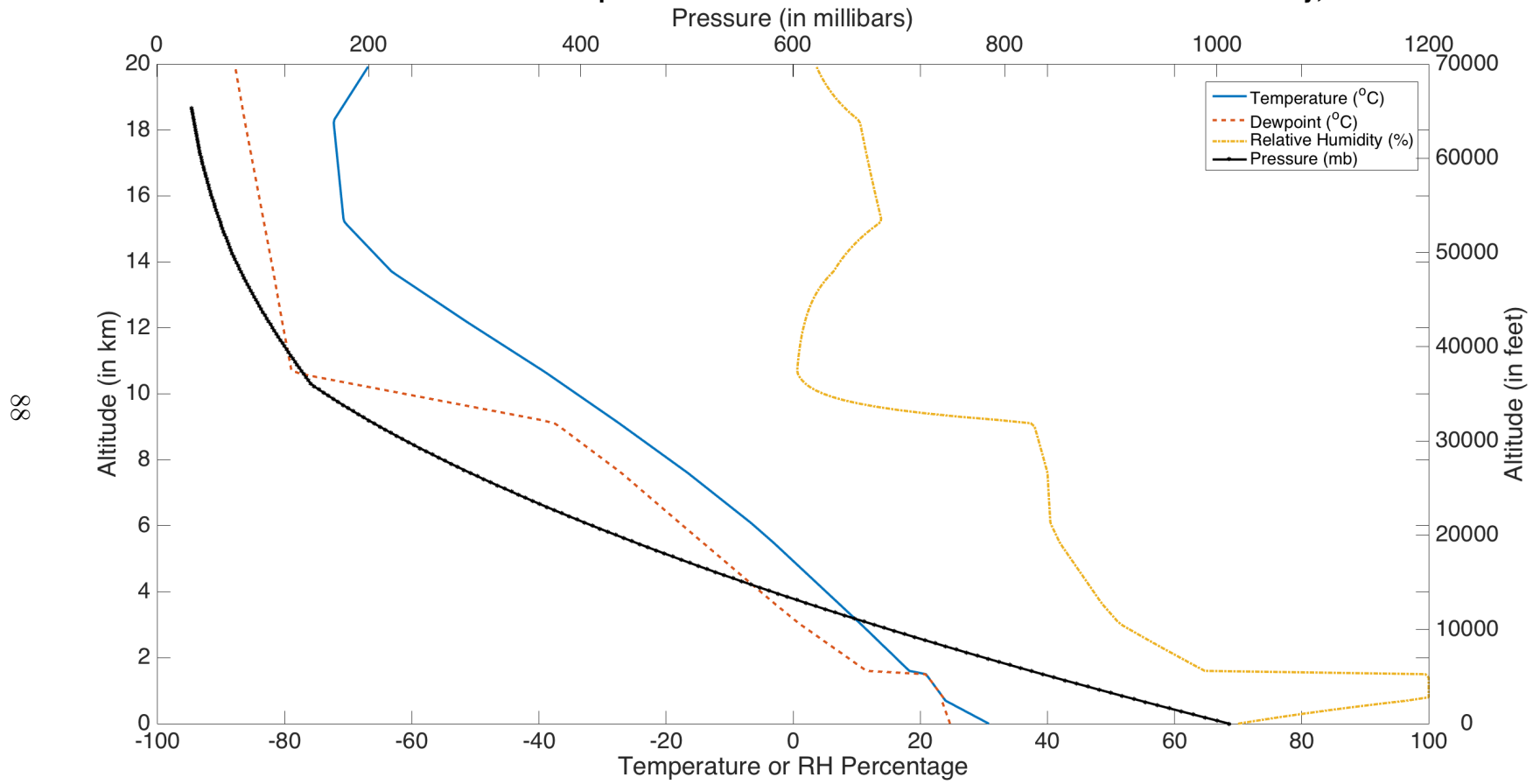
Figure 36. Vertical Atmospheric Profile for ExPERT Atmosphere in HELEEOS

The following examples show HELEEOS results in which an atmosphere using ExPERT climatology and boundary layer characterization was employed. Figures 37a and 37b models a PPA 35 GHz and 94 GHz radar at 300 meters in an air-to-air scenario. Note the greater attenuation in the pattern, specifically in sidelobes, than present in the higher altitudes of the standard atmosphere.
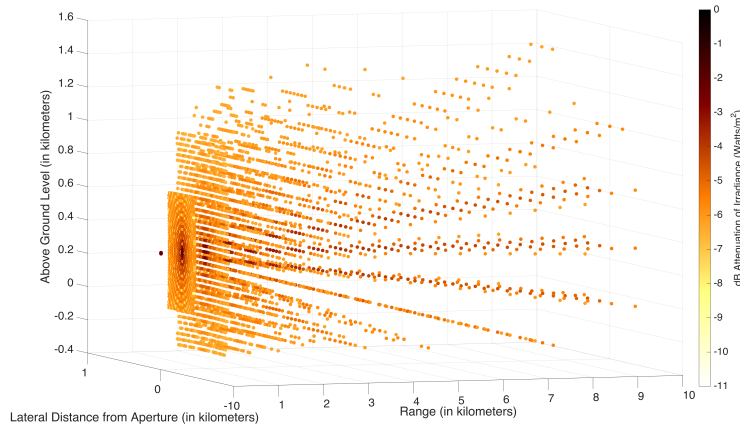
(a) PPA 35 GHz at 300 meters in an ExPERT Atmosphere.
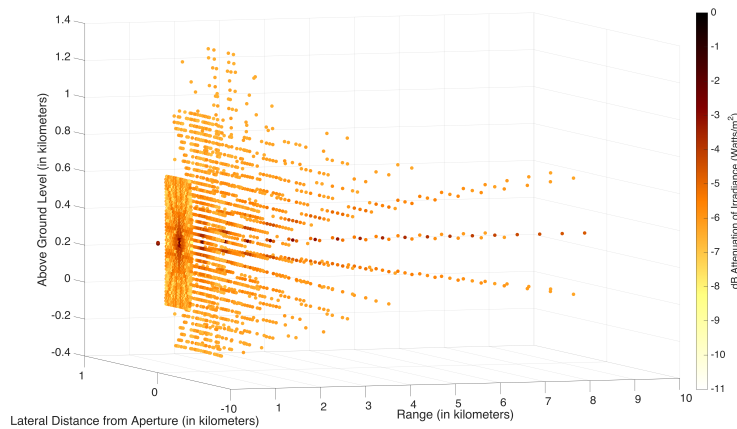
(b) PPA 94 GHz at 300 meters in an ExPERT Atmosphere.

Figure 37. PPA 35 and 94 GHz at 300 Meters in ExPERT Atmosphere

In the following surface-to-air and air-to-surface scenarios, ExPERT shows slight affects in attenuation (shape and strength of signal) that is not captured in the standard atmosphere to include the lower elevations of the beam being slightly more

attenuated than the top portion of the beam. Also, the change in decibel attenuation is over distance is different as will be discussed in Section 4.7.
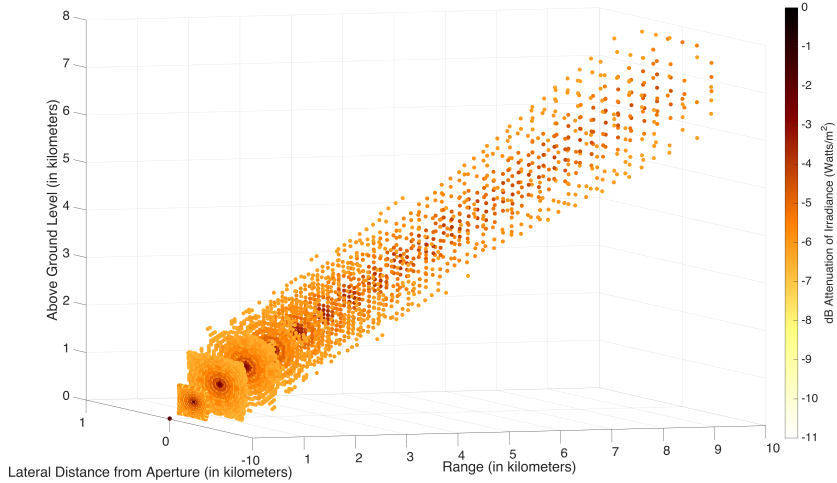
(a) PPA 35 GHz Surface-to-Air in ExPERT Atmosphere
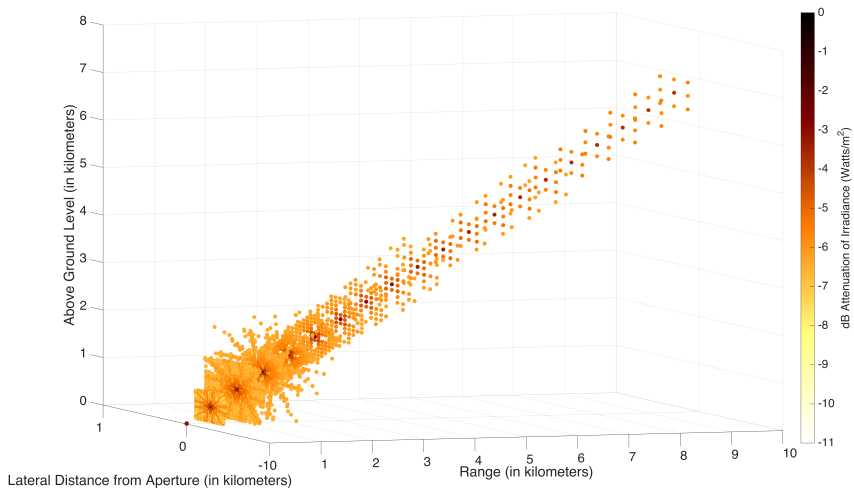
(b) PPA 94 GHz Surface-to-Air in ExPERT Atmosphere

Figure 38. Surface-to-Air Scenarios, PPA 35 and 94 GHz (ExPERT Atmosphere)

4.4 Numerical Weather Prediction Generated Atmosphere

By using numerical weather model information ingested via the NOMADS database, real time environmental effects can be introduced into the calculation rater than composite climatology captured in ExPERT. The weather model information ingested is from the Global Forecast System (GFS). It is important to consider that models may not be as accurate in observation sparse regions as they are in areas where there are a lot of observations. Mountainous and low population density regions do not have sufficient infrastructure to support a large array of surface based observations which means that model outputs in those regions may not be as quality as in other regions. With satellite and aircraft observations being ingested, this model quality is improved; however, it is still an important consideration when relying upon NWP information to provide a realistic forecast.

On the particular day of 1 Sept 2015, the GFS run was chosen to be the morning (7 am local) the day of a thunderstorm. The ground layer of fog had just warmed up enough to dissipate and create a very humid morning. The Aviation Routine Weather Report (METAR) closest to the weather model run gave the following observations listed below [31]. Note that presence of weather phenomena such as clouds does not mean the clouds are included in NWP models. Their inclusion from the METAR is meant to serve as an indicator of the presence of moist rising air which would affect temperature and dew point levels.

- Temperature and dew point of 78.8^o F (26° C)

- Relative Humidity of 100%

- Barometer rising through 29.89 inches mercury (1012.19 millibars)

- Few cumulus clouds at 800 and 1600 feet

- Few towering cumulonimbus clouds with bases at 1800 feet

- Scattered clouds at 9000 feet

- Winds calm

Because Panama City, Panama is a coastal environment where temperatures are very warm (even in September), there was a lot of moisture in the air this day. Because there was a thunderstorm in the afternoon, it can be inferred there was a lot of instability and lifting action as well. This is demonstrated in Figure 39 where the relative humidity is relatively high at higher altitudes indicative of lifting mechanisms which are present and indicative of moisture being brought higher in the atmosphere. Also the planetary boundary layer appears to be present (note the spike in the RH), however a temperature inversion at the top of the boundary layer is not present according to the NWP data. When HELEEOS calculated the boundary layer, the value given for this particular scenario was at 500 meters indicating its characterization as an ocean environment. This is likely realistic due to its close proximity to two oceans. This adds additional utility and realism to the atmospheric model.
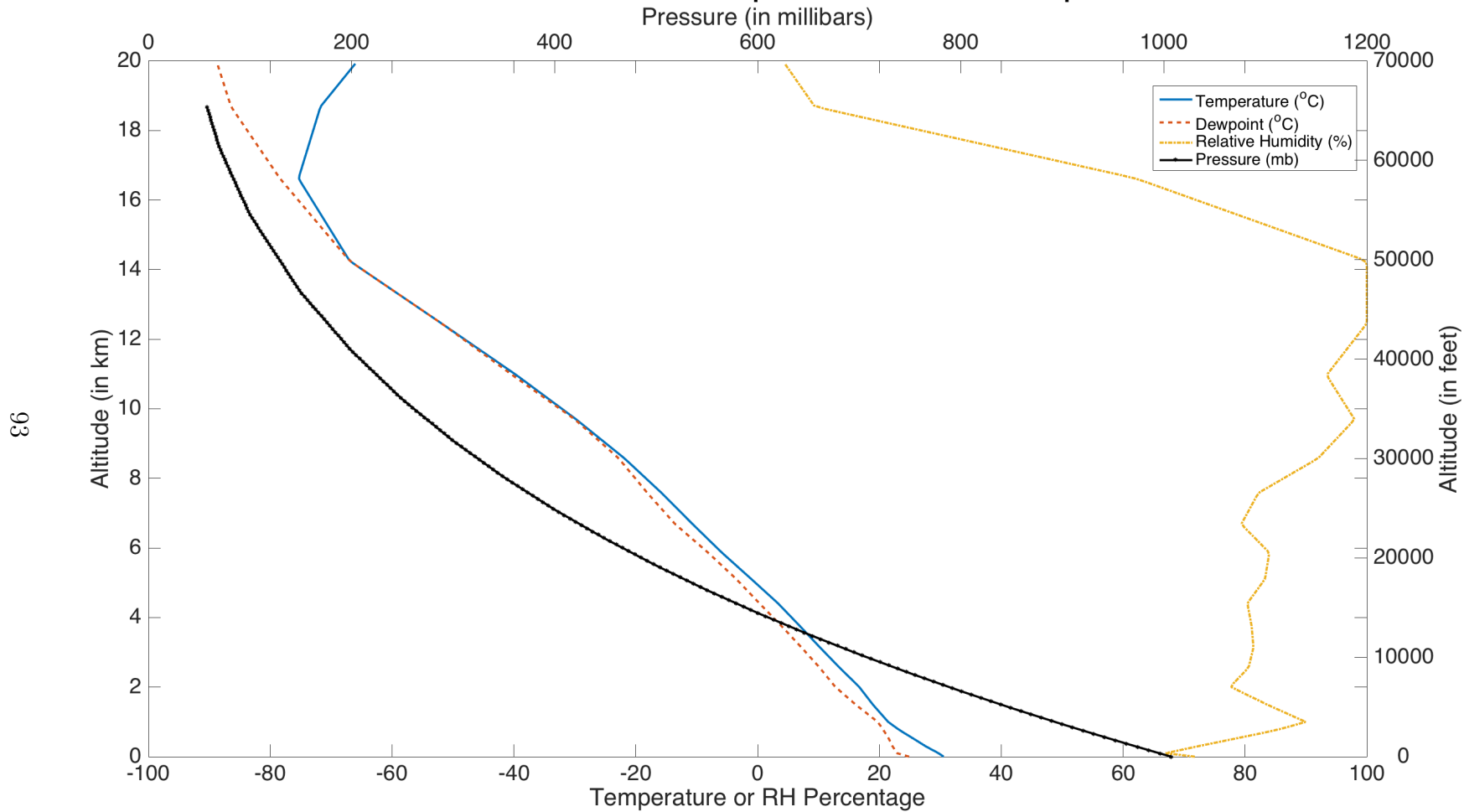
Figure 39. Atmospheric Profile for NWP Atmosphere in HELEEOS

Figure 40 shows the impact that a NWP atmosphere has at 300 meters altitude. This is not significantly different than a standard or ExPERT atmosphere at this altitude. However, one can see the additional attenuation present in the sidelobes and highlighted in the figures. Because the 35 GHz antenna was more spread out, there was more energy in sidelobes to be attenuated. This effect was not noticed with the 94 GHz scenario. Likewise, the ULA antennas at altitude also had little distinguishable differences between the ExPERT and standard atmospheres.
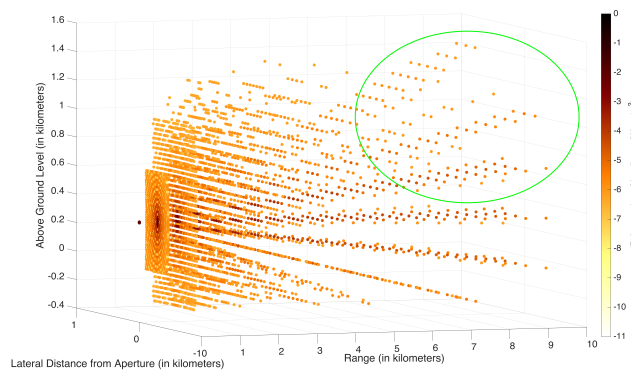
(a) PPA 35 GHz at 300 meters in NWP Atmosphere.
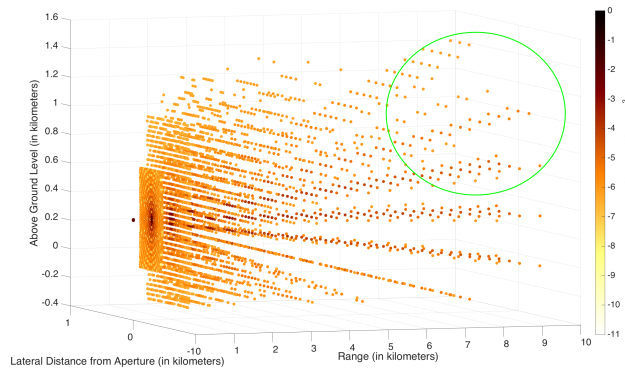
(b) PPA 35 GHz at 300 meters in Standard Tropical Atmosphere.

Figure 40. PPA 35 GHz at 300 Meters in Air-to-Air Scenario with NWP and Standard Tropical Atmosphere.

Like with ExPERT, using NWP data for scenarios in which the transmitter is near the surface, the added features of the atmosphere enhance the ability to predict the beam. Figure 41 shows a ULA transmitter looking at surface. The signal is heavily attenuated as the beam gets closer to the surface where the high humidity resides. The decreased range would not be captured with a standard atmosphere.
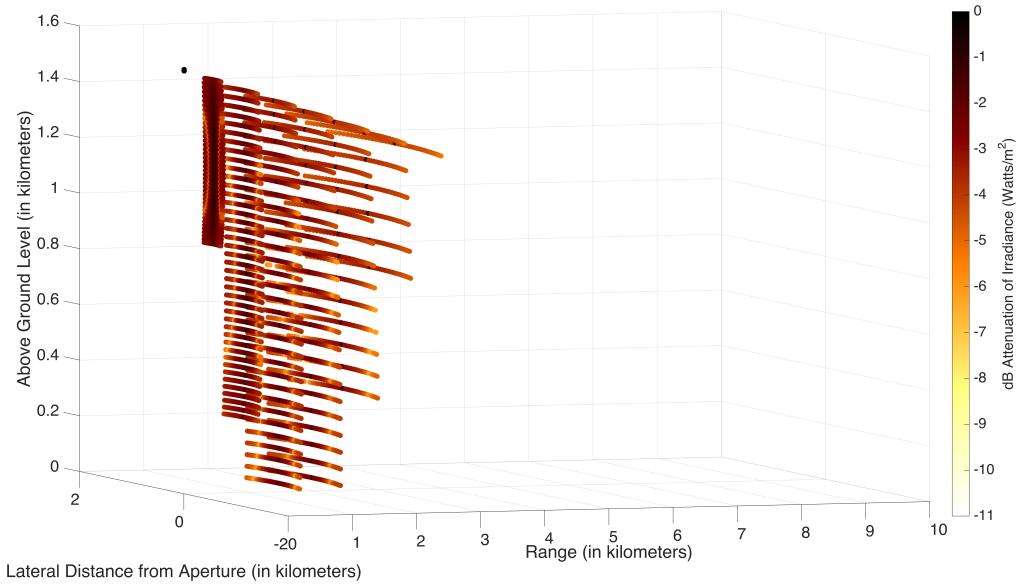

Figure 41. ULA 94 GHz from 1542 meters to Surface in NOMADS Atmosphere

The NOMADS database of NWP enables real time atmospheric conditions to be ingested into HELEEOS, which increases accuracy in range and attenuation of radar beams. This shows great promise for HELEEOS in being able to interrogate a realistic model of the atmosphere to provide insight towards MMW propagation.

4.5 Atmospheric Humidity Effects

Along with oxygen, water is a primary contributor to absorption. As discussed in Section 2.1 and shown in Figure 5, attenuation increases with frequency. Therefore, the results seen in the preceding analysis verify that the primary driver of attenuation is water content. For instance, the 94 GHz had greater amounts of attenuation than the 35 GHz. This can be seen in the plots of molecular absorption and absolute humidity in Figures 42 and 43. Note the stronger molecular absorption values for the 94 GHz versus that for the 35 GHz and also the fact that molecular absorption tracks almost exactly with water content. This explains the similarities between the two patterns in Figure 40; this similarity is directly attributable to the absolute humidity values shown in Figure 43, where the NWP, ExPERT, and Standard Tropical absolute humidity values are relatively close to the same value at 300 meters. Due to the lack of water absorption in lower frequencies, any significant effects in the 35 GHz regime will be attributed to weather phenomena such as rain or clouds. However this analysis reveals that as higher frequencies are interrogated, the amount of water absorption will become a major factor in attenuation. Figures 42 and 43 also demonstrates that the ExPERT atmosphere reverts to a standard atmosphere above the boundary layer (1500 meters).
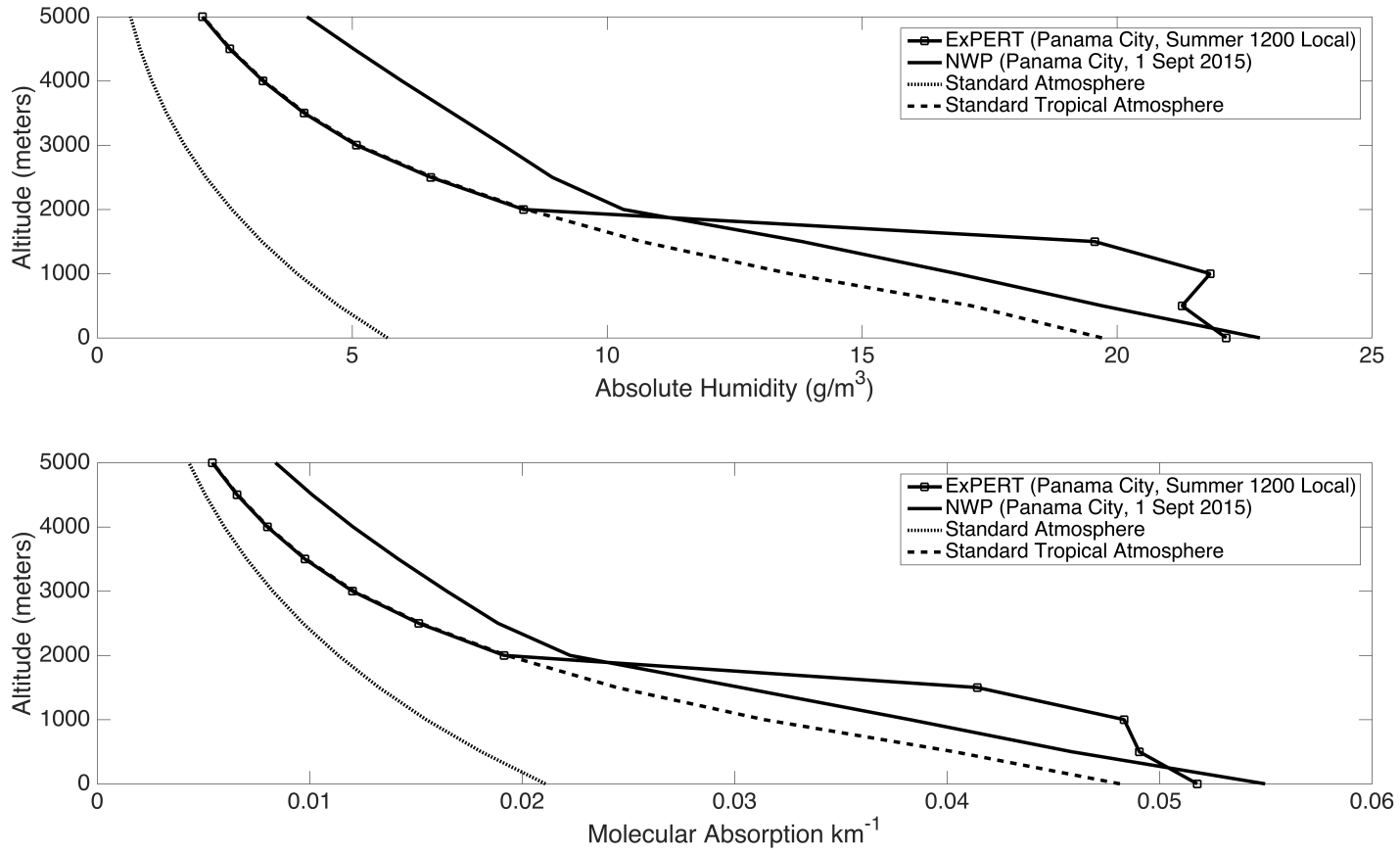
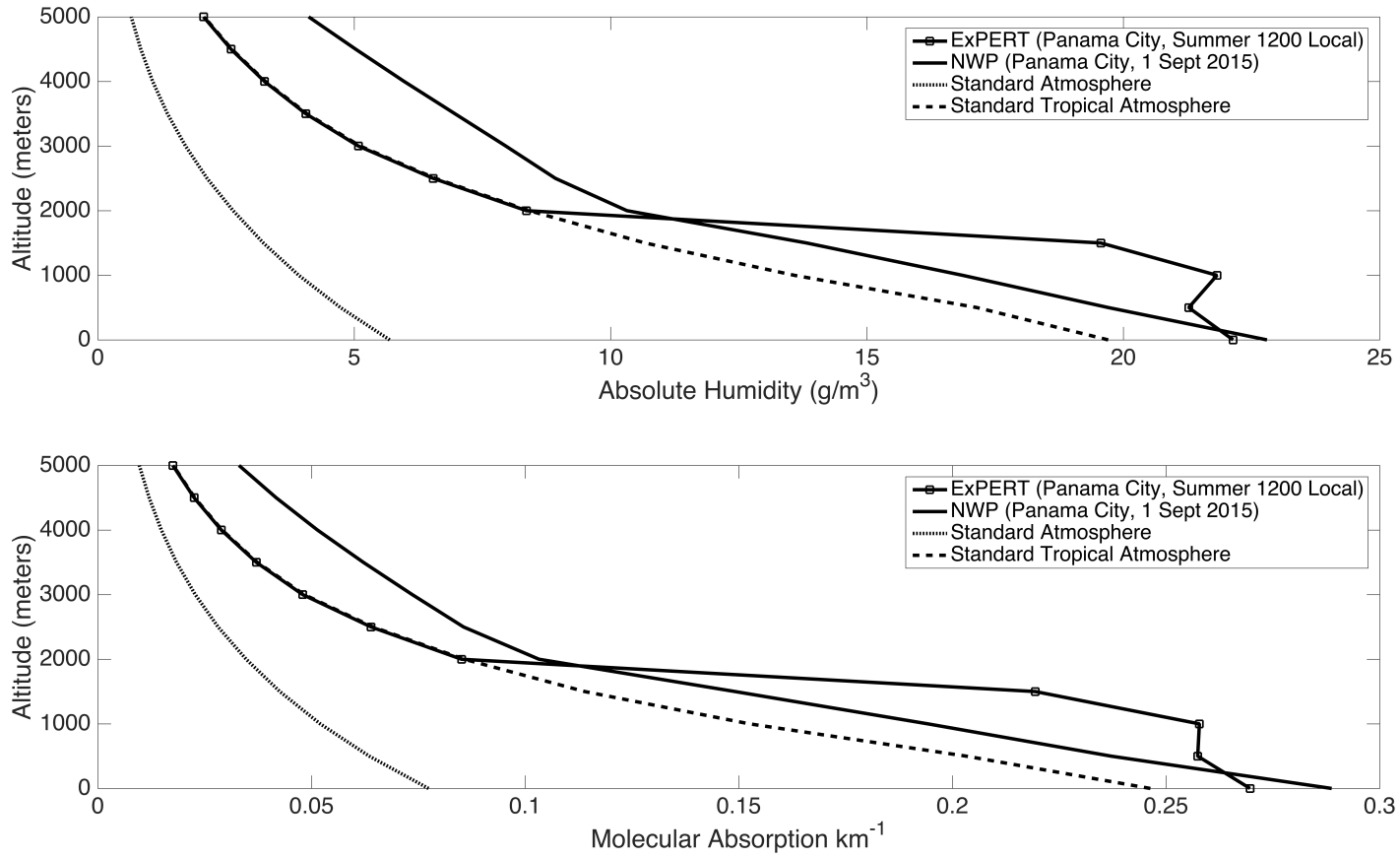Figure 42. 35 GHz Molecular Absorption and Absolute Humidity vs. Altitude

Figure 43. 94 GHz Molecular Absorption and Absolute Humidity vs. Altitude

4.6 Weather Effects

A strong advantage HELEEOS brings to HEL propagation modeling is the ability to simulate weather effects on a laser beam. A major goal of this research is to investigate if it is possible to exploit this capability for MMW radar. As mentioned in Section 2.3, by virtue of the scatterers (rain, hail, and suspended water droplets) having a size on the order of MMW wavelengths, strong attenuation can completely block a beam. This is important to account for from a tactical standpoint because weather effects can often impact operations and one's ability to employ radar capabilities.

Running the Mie code in HELEEOS for large particles such as cloud droplets and precipitation is computationally intensive and can take several seconds to compute a single data point. However, this time is well spent because it shows great promise to provide a comprehensive picture of radar patterns as they are affected by weather conditions. The remainder of this section is devoted to evaluating HELEEOS' capabilities simulating MMW propagation and observations regarding various weather effects on MMW performance.

The following figures show a PPA transmitter at 35 and 94 GHz in an air-to-air configuration at 3048 meters in a summer ExPERT atmosphere for Panama City, Panama in Summer using the 50th Percentile relative humidity (RH) conditions. Various vertical blocks of rain intensities were defined from 2500 to 3500 meters to fully obscure the radar transmitter.

Prior to proceeding, the following plotted data appears to suggest increasing RF intensity as the rain rate increases for altitudes above the transmitter. It may be tempting to conclude energy is being scattered into the upper portions of the MMW propagation pattern. However, a key limitation of this research is that the script written assigns each data point in the propagation field to a specific angle of the MMW source. Therefore, photons scattered off each lobe's central axis are not ac-

99

counted for in other areas of the pattern. Once multiple scattering is implemented into HELEEOS, it will be possible to determine if there is any enhancement of the beam due to scattering from portions of the pattern affected by weather. This would be achieved by storing a matrix of scattered values of radiation from each previous loop in the engagement.

Light Rain (5 mm/hour).

For light rain (5 mm/hr), there is a very noticeable significant attenuation after the 4 km range in Figure 44. The attenuation is similar for the 35 and 94 GHz, although it is a more abrupt drop off in strength for the 94 GHz. This is most likely due to the fact that there are more droplets in the size distribution near the 3 mm λ than the 8 mm λ. Therefore, there is more attenuation with the 94 GHz.
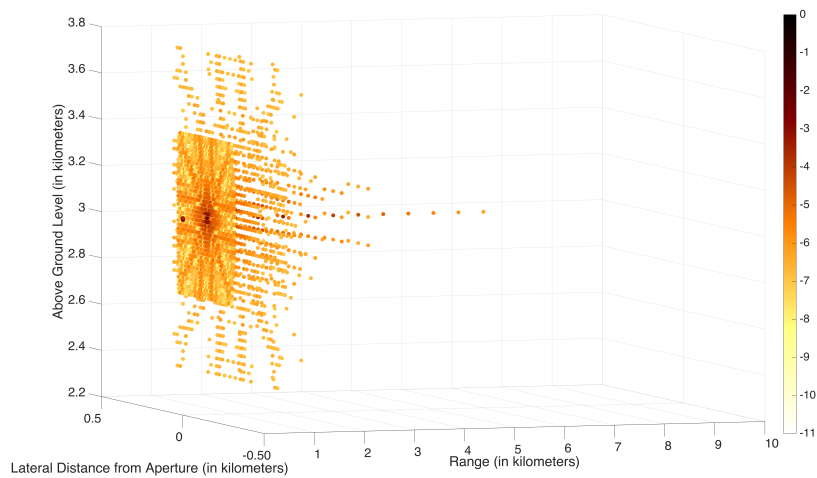
Heavy Rain (25 mm/hr).

Referencing Equation 25, which shows a direct correlation between rain rate and intensity, as the intensity increases to heavy rain (25 mm/hr), attenuation increases in areas where rain is present more than in the light rain scenarios. This relationship is also supported in Figure 15. In Figure 45, note the main beam does not travel as far in this scenario either. Furthermore, even the sidelobes are attenuated to the point of not being detectable with current radar receiver technology. This proves that at areas above 25 mm/hr rain it is possible that the weather can lead to significant decreases in MMW radar system capability especially in the 94 GHz regime due to greater beam directionality. Also, because the shorter wavelength of 3 millimeters is closer to the size of the rain which causes a greater increase in scattering.

Extreme Rain (75 mm/hr).

As shown in Figure 46, extreme rain has a substantial impact on the MMW radar ability to propagate. Propagation is heavily influenced by the frequency of the transmitter. The 94 GHz can only go a little over half of the distance the 35 GHz signal can propagate. This is simply due to the high number of scattering and absorbing particles near the 3 millimeter wavelength of the 94 GHz radar as opposed to the 35 GHz (3 millimeter) radar.
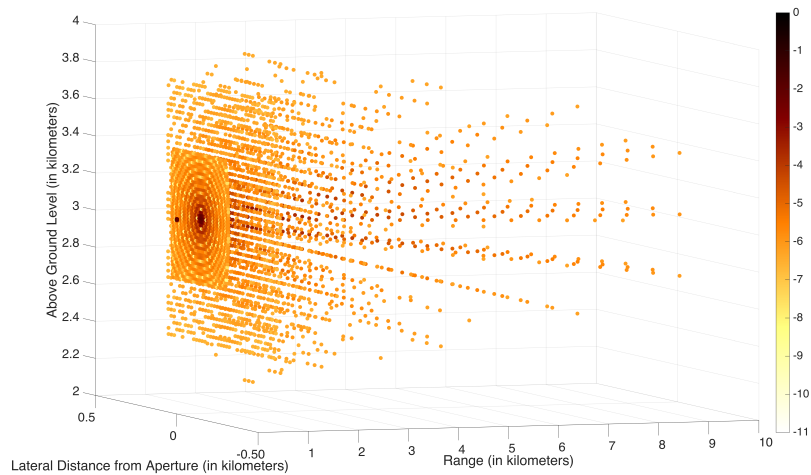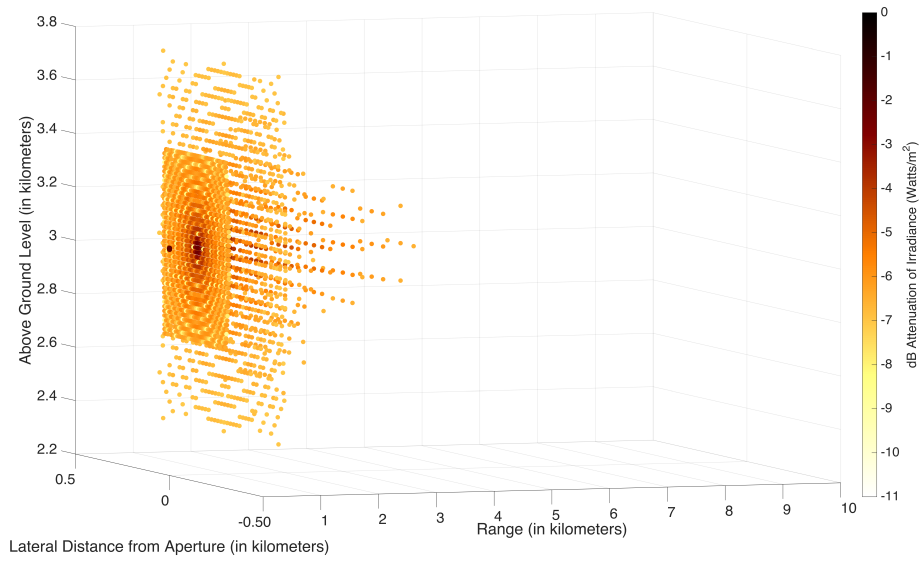
(a) PPA 35 in Light Rain at 3048 meters. Note the attenuation is much greater to the lower lobes, especially after 4 km range.
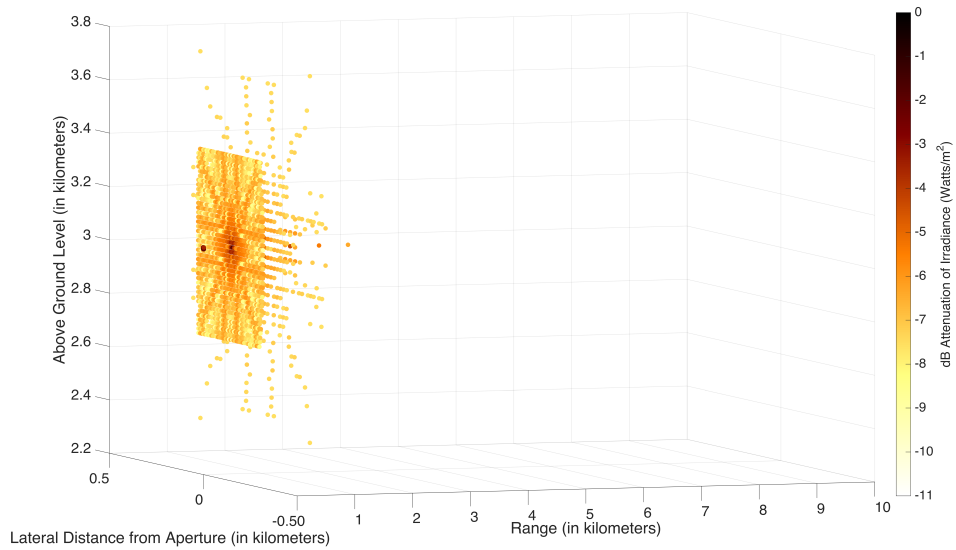

(b) PPA 94 in Light Rain at 3048 meters. Note the attenuation is much greater to the lower lobes, especially after 4 km range.

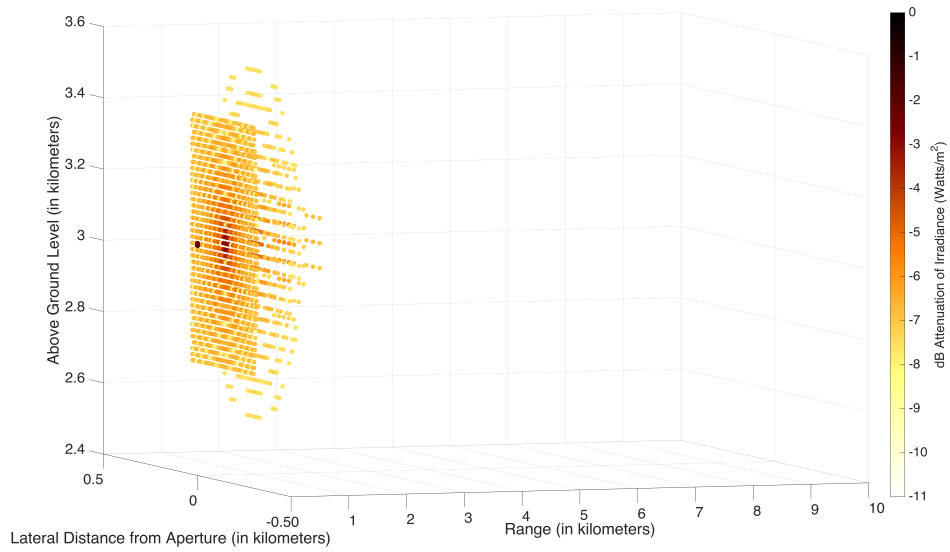Figure 44. Light Rain (5 mm/hr) in an Air-to-Air scenario at 3048 meters

(a) PPA 35 in Heavy Rain at 3048 meters. As expected, more attenuation than the light rain.
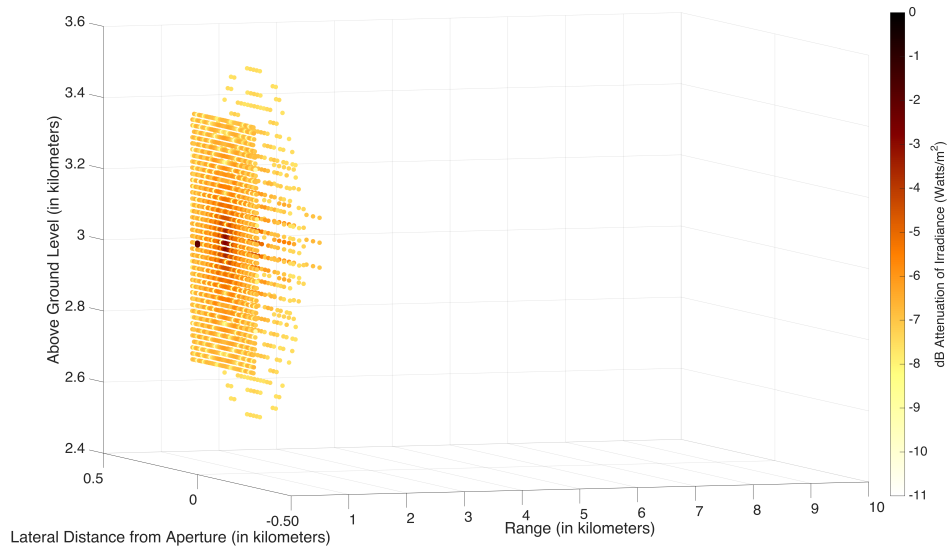

(b) PPA 94 in Heavy Rain at 3048 meters. As expected, more attenuation than the light rain. Note the range values.

Figure 45. Heavy Rain (25 mm/hr) in an Air-to-Air scenario at 3048 meters

(a) PPA 35 in Extreme Rain at 3048 meters. As expected, much greater attenuation than light or heavy rain.

(b) PPA 94 in Extreme Rain at 3048 meters. Note the range values - 94 GHz is much more attenuated than 35 GHz in the same scenario.

Figure 46. Extreme Rain (75 mm/hr) in an Air-to-Air scenario at 3048 meters

Cumulus Clouds.

The HELEEOS cloud model used was clean (no suspended pollutants) cumulus continental. The clouds were from 2500 - 3500 meters and the aperture for the air-to-air scenario was at 3048 meters. The cloud attenuates slightly the 35 GHz but not nearly the same effect as the rain has on the signal. This is important to realize that as a cloud builds and increases moisture content and vertical motion, it becomes much more opaque once rain droplets reach a size on the order of the wavelength. Furthermore, HELEEOS shows the capability to capture the effect of the rain providing more attenuation below the cloud than above or within the cloud. In an air-to-ground scenario with a cloud deck from 2500 - 3500 meters, the radar does propagate; however, HELEEOS is able to predict increased attenuation as the radar travels through the clouds.
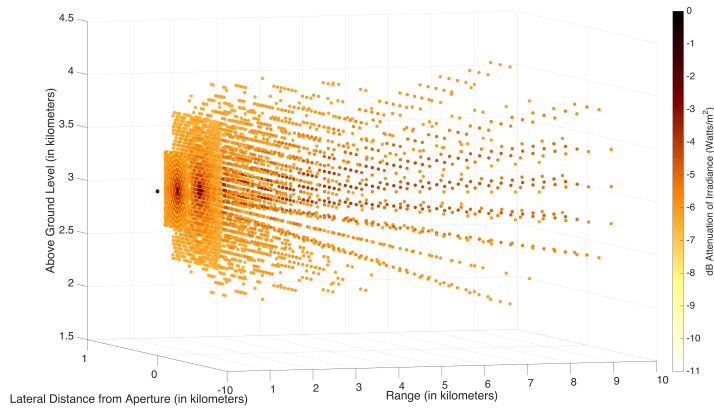

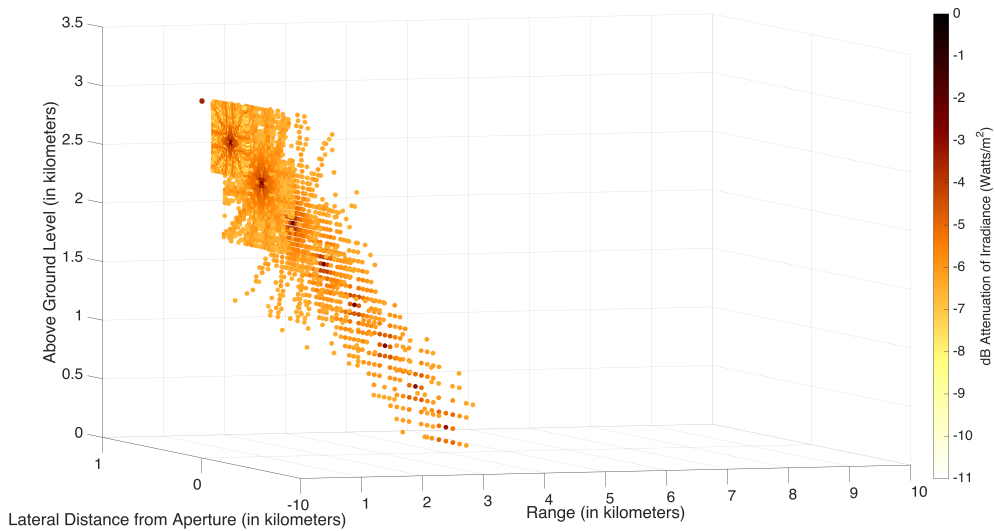Figure 47. PPA 35 GHz in NWP Atmosphere with Cumulus Cloud at 3048 meters

Figure 48. PPA 94 in Air-to-Ground in a NWP atmosphere with Clouds at 2000-3000 Feet.

Fog.

Fog is of particular interest to the surface-to-air scenarios because a large amount of moisture in the air has potential to greatly inhibit MMW transmission. In this research, fog was modeled from surface to 300 meters (roughly 1000 feet). This is very thick fog, and typically fog only extends a couple hundred feet in the air. However, modeling such a thick segment of fog gives a worst case scenarios for these radars.

Figure 49 shows a ULA pattern in a standard atmosphere with and without fog. Note the significant change in attenuation of the main beam. More interesting is that the sidelobe energy below the main beam is completely absorbed in the layer of fog. This effect is shown by a weaker signal in the far field pattern, indicated with the green oval in Figure 49a. Depending on the application, fog has the potential to completely absorb a MMW transmission. This fact certainly is a factor that many radar models do not fully account for and any additional information (provided it is appropriately validated via experiment) will add to further understanding of MMW

propagation.
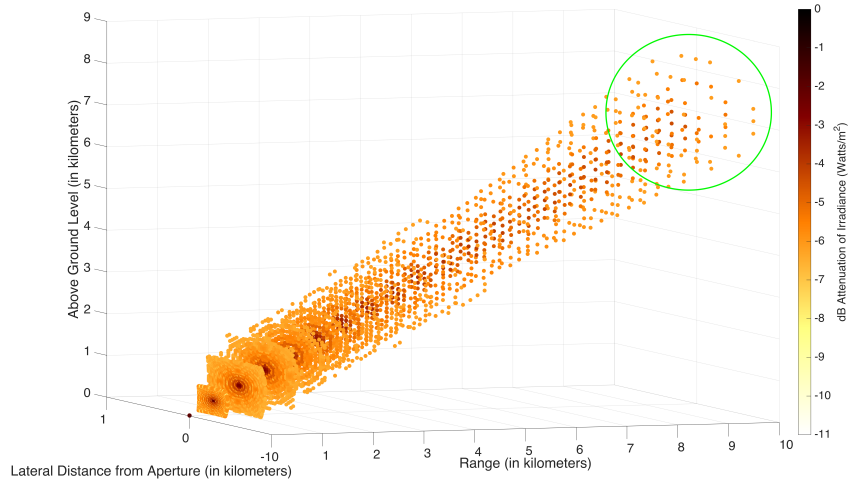
(a) PPA 35 GHz in Surface-to-Air Scenario for comparison to the same scenario with a layer of fog (Figure 49b)
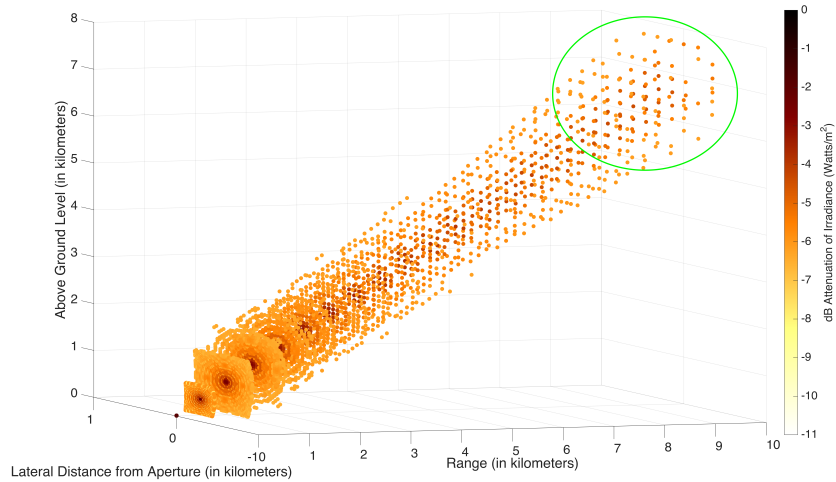
(b) PPA 35 GHz in Surface-to-Air Scenario with Fog Layer from Surface to 1000 Feet.

Figure 49. PPA 35 in Surface-to-Air Scenario using Standard Atmosphere with (Figure 49b) and without (Figure 49a) fog layer. Both scenarios are very similar, however it can be seen that the fog slightly increases attenuation

107

Ice Fog.

An Ice fog layer from surface to 305 meters(1000 feet) created a much weaker attenuation than that of regular fog, leading to the conclusion that ice fog does not cause any appreciable effects to MMW propagation at 35 and 94 GHz as anticipated from the discussion on Page 39.
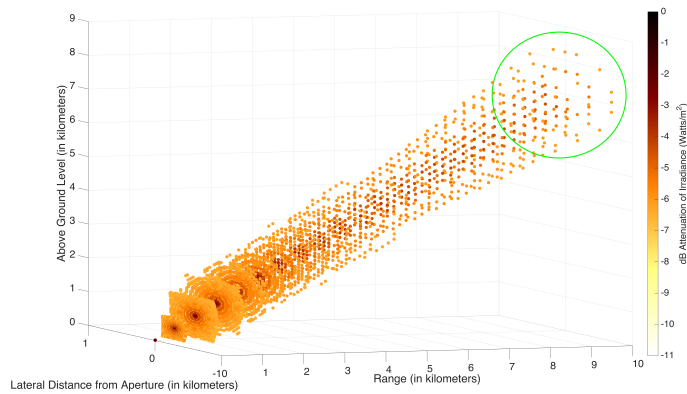
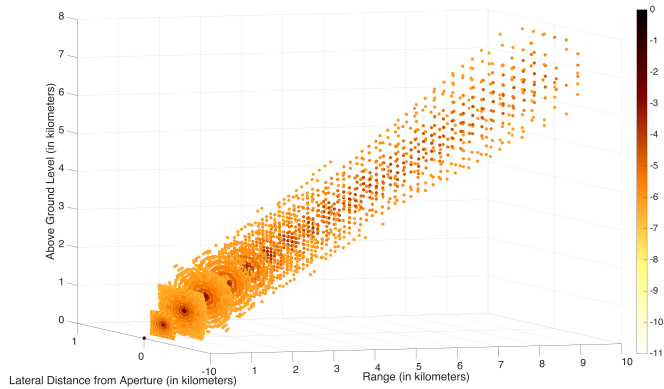

Figure 50. PPA 35 GHz in Standard Atmosphere

Figure 51. PPA 35 GHz Surface-to-Air in Ice Fog. Compare to Figure 50.

4.7 Main Beam Attenuation

The simplest way to look at the attenuation of the radar pattern is to evaluate the main beam (0° Azimuth and Elevation) and look at the attenuation at each range point. As with plotting the entire pattern, this method looks at the irradiance at

a point and compares it to the irradiance at corresponding vacuum reference point. In the following figures, they all appear to have a $1/r^2$ relationship which validates the assumptions made in Subsection 3.1. It also allows an easy way to compare the attenuation of various scenarios and demonstrate quantifiable impacts from weather and atmosphere on radar propagation. Furthermore, comparing the values between various scenarios allows a quick way to determine if HELEEOS is able to calculate a large difference in propagation strengths.

Path attenuation is heavily dependent upon any rain, for reasons discussed in Section 4.6 and on Page 39. Figure 52 shows the difference in total extinction path lengths for light, heavy, and extreme rain. HELEEOS, with the help of LEEDR, is able to account for the fact that during 75 mm/hr rain, the effective range is less than half of that in light rain.

As mentioned earlier, frequency effects in the MMW regime are very important to capture, and while the different frequencies may not have appreciable differences in attenuation in scenarios without weather, such as Figure 54, there are accountable differences when in heavy rain situations such as Figure 53.

In order to see how closely the HELEEOS results correlate with equations derived in Section 2.3, Equation 25 was applied to the 35 and 94 GHz frequencies and calculated attenuations displayed in Table 8. Comparing Table 8 with Figure 52, the dB attenuations do not align well at all. This is because irradiance needs to scale differently and there needs to be a correlation study done as well as ensuring the dB attenuation is accurately matching up with expected values. However, as expected, the higher rain rates and frequencies do cause a greater loss of the signal but it is not clear why this was not represented to the same value in the HELEEOS script.

The type of atmosphere obviously has an impact on main beam attenuation. Using main beam analysis on various atmospheres sampled, HELEEOS can break out

the effects on the main beam. Interestingly enough, Figure 55 demonstrates strong similarities between a ExPERT and NWP atmosphere at 35 GHz. This similarity is anticipated by referring back to Figure 42 where the ExPERT and NWP profiles have a very similar absolute humidity profile for this given day. Having experimental data will provide a real truth to allow a fit to which atmosphere can produce the most realistic radar strength measurements. Nonetheless, there are differences in the 35 and 94 GHz that are significant enough to make a difference in path loss. The real value of HELEEOS may lie in capturing the energy spread in various atmospheres.

While not the entire picture, looking at main beam attenuation allows a quick analysis of atmospheric effects on power loss of the radar. Comparing various scenarios communicates which effects are important to capture in tactical scenario development.

Table 8. Calculated Rain Attenuation Intensities for 35 and 94 GHz

Rain Rate	5		25		75	
Frequency (GHz)	35	94	35	94	35	94
Alpha	0.242	0.94	0.242	0.940	0.242	0.940
Beta	1.04	0.720	1.040	0.720	1.04	0.720
Attenuation (dB/km)	5.746	24.873	11.015	27.103	22.851	34.110
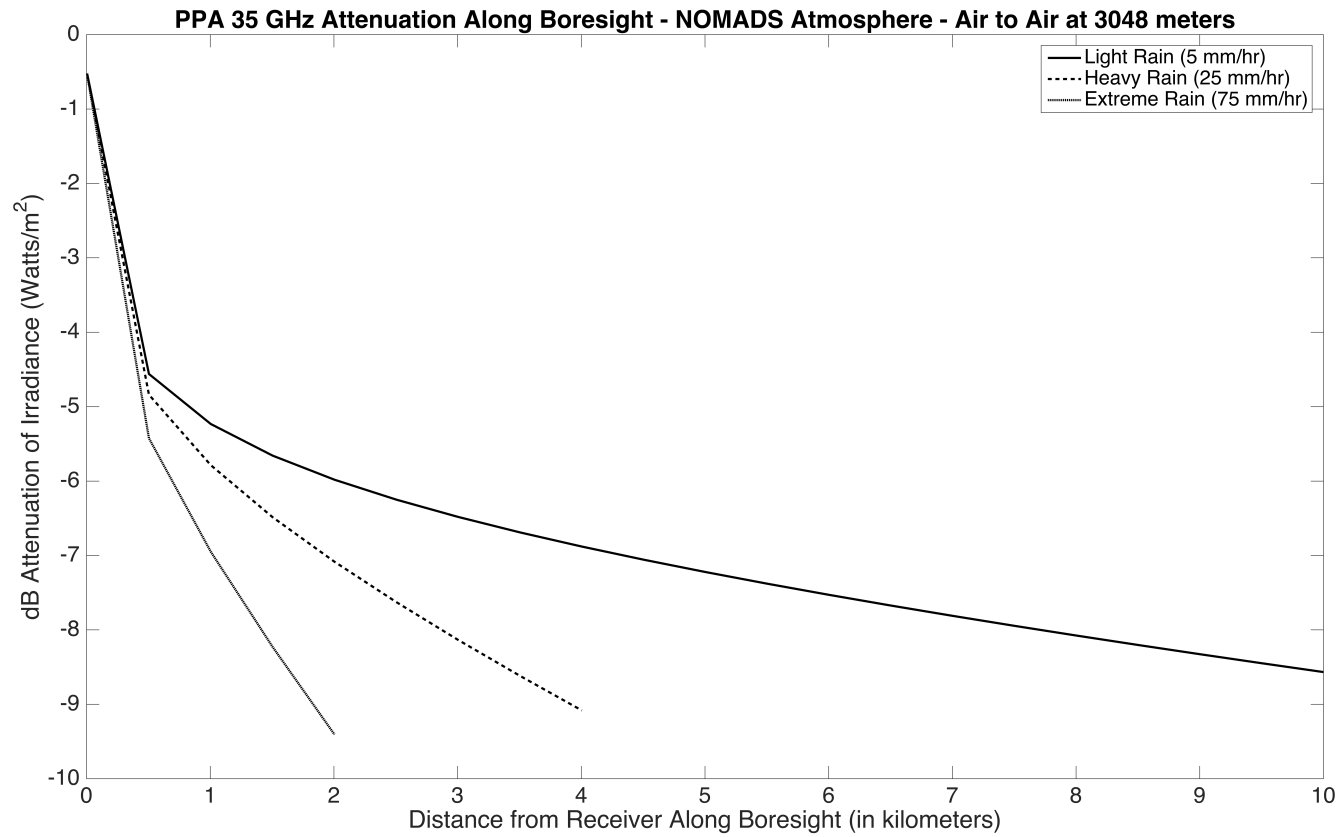
Figure 52. Decibel Attenuation Comparison for Main Beam in Varying Levels of Rain for PPA 35 GHz
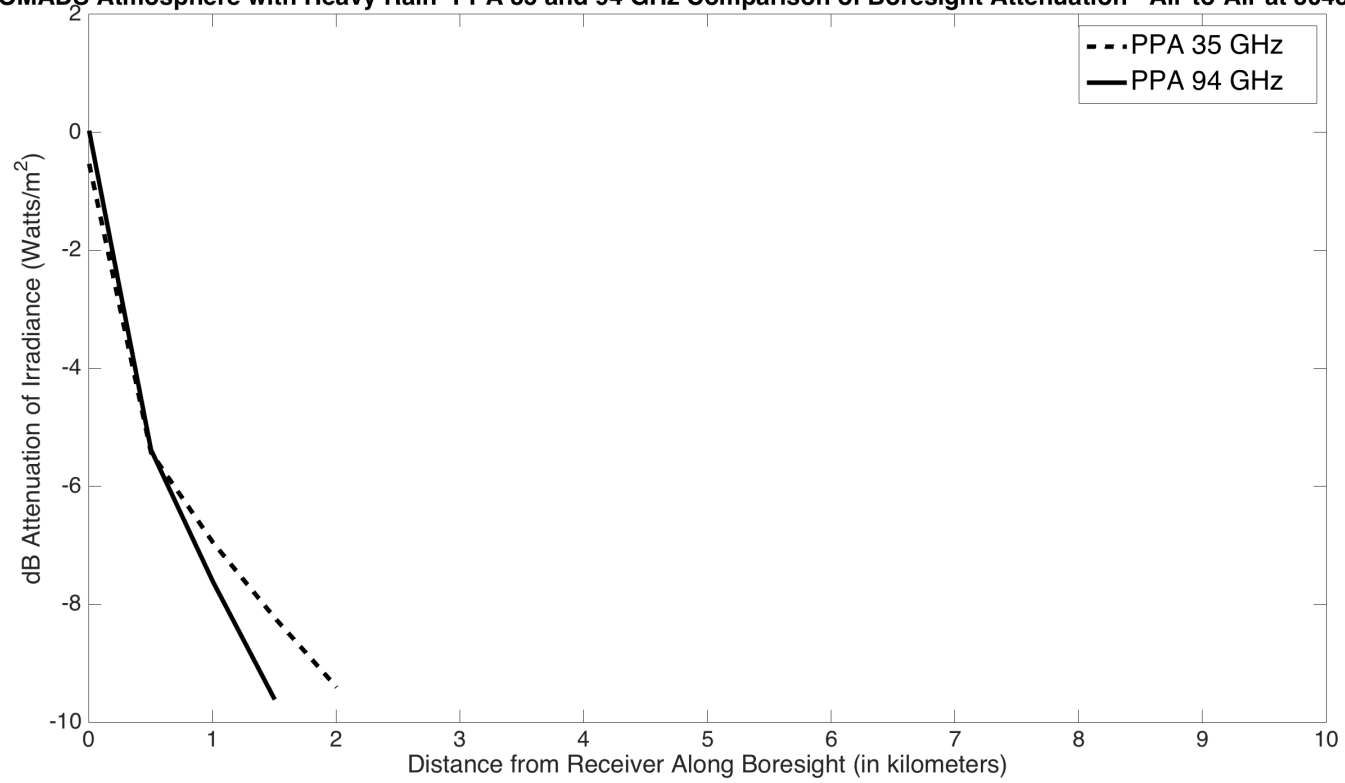
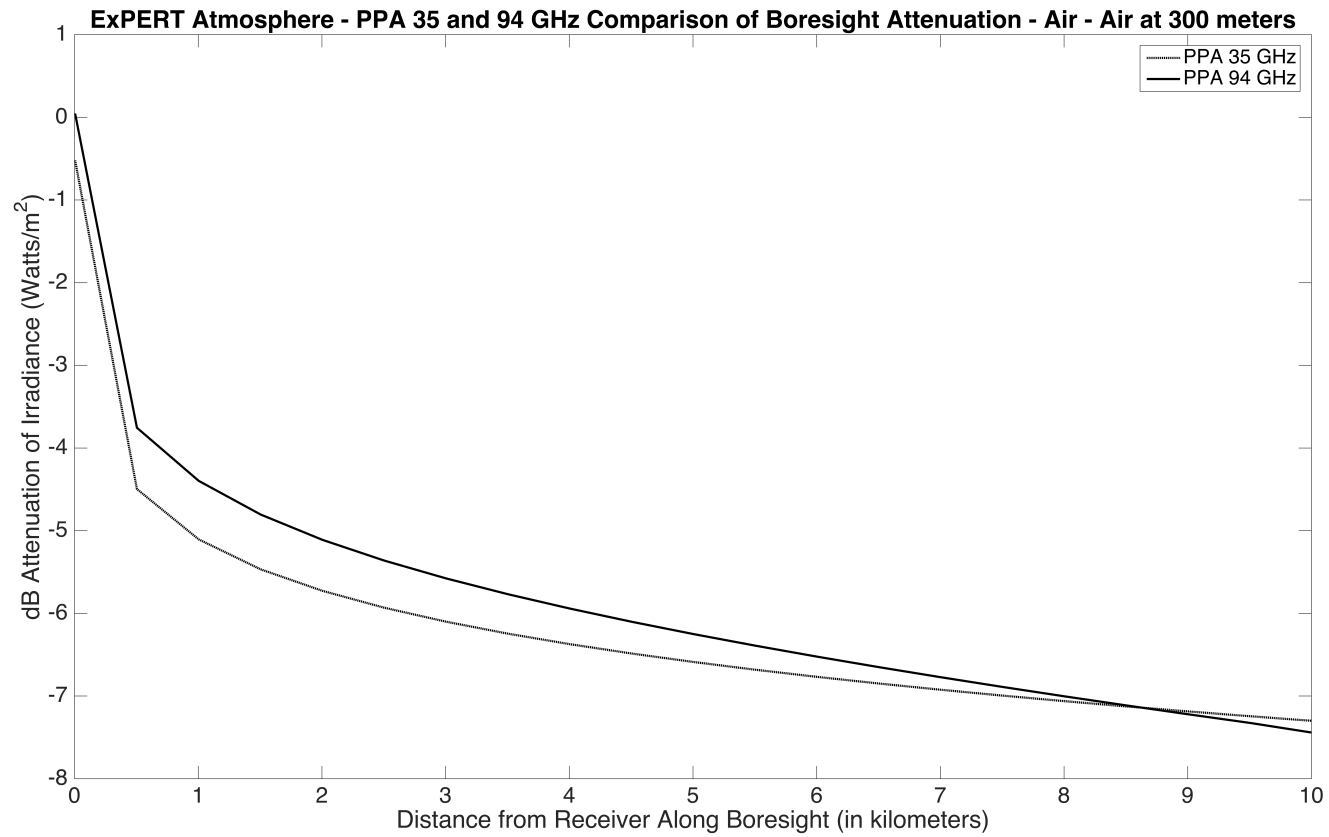Figure 53. Decibel Attenuation Comparison for Main Beam in Varying Levels of Rain for PPA 94 GHz

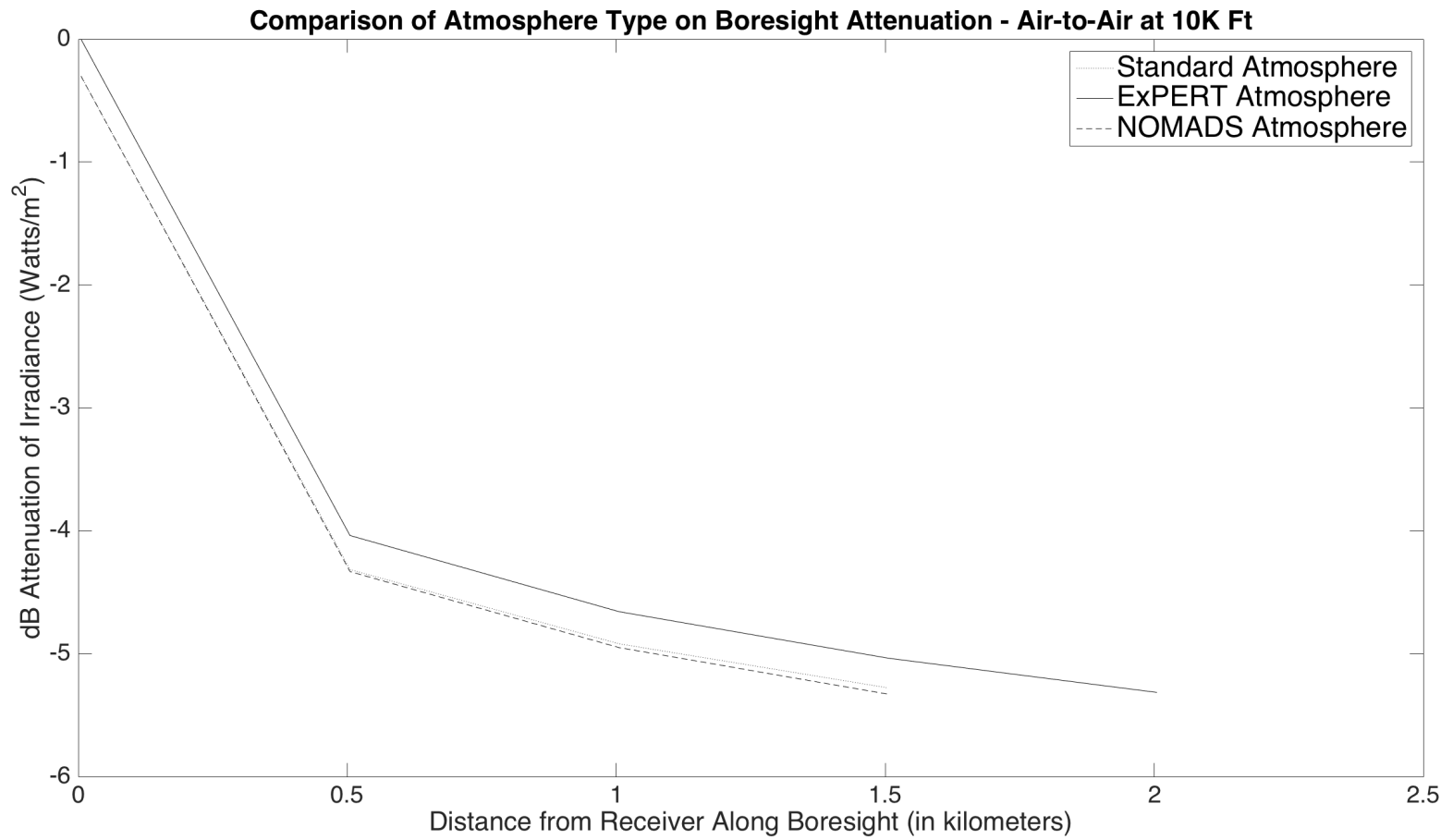Figure 54. PPA 35 GHz and 94 GHz Main Beam dB Attenuation in ExPERT Atmosphere

Figure 55. Comparison of Types of Atmospheres in Main Beam Attenuation at 35 GHz

4.8 Comparing HELEEOS Outputs to AREPS and IMOM

Both AREPS and IMOM have unique issues that made it difficult for a full quantitative analysis of the correlation between HELEEOS outputs with AREPS and IMOM. The most obvious advantage to a HELEEOS analysis is the three dimensional aspect. Both AREPS and IMOM were only able to produce two dimensional altitude-range plots for one azimuth angle. This meant that HELEEOS can give a three dimensional propagation for non-symmetric and complex patterns as it propagates through an atmosphere that varies not only in the vertical, but horizontal as well. Another strength of HELEEOS is the fact that weather conditions could be inserted whereas AREPS and IMOM did not have the ability to put in precipitation and cloud layers. This amount of fidelity and detail came at a cost; HELEEOS was the most time intensive to run (on the order of hours) and AREPS ran the quickest (under one minute for a scenario). Time to run an IMOM scenario varied between 1-3 minutes.

Comparison to AREPS.

The GUI for AREPS only allows frequencies of radar up to 57 GHz. Because of this, only the 35 GHz PPA comparison was performed. The propagation was assumed to be similar between PPA and ULA due to the same frequency. The following atmospheres were tested in the AREPS program:

- Standard Atmosphere

- ExPERT Atmosphere (Using imported data from HELEEOS)

- NOMADS Atmosphere (Using imported data from HELEEOS)

AREPS enabled the direct input of temperature, dew point, humidity, and wind profiles from the LEEDR generated atmospheres. Each atmosphere was tested at

3048 meters, and in a surface-to-air and air-to-surface configuration. AREPS also only allows for elevation angles of $\pm 10^o$. This led to some bouncing off the ground for the surface-to-air scenario, this effect was ignored in the HELEEOS scripts. However, even with these limitations, it is still possible to evaluate HELEEOS' performance relative to traditional radar code, if the two programs produce similar patterns and strengths. Recall in Subsection 2.2 that AREPS is able to generate propagation factor and propagation loss. While propagation loss will be the primary method of analysis, propagation factor charts will be included as well for reference in Appendix A.

Standard Atmosphere.

In the air-to-air scenario, AREPS produced lobe patterns similar to those generated from HELEEOS. The pattern also appeared to propagate in strongest form out to 10 kilometers. The angular dispersion from boresight was similar and the strongest areas of energy are towards the center. The propagation factor chart supports this "cone" of energy radiating from the antenna. For comparison to the HELEEOS model generated, Figure 57 show just the 0° azimuth value pulled from the standard moist atmosphere model run. As performed in this research, HELEEOS did not provide as much fidelity as the AREPS model. However, with more computation power, HELEEOS would be able to provide a more fine grid of computed irradiances. Nonetheless, there is still evidence of the patterns correlating and propagating at similar lengths and shapes.

Being limited to a maximum of 10° declination created issues with being able to see any changes occur with decreasing altitude, such as in Figure 58. The air-to-surface scenario is similar to the air-to-air scenario in pattern and attenuation.
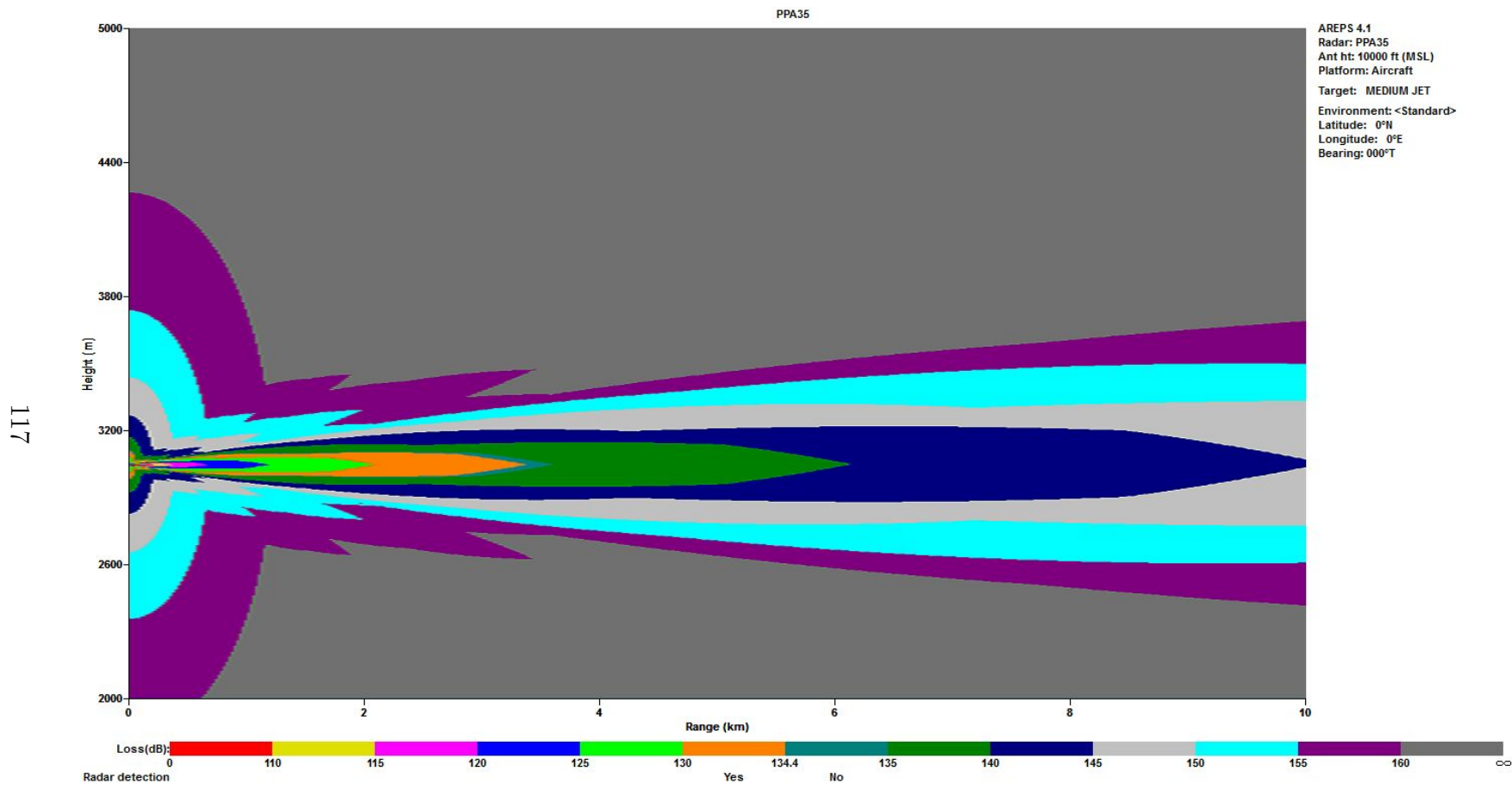
Figure 56. 35 GHz AREPS Propagation Loss for Air-to-Air Scenario in Standard Atmosphere at 3048 meters
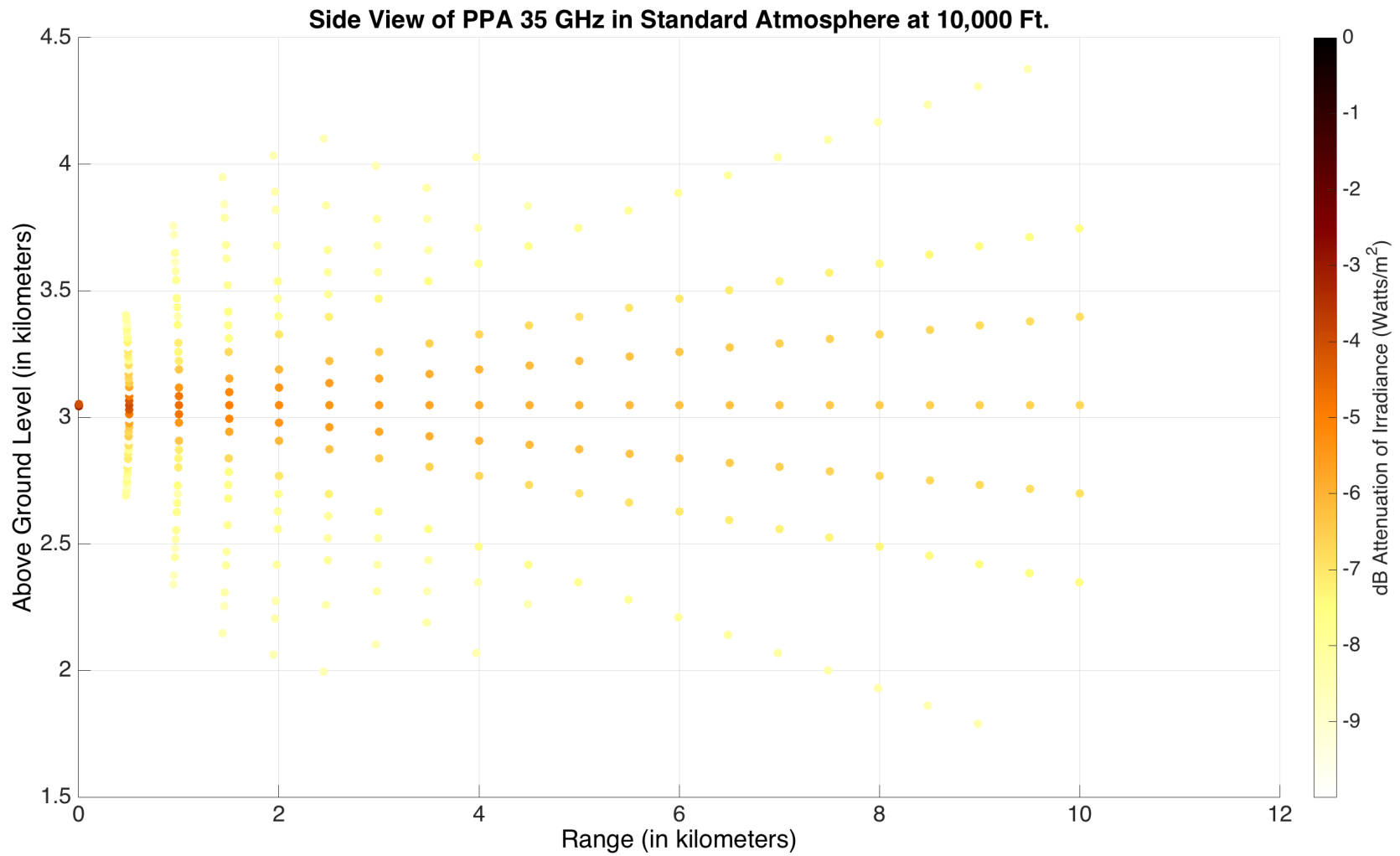
Figure 57. HELEEOS Side Cut for 35 GHz AREPS Propagation Factor for Air-to-Air Scenario in Standard Atmosphere
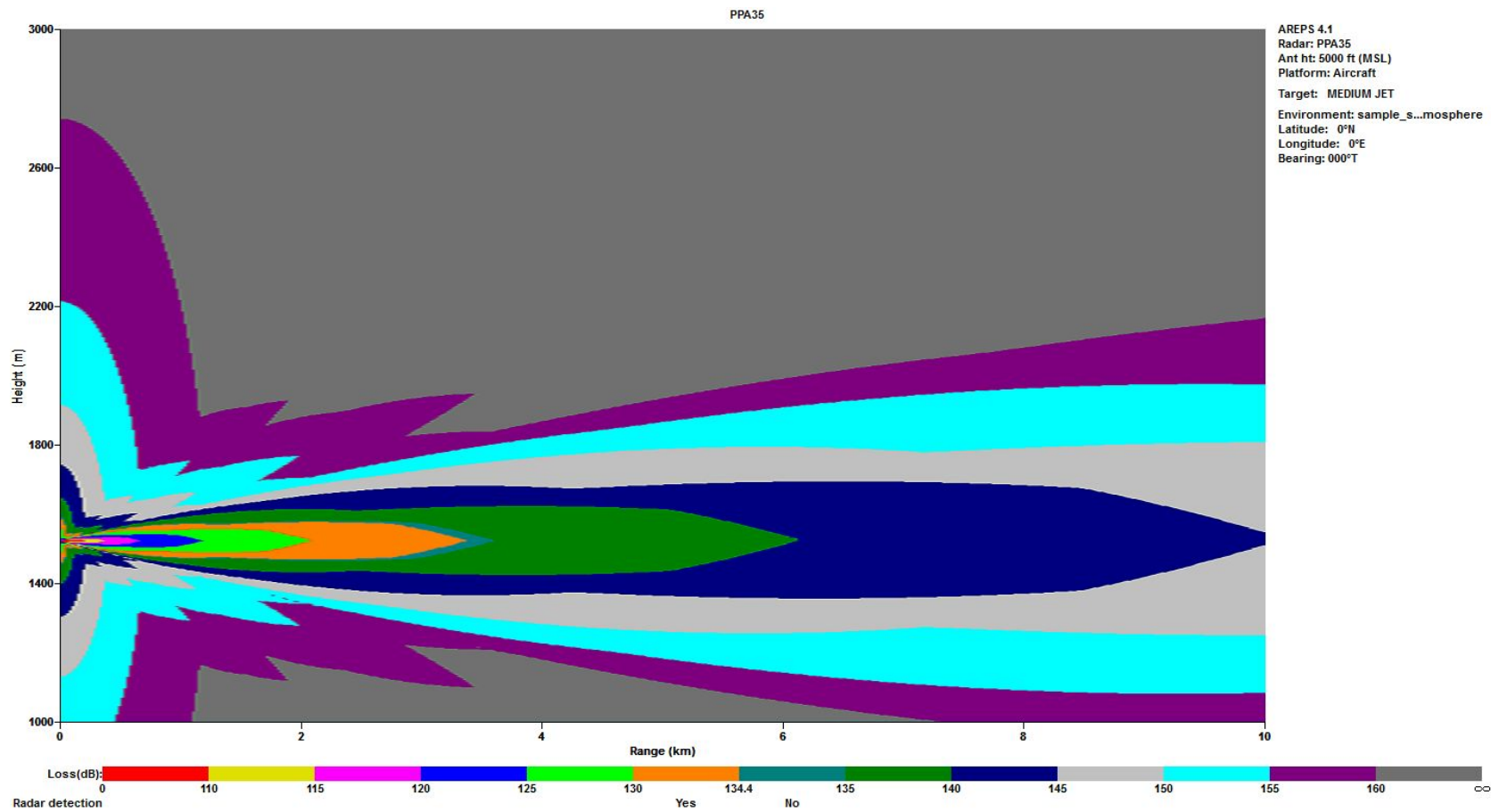
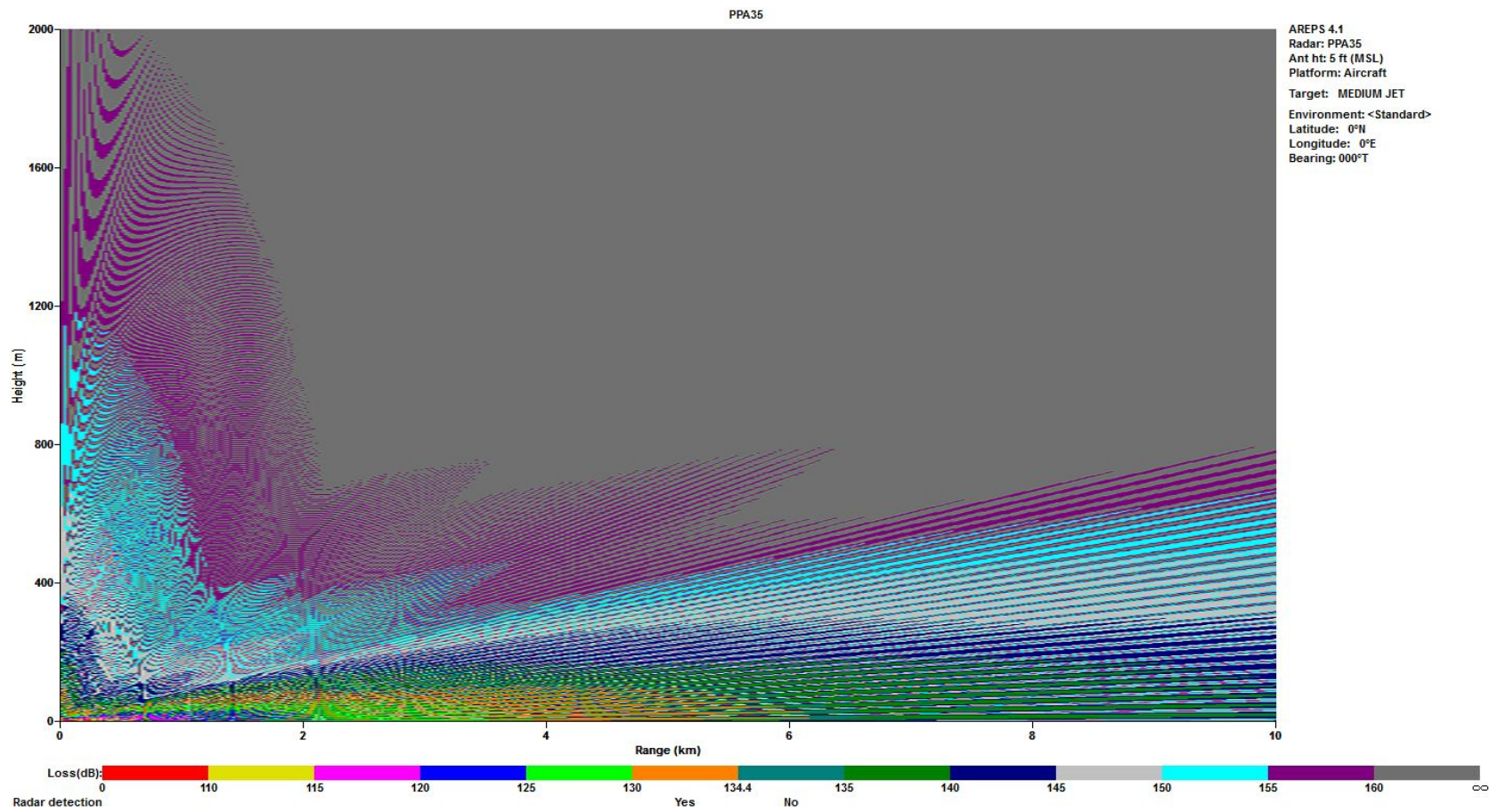Figure 58. 35 GHz AREPS Propagation Loss for Air-to-Surface Scenario in Standard Atmosphere at 5,000 Feet

Figure 59. 35 GHz AREPS Propagation Loss for Surface-to-Air Scenario in Standard Atmosphere

The surface-to-air scenario had interesting effects from the surface bounce and the low altitude of the transmitter. The low altitude also had strong attenuation effects on the signal. This example of multipath effects is a prime example of a capability that needs to be implemented into HELEEOS in order to provide a more robust capability to predict MMW radar propagation.

ExPERT Atmosphere.

Using the atmosphere generated by HELEEOS, the atmospheric profile for Panama City, Panama was able to be generated and imported into an AREPS environment. Figure 61 shows the corresponding HELEEOS script run that calculated the same scenario. Like the standard atmosphere, HELEEOS was able to calculate similar angles and patterns. However, again, the structure is lost with the coarse grid of points.

Figures 62 through 79 show the air-to-surface and surface-to-air AREPS plots and they are very similar to the standard atmosphere in terms of beam shape and propagation distance.
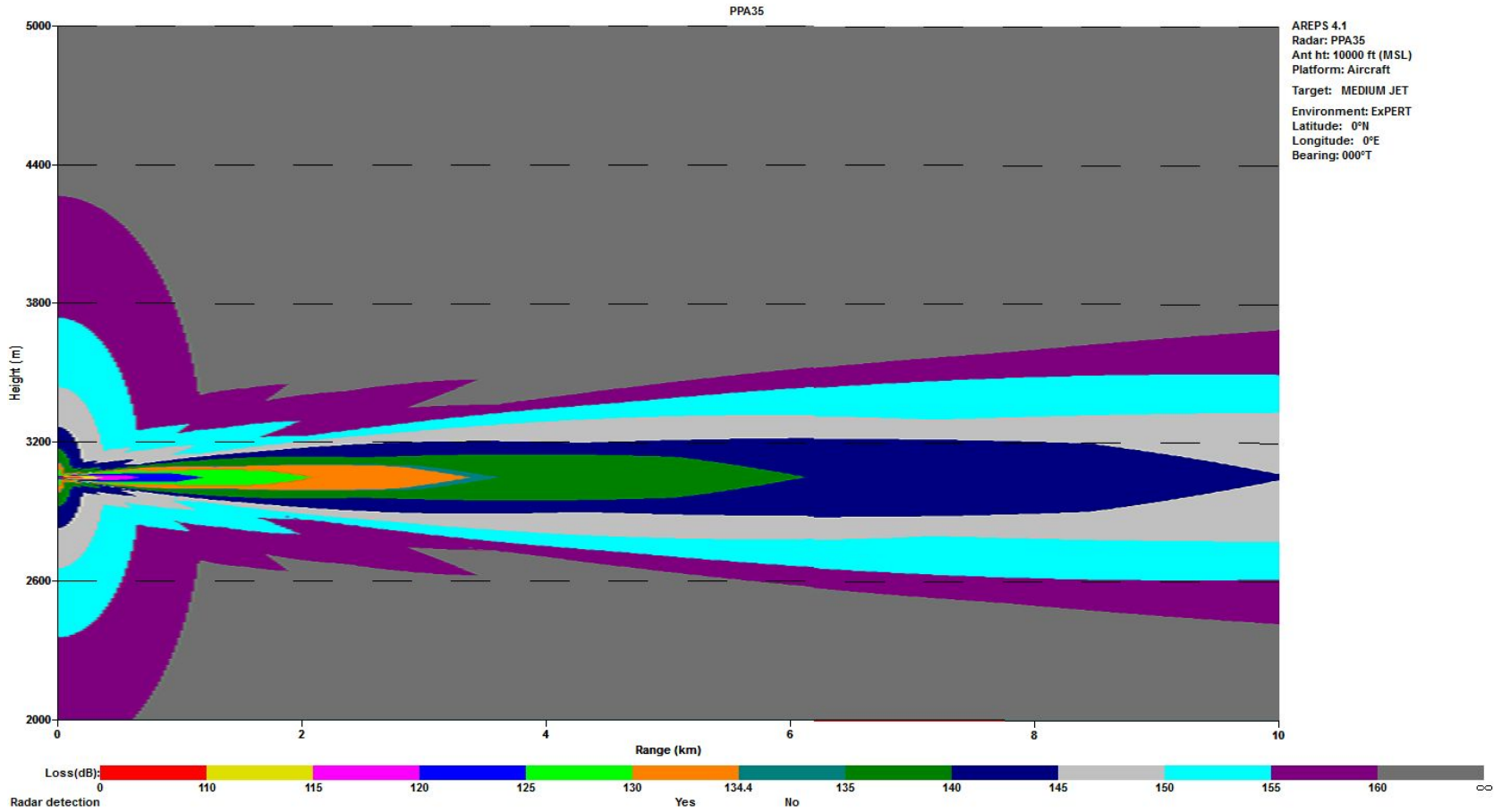
Figure 60. 35 GHz AREPS Propagation Loss for Air-to-Air Scenario in ExPERT Atmosphere at 3048 meters
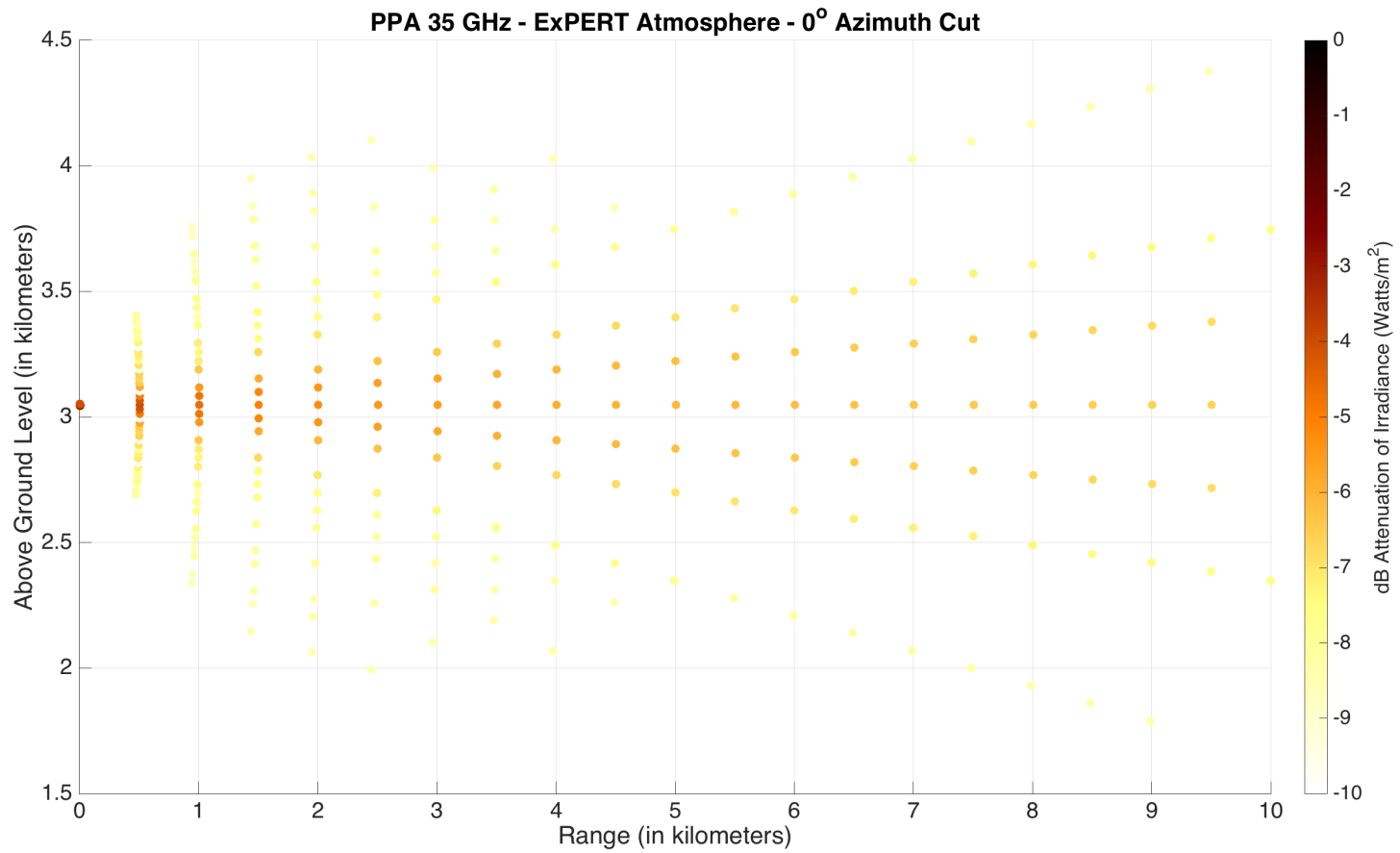
Figure 61. HELEEOS Side Cut for 35 GHz AREPS Propagation Factor for Surface-to-Air Scenario in ExPERT Atmosphere
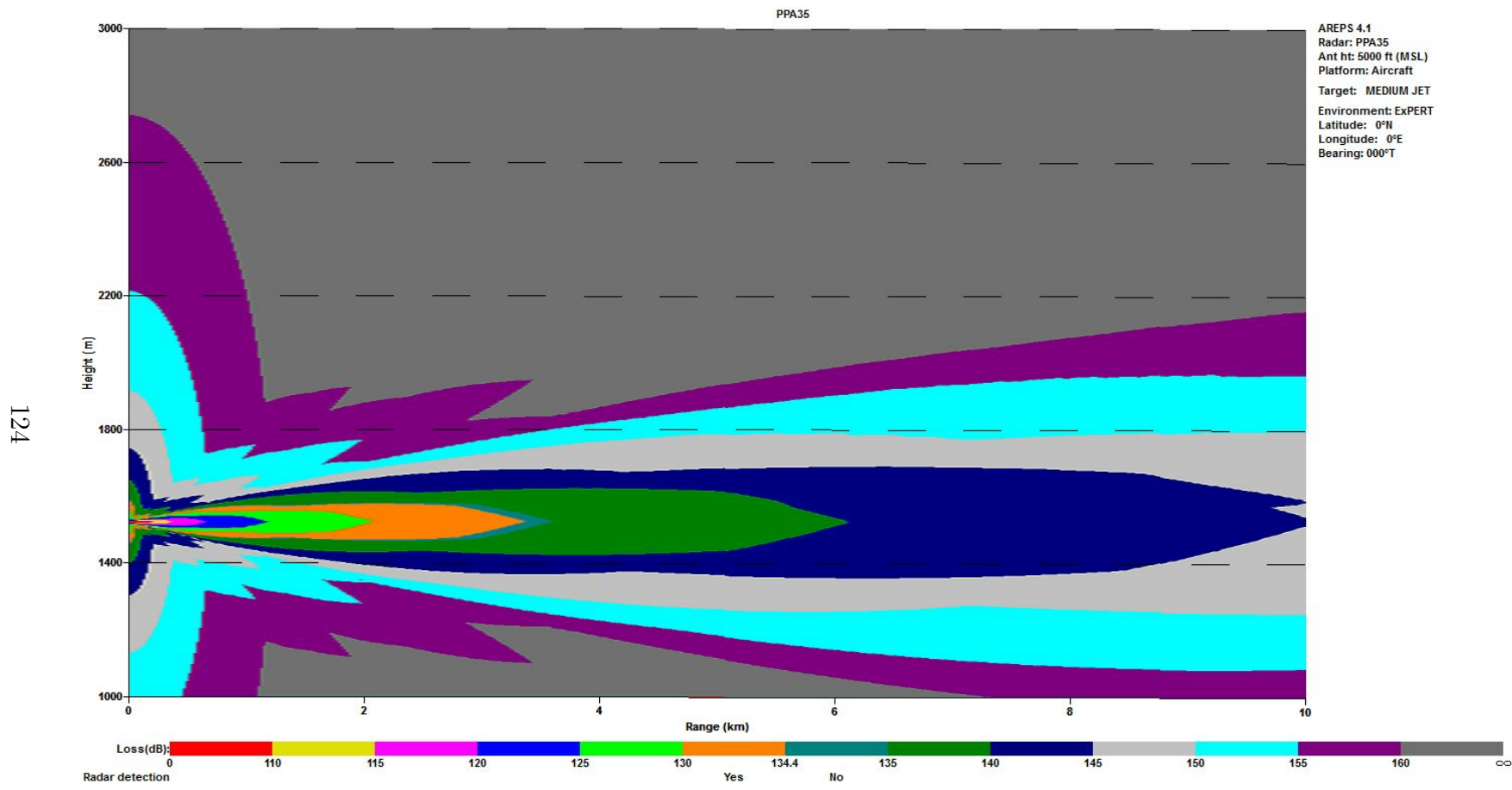
Figure 62. 35 GHz AREPS Propagation Loss for Air-to-Surface Scenario in ExPERT Atmosphere at 5,000 Feet
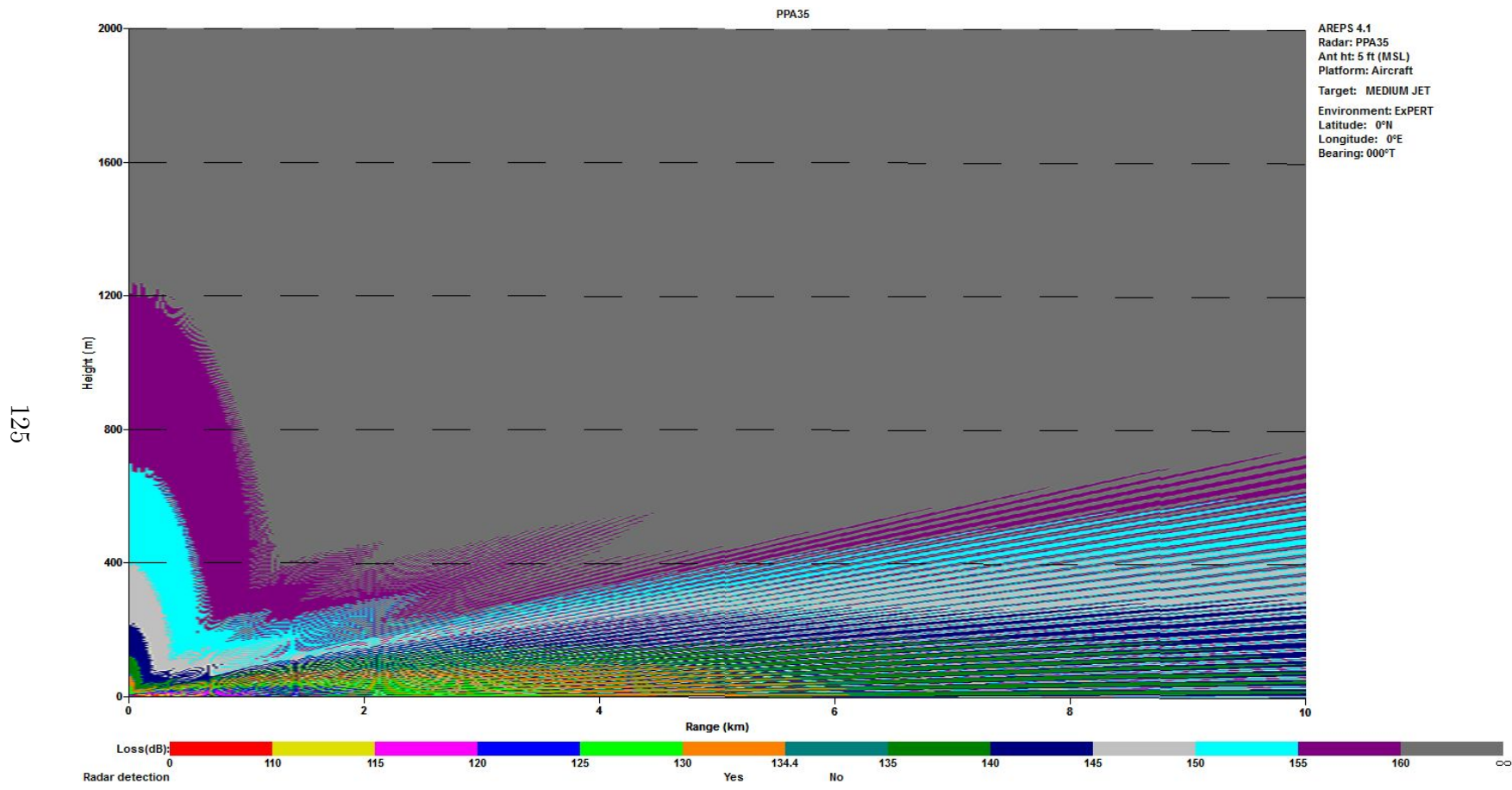
PPA35

AREPS 4.1
Radar: PPA35
Ant ht: 5 ft (MSL)
Platform: Aircraft

Target: MEDIUM JET

Environment: ExPERT
Latitude: 0°N
Longitude: 0°E
Bearing: 000°T

Figure 63. 35 GHz AREPS Propagation Loss for Surface-to-Air Scenario in ExPERT Atmosphere

NWP Atmosphere.

Because the NWP and ExPERT atmosphere were similar in values, the AREPS propagation is very similar to the ExPERT propagation paths. The HELEEOS side cut (in Figure 65) agrees with the AREPS pattern as well, however the AREPS pattern slightly more attenuated than it was in the standard atmosphere. The air-to-surface and surface-to-air scenarios are similar as well and shown in Figures 66 through 77.
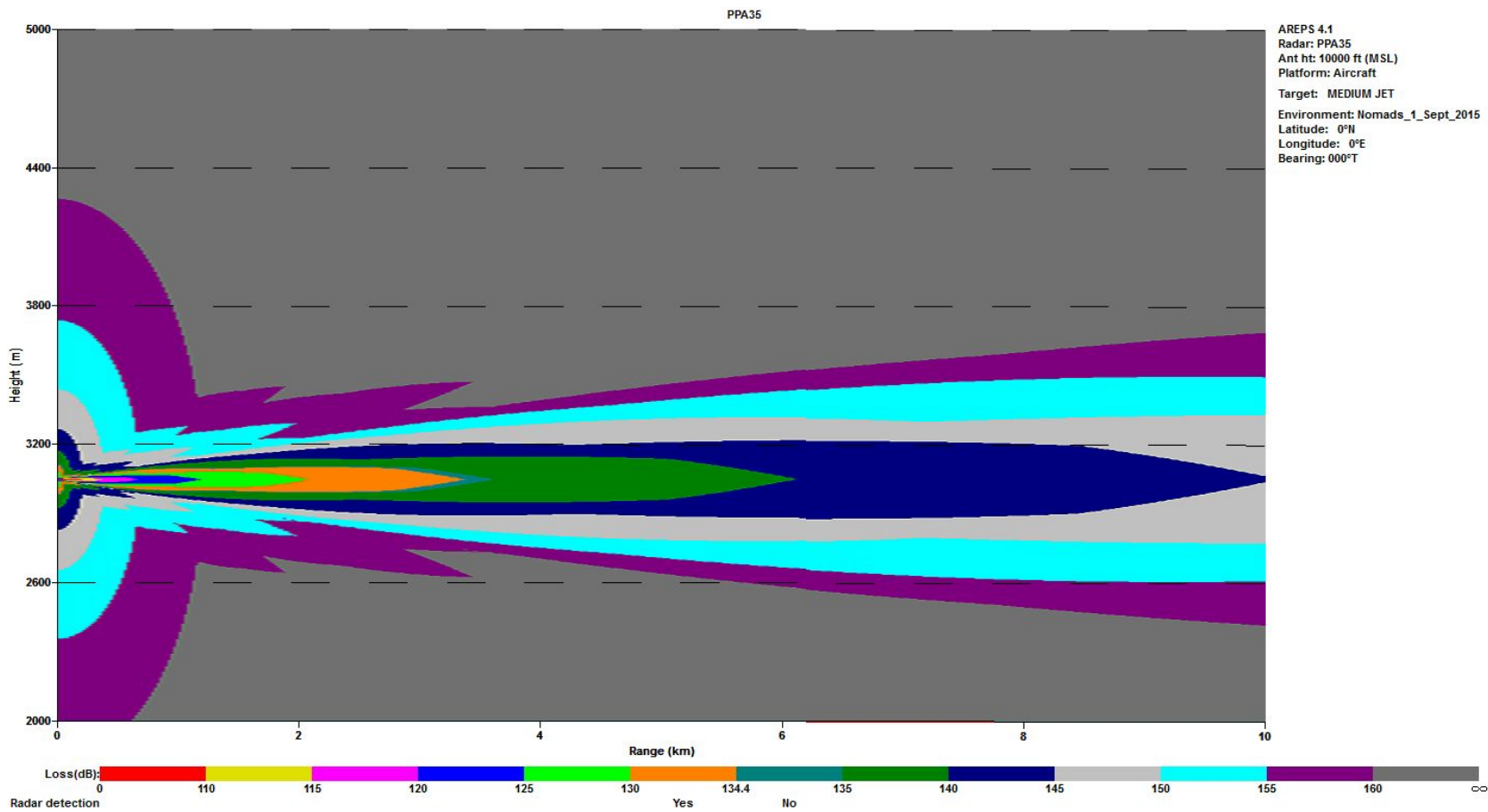
Figure 64. 35 GHz AREPS Propagation Loss for Air-to-Air Scenario in NOMADS Atmosphere at 3048 meters
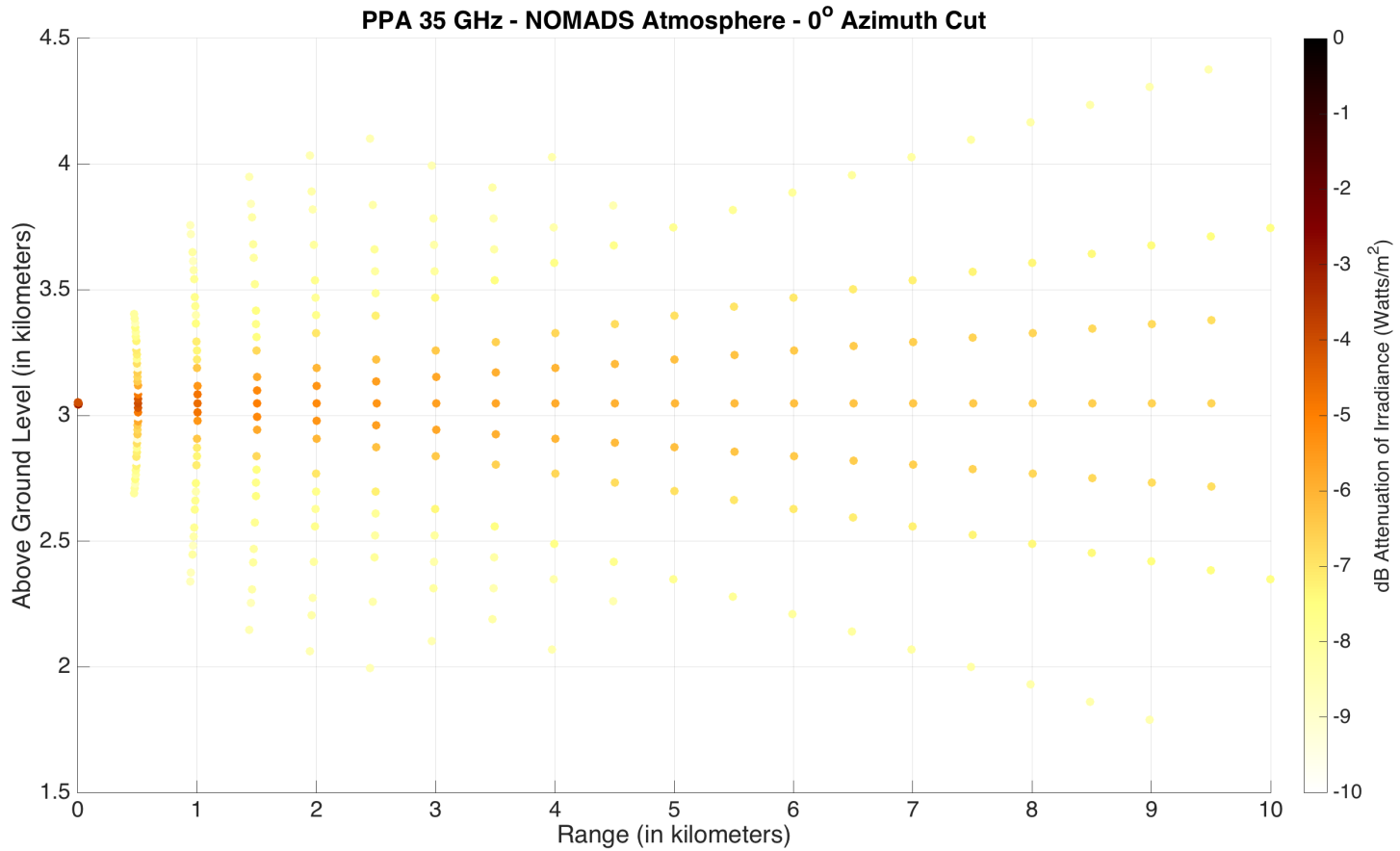
Figure 65. HELEEOS Side Cut for 35 GHz AREPS Propagation Factor for Air-to-Air Scenario in NOMADS Atmosphere
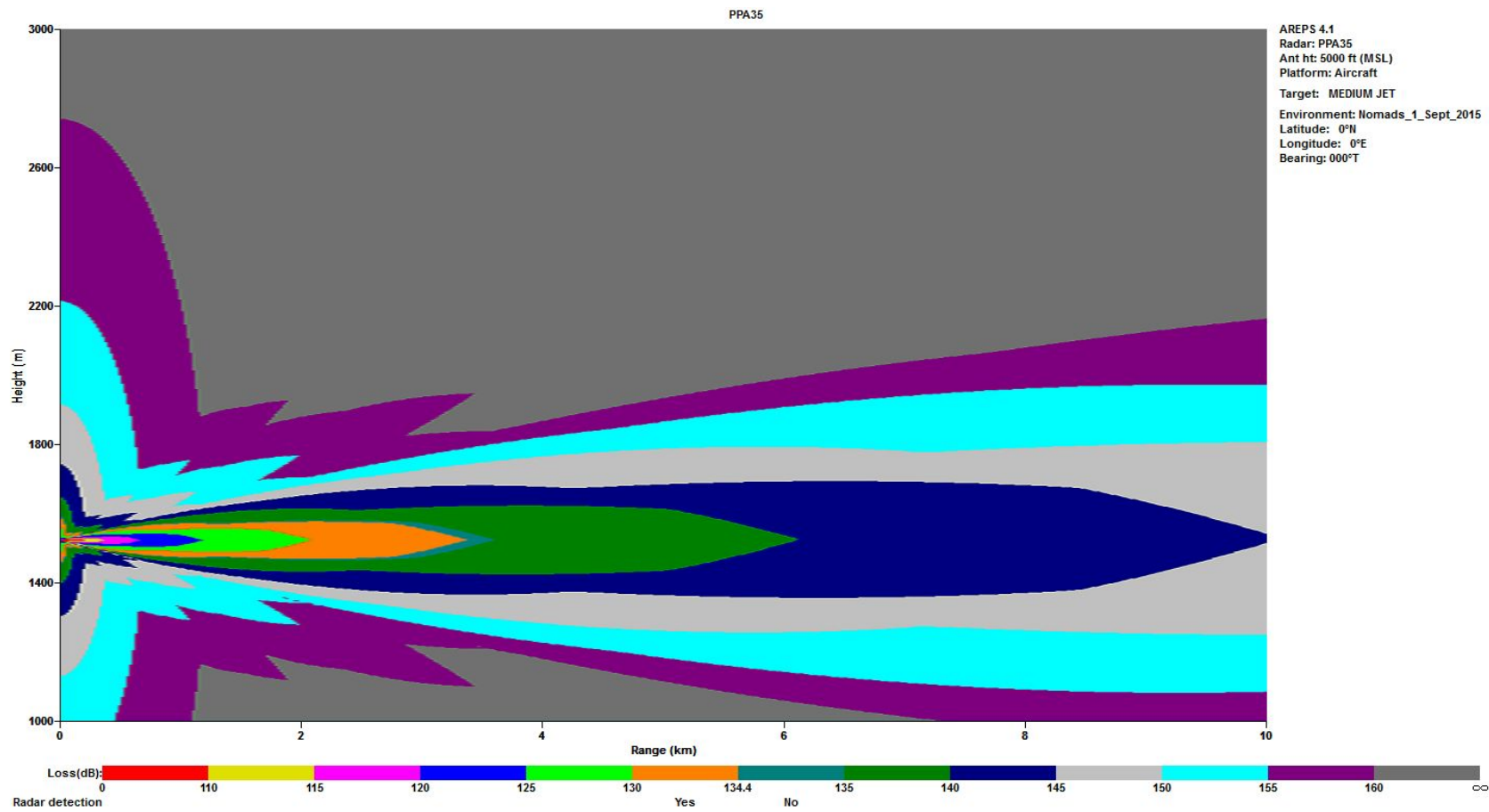
Figure 66. 35 GHz AREPS Propagation Loss for Air-to-Surface Scenario in NOMADS Atmosphere at 5,000 Feet
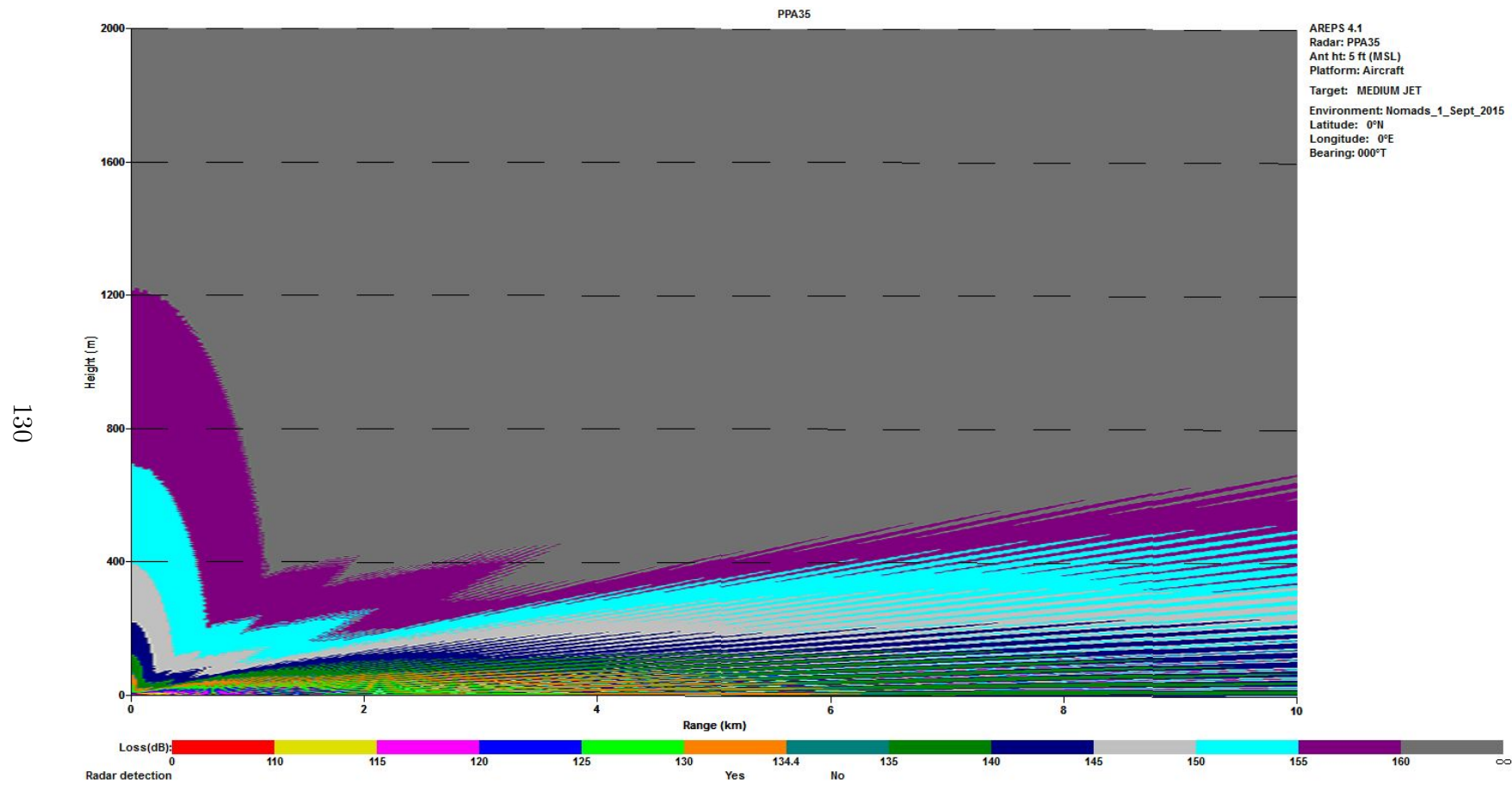
Figure 67. 35 GHz AREPS Propagation Loss for Surface-to-Air Scenario in ExPERT Atmosphere at

Comparison to IMOM.

As discussed in Section 2.2, IMOM does not have the capability to define a custom atmosphere with temperature, pressure, and humidity gradients like that in HELEEOS and even AREPS. The following analysis of the PPA and ULA radar antennas were done using the Signal Analyzer tool and choosing MMWave propagation engine with a humid atmosphere. All four patterns show similar results to HELEEOS and AREPS. IMOM's frequency dependence and resolution seems to be better than AREPS, however it is difficult to tell due to the differences in presenting the information. Both IMOM and HELEEOS appear to provide adequate pattern information of the radar. It is apparent a more careful evaluation comparing the capabilities of the various models is needed.
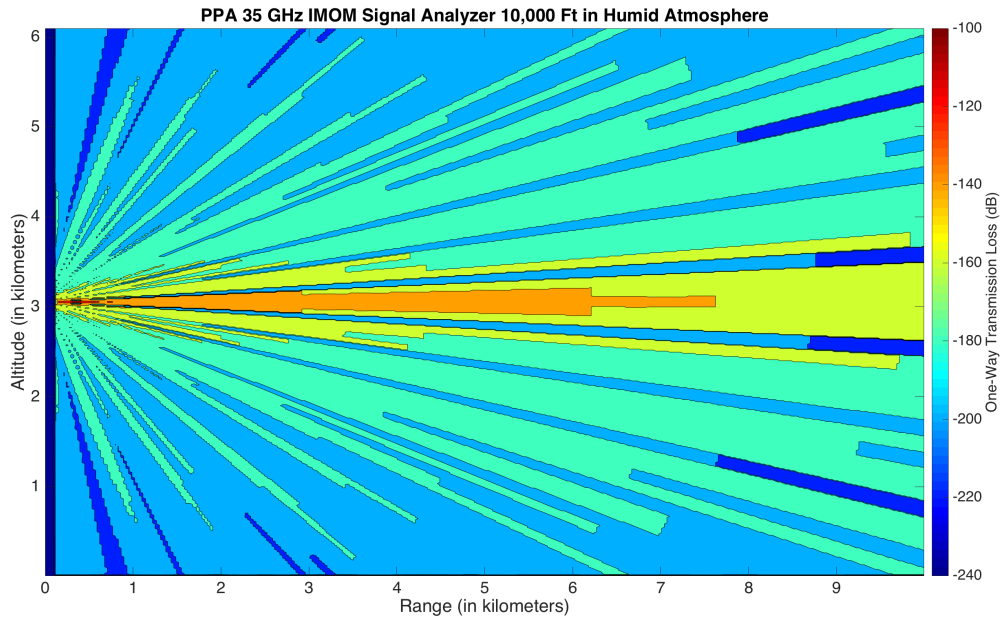

Figure 68. IMOM PPA 35 GHz Humid Atmosphere at 3048 meters
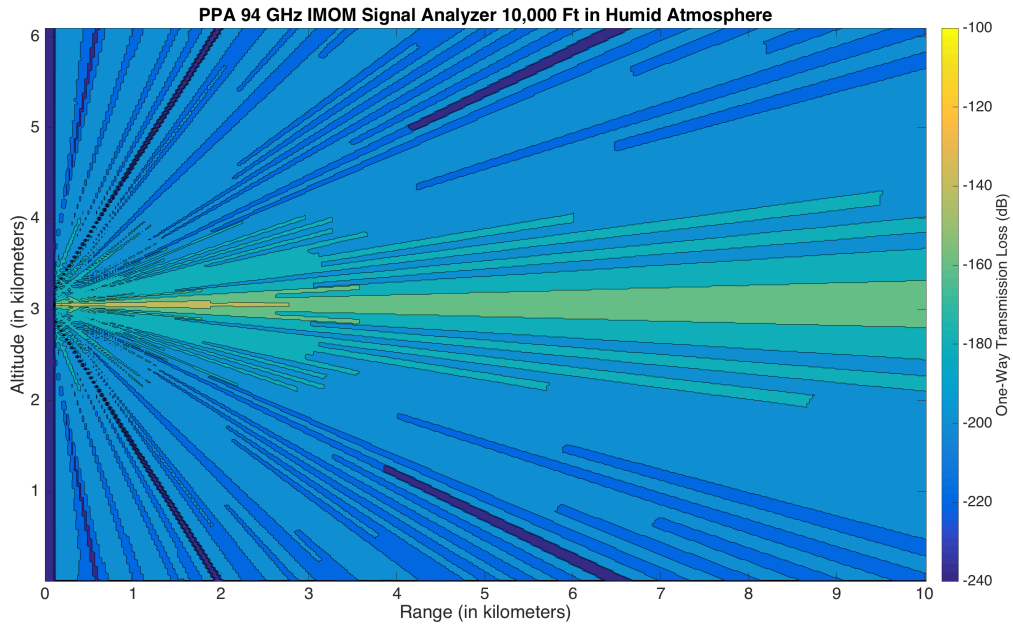
Figure 69. IMOM PPA 94 GHz Humid Atmosphere at 3048 meters
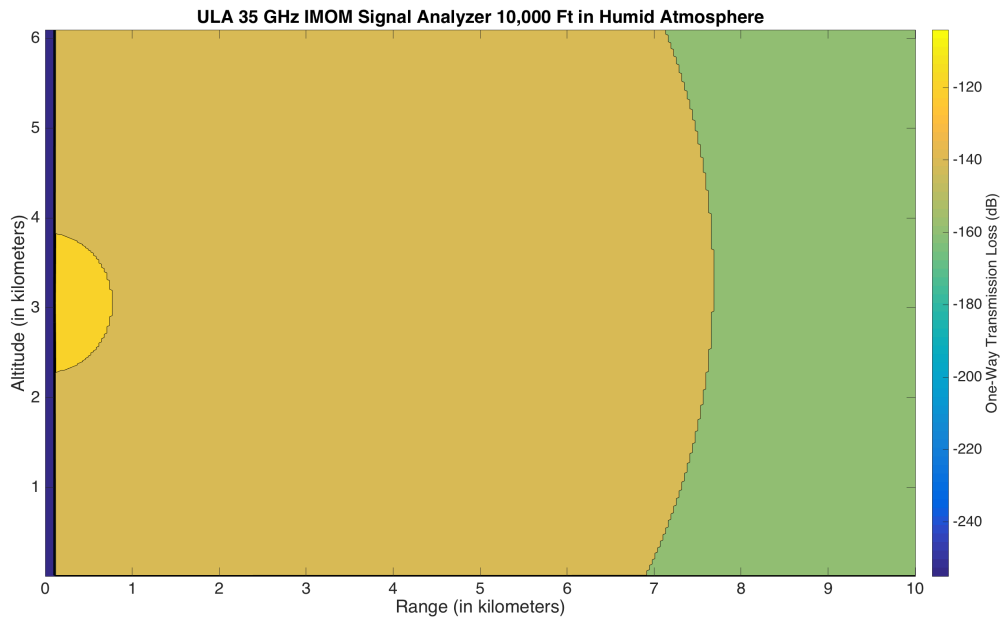
Figure 70. IMOM ULA 35 GHz Humid Atmosphere at 3048 meters
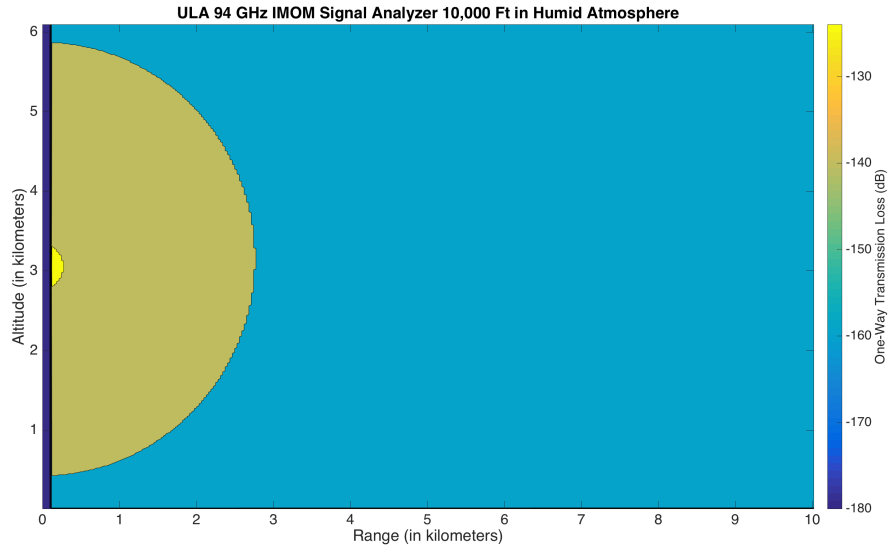
Figure 71. IMOM ULA 94 GHz Humid Atmosphere at 3048 meters

Qualitatively, utilizing AREPS and IMOM models demonstrate that HELEEOS is capable of reproducing a pattern with similar range values and provides strong support to the hypothesis that HELEEOS is able to be engineered into a tactical decision and research aid for MMW radar propagation with complex patterns. However, much research needs to be performed on correlating the alternative reference power used in this research with typical reference powers for radar research. This is the next logical step in enabling HELEEOS to perform as a MMW radar modeling tool.

V. Conclusion

5.1 Summary of Results and Significance

HELEEOS has shown the potential to provide a more comprehensive view of a radar pattern as it propagates through a real atmosphere in three dimensions than current radar models. This capability is crucial towards enhancing the understanding of atmospheric effects on MMW frequencies. HELEEOS shows the potential to demonstrate the fact that certain phenomena are more critical to consider. Areas with high humidity, clouds, and precipitation can heavily attenuate, if not completely block, a radar signal.

At higher altitudes (3048 meters and above), there are far fewer attenuation effects that require attention. However, when operating in lower atmosphere or in weather conditions, MMW radar experiences frequency dependent effects that must be accounted for. These effects drastically affect the usable range of the system as well as where energy from the sidelobes are directed to.

By ingesting ExPERT atmospheric climatology data, a radar pattern can be propagated in an atmosphere that is climatologically typical for a given location. If looking for real-time data, internet-based NWP meteorological data can be ingested, which provides numerical weather model output to build the atmosphere and provide attenuation data via LEEDR.

These capabilities are useful for military and civil applications, as weather conditions are never standard and tactical implications of weather should always be considered. As radar technology continues to mature in the MMW regime, thorough understanding of the first principles of radiative transfer and their effects on propagation become increasingly important to understanding limitations and capabilities of these systems.

5.2 Future Work

While this thesis has provided a successful proof of concept for enabling radar patterns to be propagated with HELEEOS and LEEDR software packages, there is still much to be done to ensure atmospheric effects are captured as completely and accurately as possible. It would be ideal to have future work based on actual radar propagation experimental data that enables validation of the LEEDR and HELEEOS code in the MMW regime. Determining how the ShARE toolbox is focusing the beam and how realistic a focused beam is to MMW radar propagation will further enhance understanding of HELEEOS' effectiveness in predicting propagation patterns.

Despite the coding efficiencies added in Section 3.3, the amount of time to compute a full radar pattern was much greater than the time that would be available for conducting large batch runs for parameterization studies and operational studies. Naturally, as computer processing speed grows in accordance with Moore's Law, computation time will decrease. However, in the near term, there is much optimization to be done with parallel computing and other mechanisms to decrease computation time from hours to minutes or even seconds. A different means of parallelizing the code and running the scripts on a high performance computer will allow for much quicker analysis that could potentially aid in creating a real-time decision aid.

More evaluation needs to be done in the realms of turbulence effects on MMW beams. Furthermore, analysis on existing field studies can be expanded upon to determine if the scaling laws HELEEOS use is applicable to MMW frequencies. HELEEOS is able to calculate extinction due to turbulent effects, but it remains to be known how accurate the specific turbulence profiles and C_n^2 values, and derived radiative effects, are for the MMW regimes.

Furthermore, much evaluation needs to be done to ensure that refractive bending is more easily and accurately implemented in code. A metric could be developed that

will relate how much a beam is bent over a path length. This metric will characterize how much correction would need to be applied in order to ensure a radar is pointing where it needs to point, thus increasing targeting accuracy. Refraction research will also enable engineers to understand the effects of ducting in the MMW regime and more thoroughly understand the possibilities of ducting and trapping due to the fact that MMW may respond differently than traditional radar wavelengths.

Another area of interest concerns multiple scattering. Once HELEEOS has the capability to implement multiple scattering, radar in the MMW regime may have some unique characteristics that are captured. For instance, if a rain deck heavily scatters energy in a certain direction, it is possible that other areas of the radar pattern may be enhanced by the scattered energy. However, this will require much additional research and the code to calculate these effects will be much more computationally intensive than this research.

It is also important to note that this research did not account for multipath radar. When a propagation path intersected the surface, the code stopped calculating. Future research could evaluate the dielectric constant at the surface and determine the direction and strength of any bounced signal and examine if LEEDR and HELEEOS give realistic results for multipath scenarios.

Multipath effects also closely relate to the RCS calculation aspect of MMW radar. Of unique interest to the Department of Defense is the effect of MMW radar on existing RCS data. It is possible that HELEEOS could be adapted to predict how MMW radar will scatter off smaller portions of a target's surface. If it is possible to determine the amount of energy that will be reflected normal to path of incidence, the capability to calculate a target's monostatic RCS at a specific frequency can be proven.

This research only evaluated two MMW arrays and frequencies. Evaluating dif-

ferent transmitters such as a Horn Antenna and Luneburg Lens will continue to demonstrate the utility of HELEEOS in radar propagation prediction. Furthermore, experimental validation will also show which frequencies HELEEOS provides realistic results.

It is important to note these radar patterns were highly idealized and there are very specific patterns and powers that can be calculated using HELEEOS. However,this research had little or no experimental data for comparison that could be used to exactly correlate to atmospheric conditions observed and frequency and patterns of radars used. The next step of research should be to gather actual data from a transmitter receiver setup, import the radar pattern to HELEEOS using methods derived here, and use the HELEEOS output to correlate dB attenuation values to what was actually received. With enough data points, it would be possible to ensure HELEEOS has the corrections necessary to provide actual attenuation information for a three dimensional pattern. The comparisons against AREPS and IMOM were useful for determining similarities in patterns; however, even AREPS and IMOM may not be accurate for strength values in the MMW regime.

Long term, a merging of capabilities between existing radar propagation models that excel in radar frequency and waveform calculations and LEEDR/HELEEOS which excel in three dimensional atmospheric effects, could provide a very powerful program that would enable MMW radar propagation to be done very accurately and for much less computational cost. Exploiting these research efforts could perhaps lead to a very capable scenario and engagement package able to simulate the full MMW pattern effects throughout a three dimensional atmosphere.

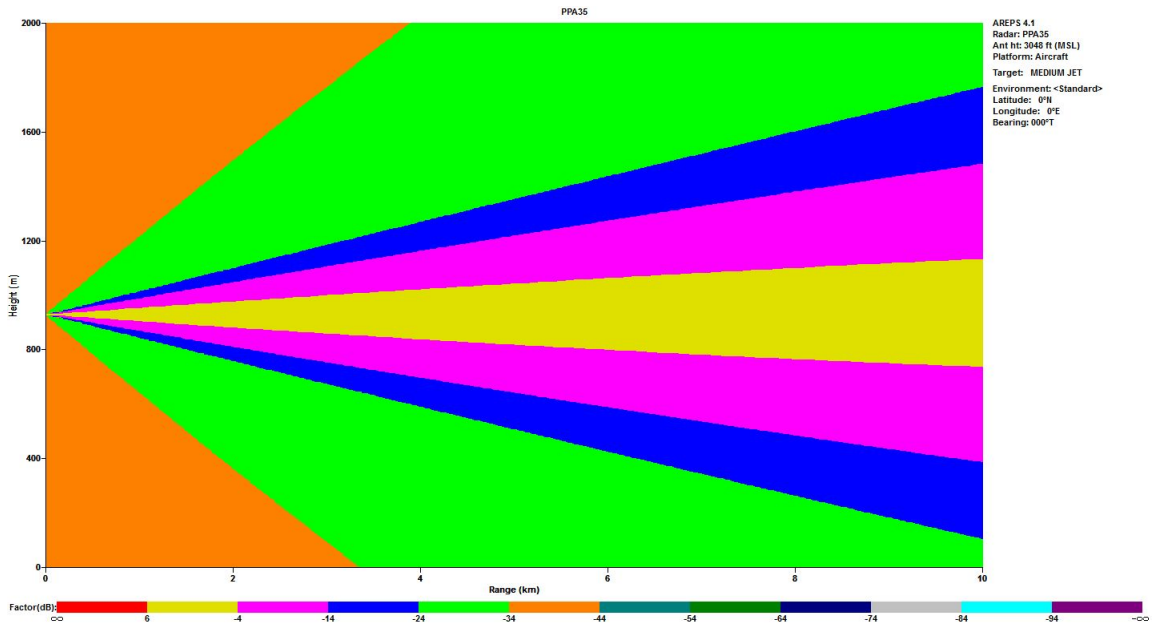# Appendix A.   AREPS Propagation Factor Figures

Figure 72. 35 GHz AREPS Propagation Factor for Air-to-Air Scenario in Standard Atmosphere at 3048 meters
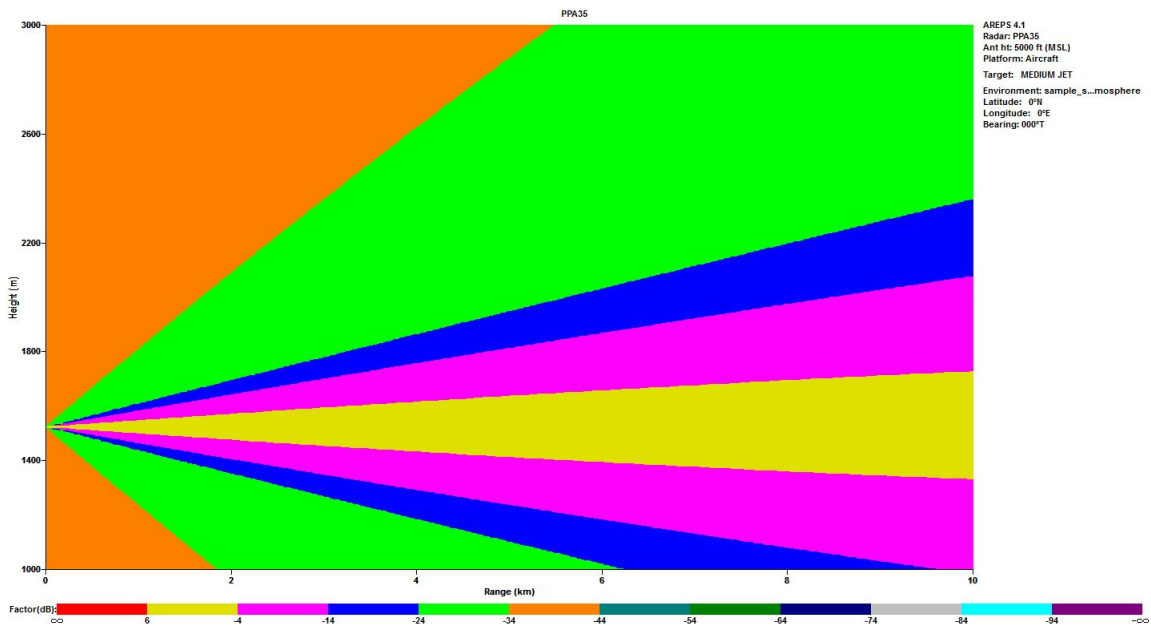
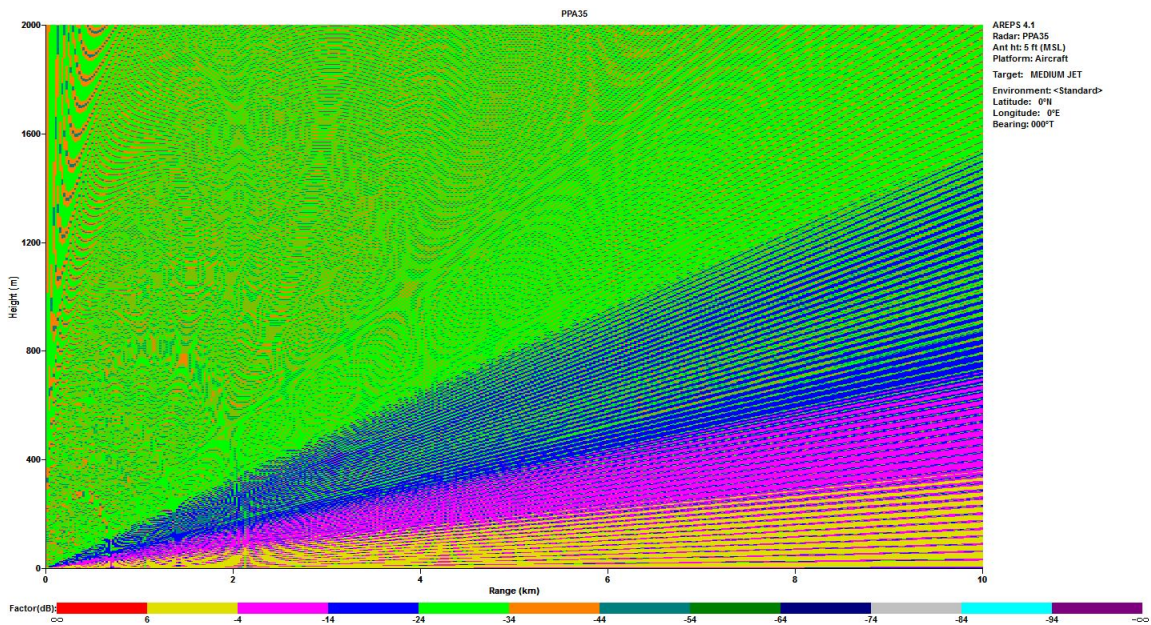Figure 73. 35 GHz AREPS Propagation Factor for Air-to-Surface Scenario in Standard Atmosphere at 5,000 Feet

Figure 74. 35 GHz AREPS Propagation Factor for Surface-to-Air Scenario in Standard Atmosphere
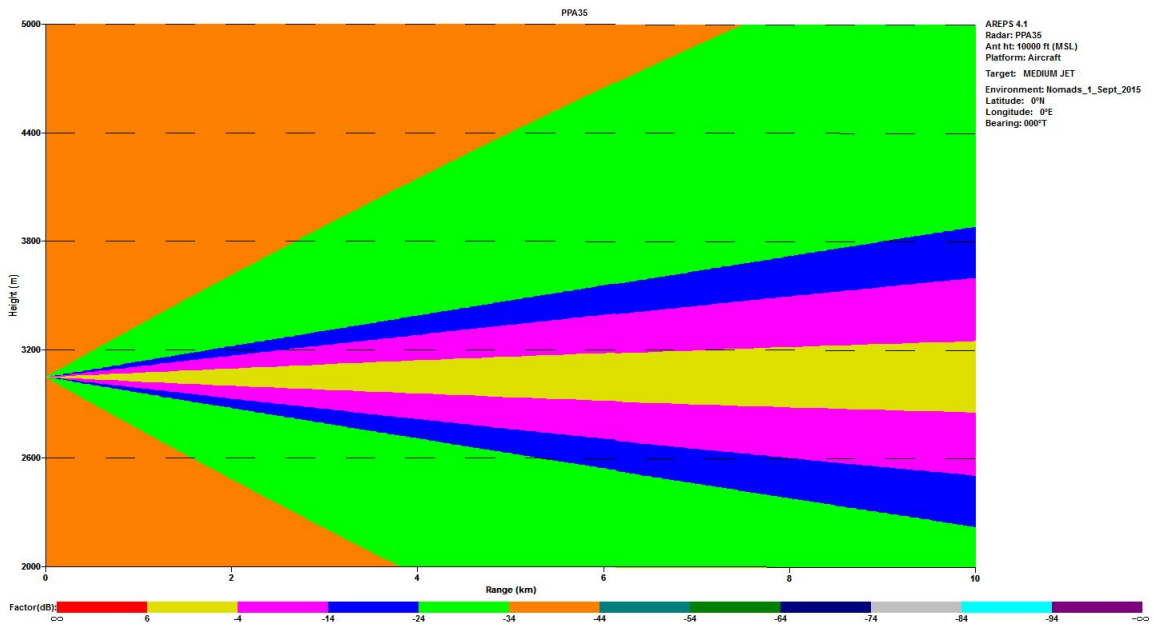
139

Figure 75. 35 GHz AREPS Propagation Factor for Air-to-Air Scenario in NOMADS Atmosphere at 3048 meters
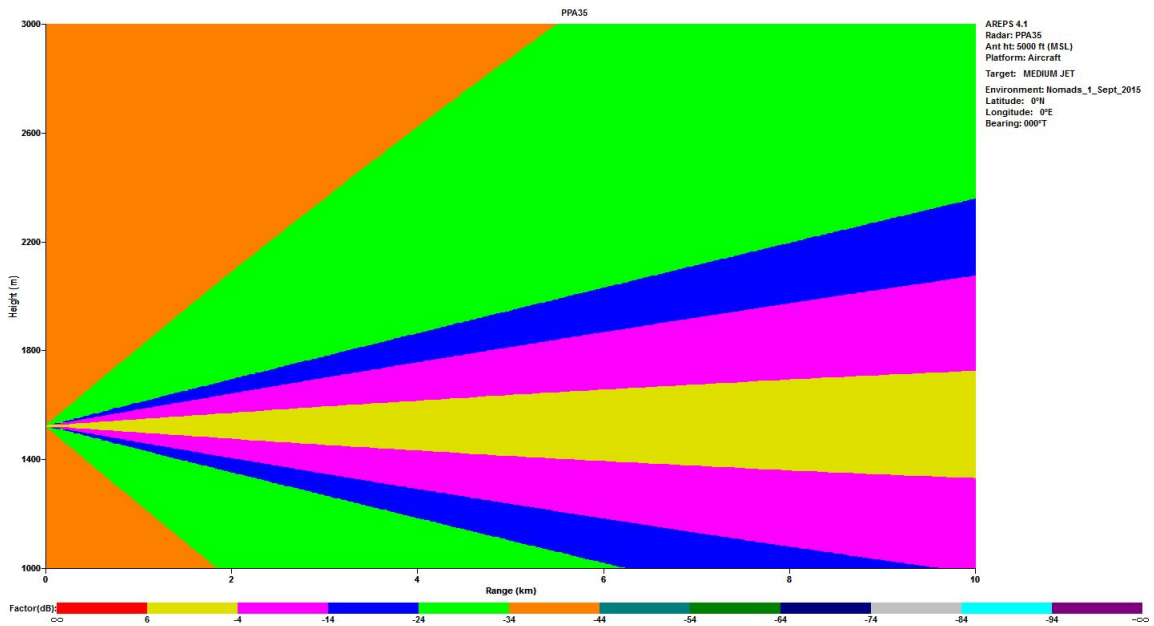

Figure 76. 35 GHz AREPS Propagation Factor for Air-to-Surface Scenario in NO-MADS Atmosphere at 5,000 Feet

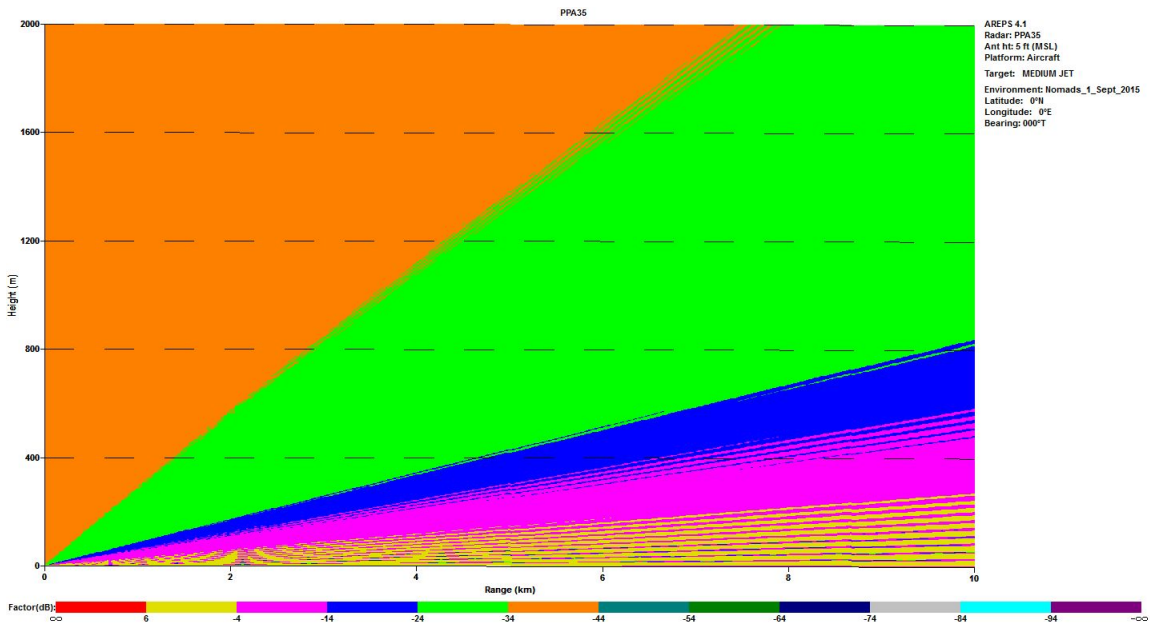Figure 77. 35 GHz AREPS Propagation Factor for Surface-to-Air Scenario in NO-MADS Atmosphere
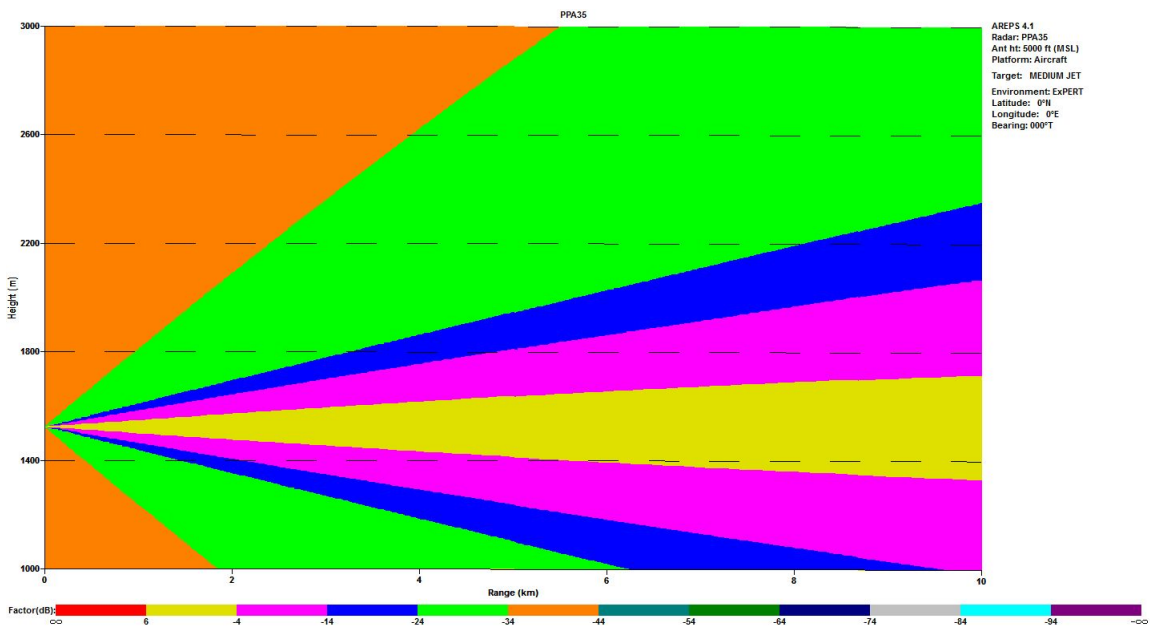

Figure 78. 35 GHz AREPS Propagation Factor for Air-to-Surface Scenario in ExPERT Atmosphere at 5,000 Feet
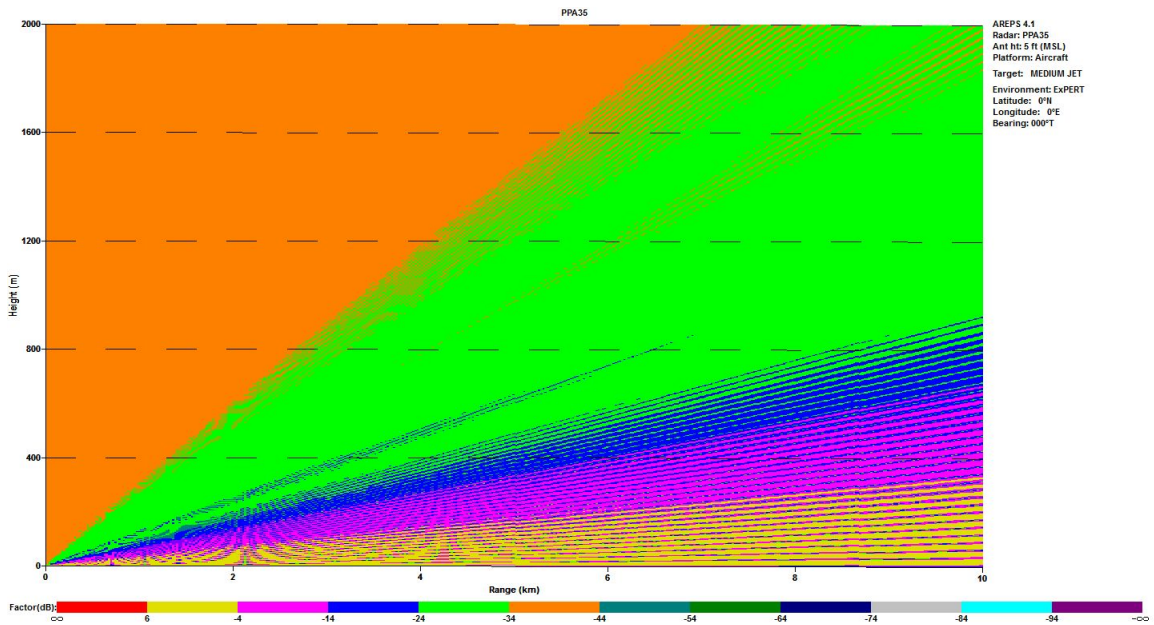
Figure 79. 35 GHz AREPS Propagation Factor for Surface-to-Air Scenario in Ex-PERT Atmosphere
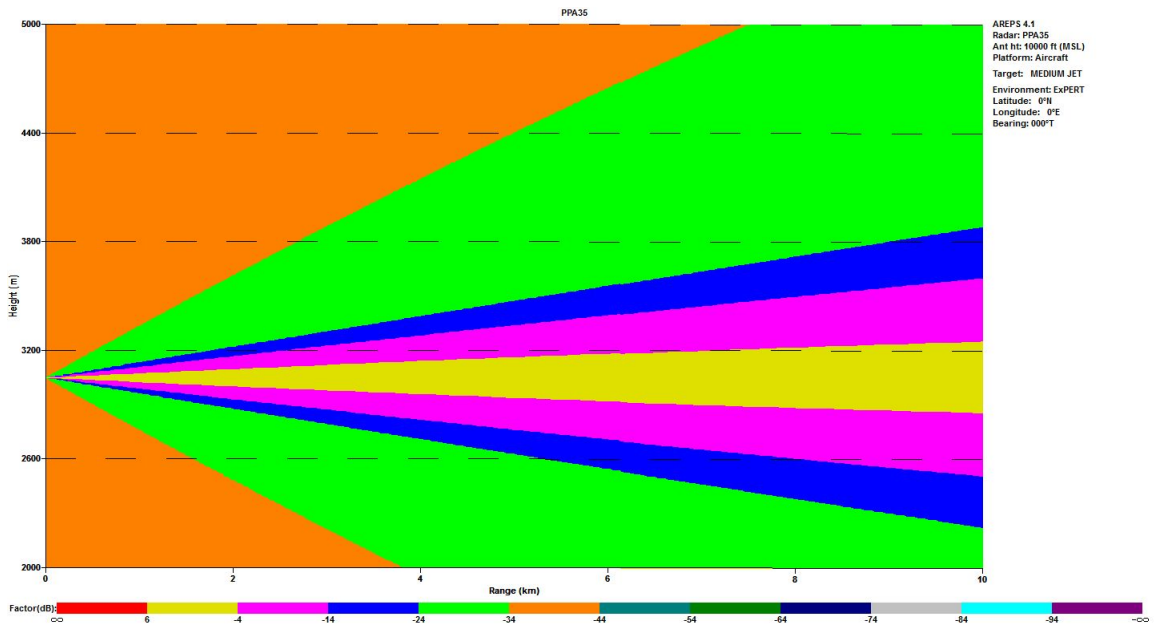
Figure 80. 35 GHz AREPS Propagation Loss for Air-to-Air Scenario in ExPERT Atmosphere at 3048 meters

Appendix B. How To Use MATLAB Sensor Array Analyzer to Generate Radar Patterns

2.1   Step 1: Open Sensor Array Analyzer in MATLAB R2015a or Later

Note that this is an extra toolbox that must be purchased on your respective license and then installed.
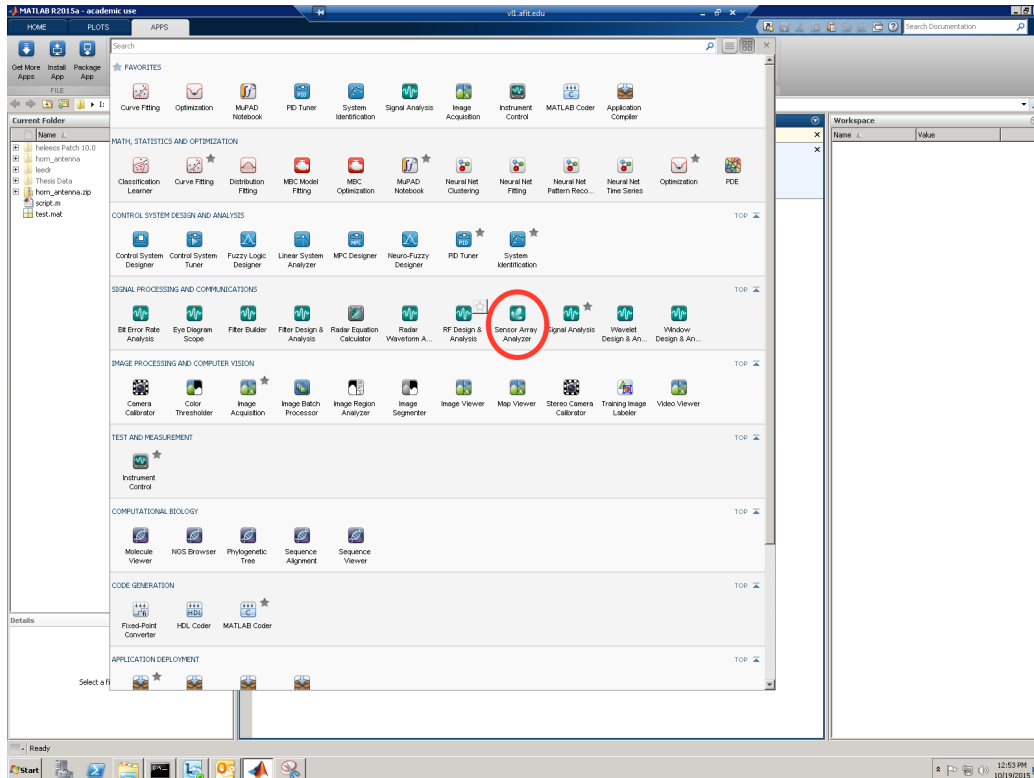
Figure 81. Sensor Array Analyzer Toolbox

2.2   Step 2: Define Radar Antenna Parameters

The toolbox supports various styles of antennas. This research used circular planar and uniform linear arrays. Various parameters are self explanatory and easily customizable. The figure on the right side of the toolbox allows for a preview of what the array looks like once hitting the "Apply" button.
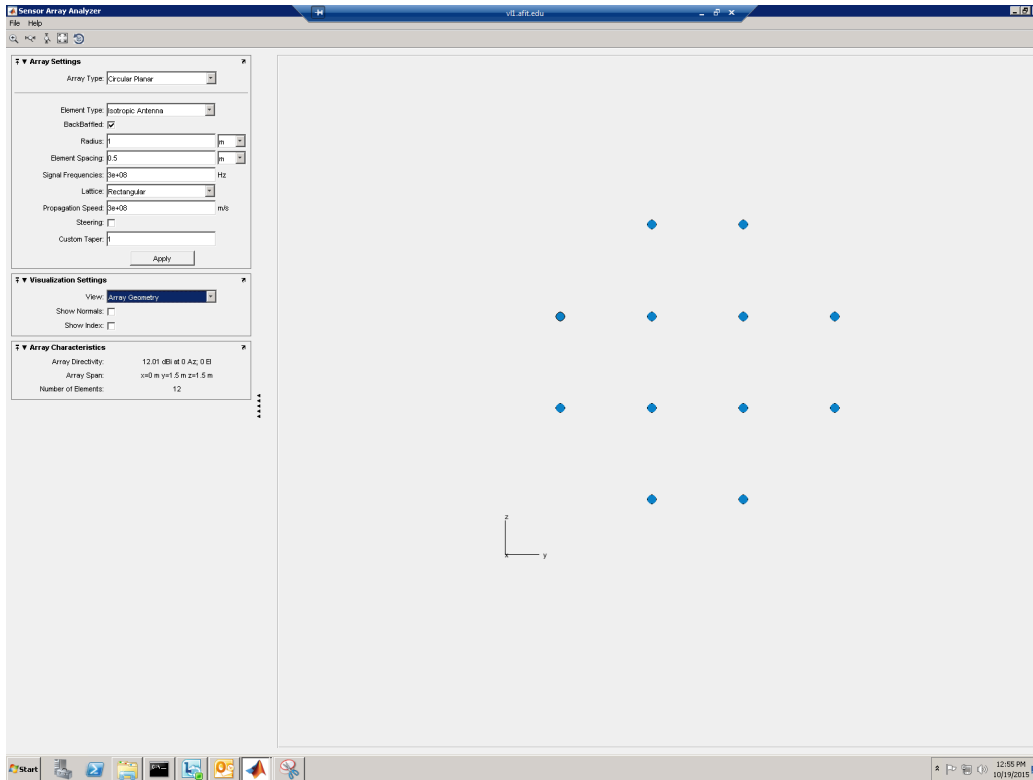
Figure 82. Sensor Array Analyzer: Defining Parameters

2.3   Step 3: Select Various Displays of Radar Pattern

By selecting different options from the drop down menu in the "Visualizations" section, various plots can be generated to give a preview of what the radar pattern will look like.
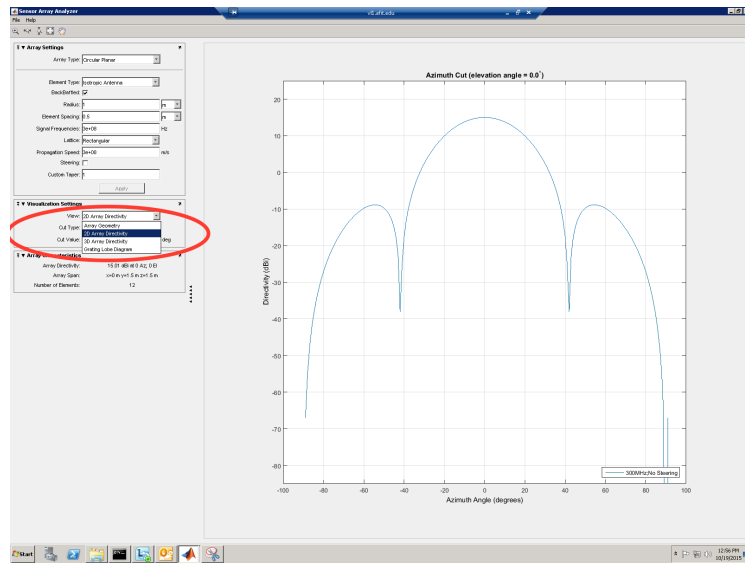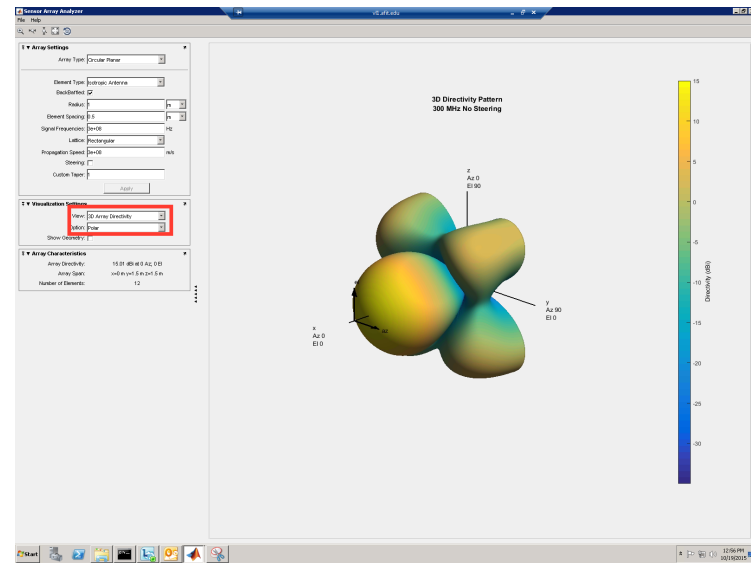
(a) 2-D Representation of Radar Pattern Preview (b) 2-D Representation of Radar Pattern Preview

Figure 83. Sensor Array Analyzer: Various Pattern Representations

Once satisfied with the antenna and pattern, code can be generated (File > Generate MATLAB Code) to allow the user to create exportable and savable figure files (.fig or .png) (see Section 2.4) or generate tabulated data that includes the decibel directivity of the pattern (see Section 2.5).

2.4 Step 4: Use Generated Code to Produce Exportable Figures

Below is what the output of code may look like (may vary depending on if you selected 2-D or 3-D visualization)
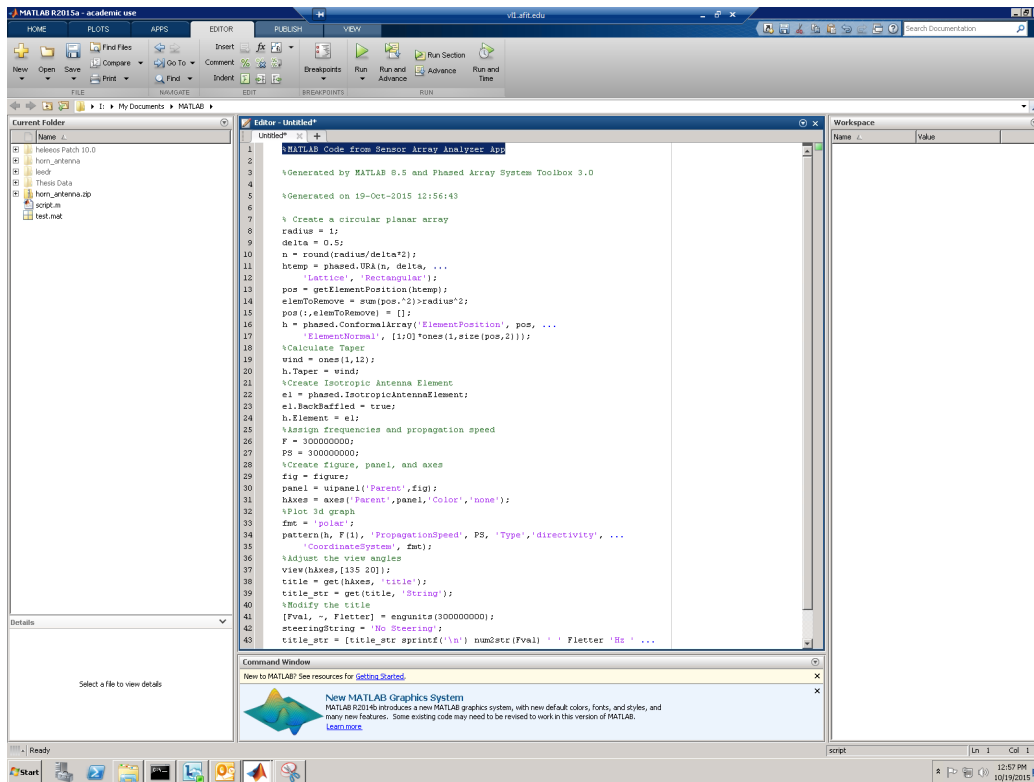
Figure 84. Sensor Array Analyzer: MATLAB Generated Code

Ensure you change "directivity" to "powerdB" in the pattern command. This ensures that output data is normalized such that 0 dB is the maximum power of the antenna.

146
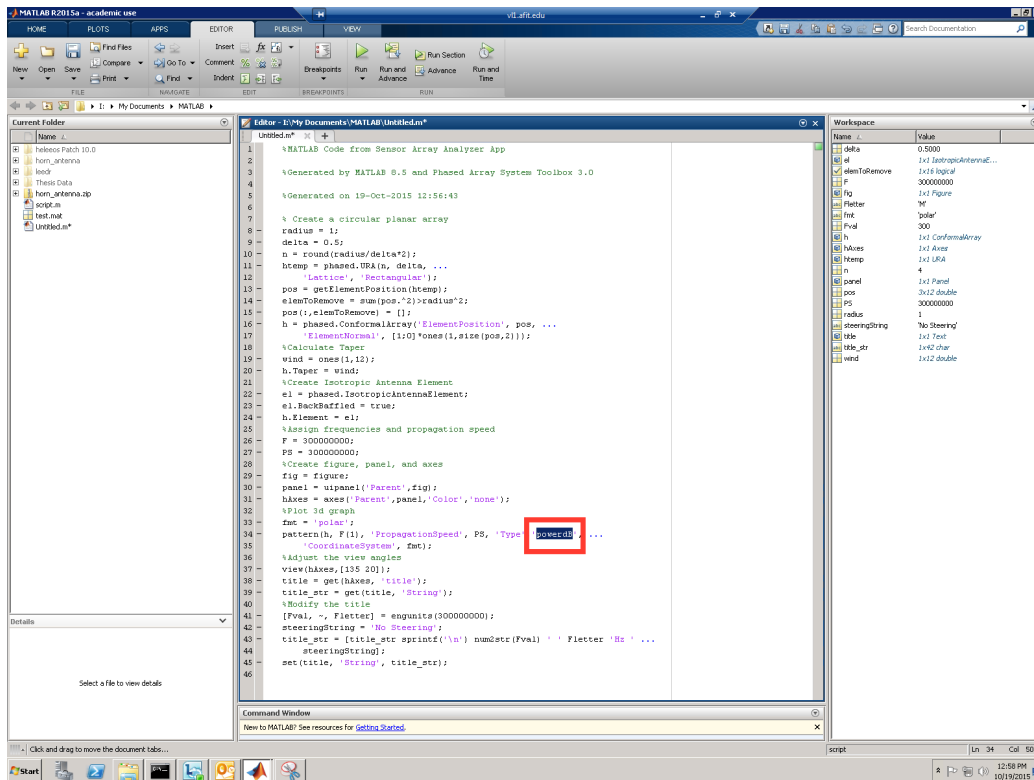
Figure 85. Generated Code: Ensure "directivity" is Changed to "powerdB" to Normalize Power Data

Once you run the script, a figure is generated that can be manipulated and saved as MATLAB's .fig or a portable network graphics (.png) file.
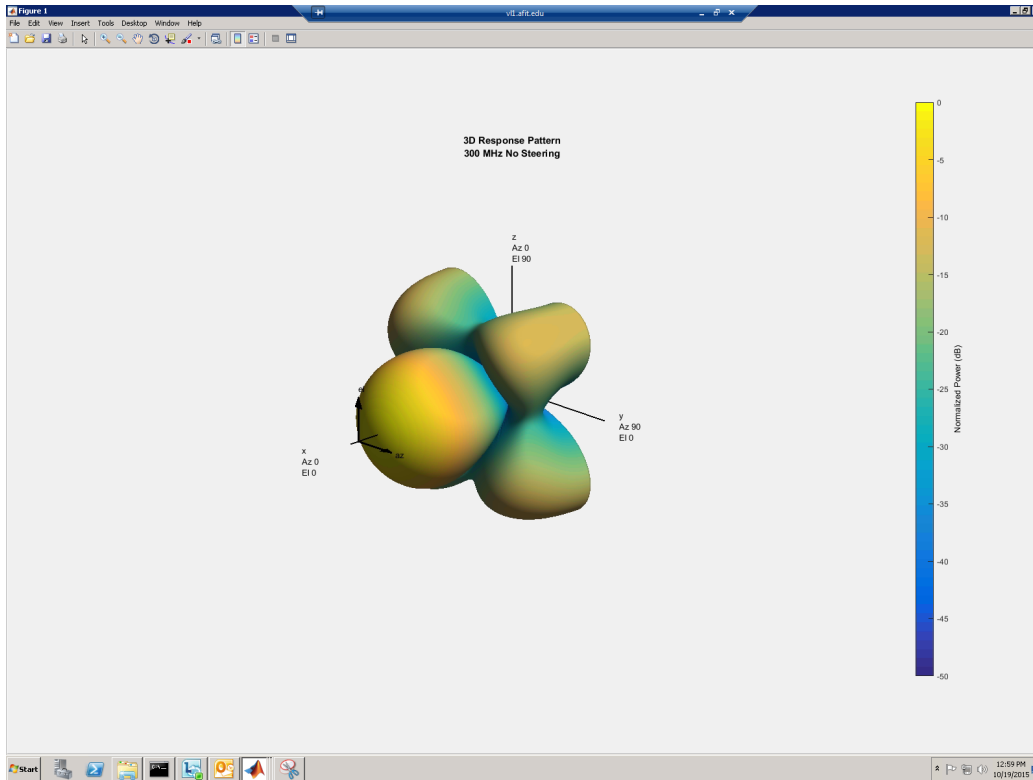
Figure 86. Exportable Radar Pattern Image

2.5   Use Generated Code to Produce Decibel Data

In the generated code, add the following output to the pattern function line:

```
[PAT, AZ_ANG, EL_ANG] = pattern(...)
```
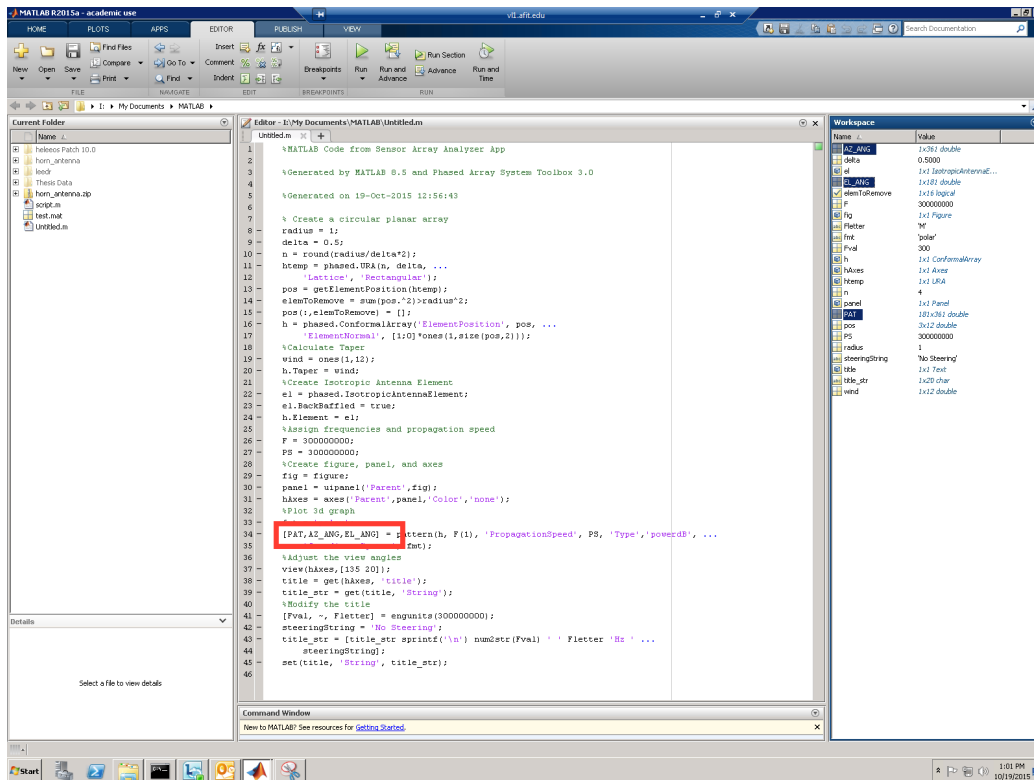
Figure 87. Exporting Power Data for Radar Pattern

After running the script, the PAT, AZ_ANG, and EL_ANG variable will be present in the workspace. Run the following commands using the command window to convert the PAT data to Watts in order to ingest the information into your HELEEOS script:

```
% This corrects for antenna efficiency, default is ant_eff = 1
P_o = ant_PWR * ant_eff;


% This changes the dB power to actual Watts for each angle
PAT_W = 10.^(PAT ./ 10) * P_o;


% Save all the variables to a .MAT file
% (replace filename with preferred name)
save('filename','PAT_W','AZ_ANG','EL_ANG');
```

Appendix C. MATLAB Script for Running Pattern Through Various Engagements

```matlab
function cook_RunHELEEOS()
clear all; close all;
% Version 2.0
% Fixed issue where wavelength was not being assigned before runAtmosphere.
% Improved radar data retrieval


% clear all; close all;
format long



%% Load all the various engagement scenarios
load('engagements_final.mat');


% Input the folder for all the radar files
radar_folder = 'W:\Documents\Cook\cook_RunHELEEOS\radarData';


% Define power thresholds and maximum zenith and azimuth angles
threshold = .1; % For PIB
irr_threshold = 1; % Irradiance Peak
max_azimuth = 20;
max_zenith = 20;


% Define boresight range distances
bs_ranges = [5:500:10005]';


% Initiate RunHELEEOS Wrapper
R = RunHELEEOS([]);
R.resetCache();
```

```matlab
% Turn on file output

R.toggleFileOutputOff();

R.toggleDebuggerOff;




for engage_ind = 29 % loop through all engagements




% Get Radar Data for PPA or ULA and 35 or 94 GHz


wavelength = 2.99e8/(engagement_list.Frequency(engage_ind)*10^9);




% Get radar data

[azimuths, zeniths, powers] = inputRadarData(engagement_list.RadarArray(engage_ind),

    engagement_list.Frequency(engage_ind), radar_folder, threshold, max_azimuth, ma:


% Set up inputs

in = RunHELEEOS.getDefaultInputs();

platAngle = engagement_list.platformAngle(engage_ind);

platAlt = engagement_list.platformAltitude(engage_ind);

in.platform.setInitialAltitude(platAlt);

% Turn on observer (causes problems in the Phase function calc - see ln 226 of RunHI

in.setUseObserver(true);

in.setWindGroundSpeed(0); % Turn off wind speed

% Set turbulence defined in engagement list

in.turbulence.setType(Turbulence.zero);

in.setAerosols(Aerosols.standard)

in.setAerosolsStandardType(Aerosols.standardModels.clear)
```

```matlab
% Input Weather Conditions (if applicable)
TYPE_LIST = {'Cumulus Continental Clean (cucc)', ...
'Cumulus Continental Polluted (cucp)', ...
'Cumulus Maritime (cuma)', ...
'Stratus Continental (stco)', ...
'Stratus Maritime (stma)', ...
'Fog', ...
'Ice Fog', ...
'Cirrus (-25C)', ...
'Cirrus (-50C)', ...
'Cirrus + Small Particles (-50C)', ...
'Drizzle (2 mm/hour)', ...
'Very Light Rain (2 mm/hour)', ...
'Light Rain (5 mm/hour)', ...
'Moderate Rain (12.5 mm/hour)', ...
'Heavy Rain (25 mm/hour)', ...
'Extreme Rain (75 mm/hour)'};


weather = engagement_list.weather{engage_ind};
weatherLowAlt =   engagement_list.weatherLowAlt(engage_ind);
weatherHighAlt = engagement_list.weatherHighAlt(engage_ind);


if ~strcmp(weather, '')
weatherType = find(strcmp(TYPE_LIST, weather));
in.addWeather(weatherType, weatherLowAlt, weatherHighAlt);
end

% Get atmosphere type from list and assign values
if strcmp(engagement_list.atmosphereType(engage_ind),'standard')
in.setAtmosphere(Atmosphere.standard);
```

```matlab
if strcmp(engagement_list.standardType(engage_ind),'us1976Dry')
in.setAtmosphereStandardType('U.S. 1976 Std Dry (No Season)')
elseif strcmp(engagement_list.standardType(engage_ind),'us1976')
in.setAtmosphereStandardType('U.S. 1976 Std (No Season)')
elseif strcmp(engagement_list.standardType(engage_ind),'tropical')
in.setAtmosphereStandardType('Tropical')
else
error('No standard atmosphere type selected (std, std dry, or tropical)')
end
elseif strcmp(engagement_list.atmosphereType(engage_ind),'expert')
in.setAtmosphere(Atmosphere.expert)
in.setLatitude(8.98); % For Panama City
in.setLongitude(-79.55);
in.setTimeOfDay(globals.ExPERT.timeOfDay.from12to15); % For time of day


else % Nomads Data
in.setAtmosphere(Atmosphere.nomads);
in.nomads.setFilename('201509010600012');


in.nomads.setYear(2015)
in.nomads.setDay(01)
in.nomads.setMonth(09)
in.nomads.setCycle('0600')
in.nomads.setTime('012')


in.setLatitude(8.98); % For Panama City
in.setLongitude(-79.55);


end % If atmosphere loop


% Upload inputs
```

```matlab
R.resetCache();

R.upload('in', in, 'new');

R.load('new')


% Set Wavelength

R.prof.inputs.setWavelength(wavelength);


% Run the atmosphere that will be standard for all engagement runs

R.runAtmosphere();




% Initialize matrix of stored values

pib = ones([length(zeniths), length(bs_ranges)]);

irradiancepeak = ones([length(zeniths), length(bs_ranges)]);

trans = ones([length(zeniths), length(bs_ranges)]);

targAlt = ones([length(zeniths), length(bs_ranges)]);

los_range = ones([length(zeniths), length(bs_ranges)]);




% Define the specific variables for this azimuth and elevation and run the
% engagement, loop through all.

for i = 1:length(powers)

R.prof.inputs.platform.setPower(powers(i));

R.prof.inputs.platform.setInitialRelativeAzimuth(azimuths(i));


for k = 1:length(bs_ranges)
% Calculate target altitude

targAlt(i,k) = bs_ranges(k)*sind(platAngle + zeniths(i)) + platAlt;
% Calculate Line of Sight Range at that particular angle

los_range(i,k) = bs_ranges(k);
```

```matlab
% Run the engagement if good geometry

if targAlt(i,k) > 0
% Set distance and altitude
R.prof.inputs.target.setInitialAltitude(targAlt(i,k));
R.prof.inputs.platform.setInitialDistance(los_range(i,k));

disp(['working on zenith: ' num2str(zeniths(i)) ' azimuth: ' ...
    num2str(azimuths(i)) ' range: ' num2str(bs_ranges(k))])
R.runEngagement();

% Store the values calculated
pib(i,k) = R.prof.outputs.averages.getIrradianceAllEffectsPib();
irradiancepeak(i,k) = R.prof.outputs.averages.getIrradianceAllEffectsPeak();
trans(i,k) = R.prof.outputs.averages.getTotalTrans();

else
pib(i,k) = NaN;
irradiancepeak(i,k) = NaN;
trans(i,k) = NaN;
end
% If values fall below threshold, stop terminating that
% range
if pib(i,k) < threshold && irradiancepeak(i,k) < irr_threshold
if i == numel(zeniths) % If very last direction
pib(i,k:end) = NaN;
irradiancepeak(i,k:end) = NaN;
trans(i,k:end) = NaN;
else
% Set rest of range to NaN
pib(i,k+1:end) = NaN;
irradiancepeak(i,k+1:end) = NaN;
```

155

```matlab
        trans(i,k+1:end) = NaN;

    end


    break


    else


    end


    end % For ranges



    end % For zeniths


    %Save power in the bucket into an output folder that will be saved in
    %the input folder


    % Create a variable of information about this engagement for
    % verification
    platform_altitude = R.prof.inputs.platform.getInitialAltitude;
    atmosphere_type = R.prof.inputs.getAtmosphere;
    std_type = R.prof.inputs.getAtmosphereStandardType;


    weather = R.prof.inputs.getWeather;
    if ~isempty(weather)
    weather_low_alt = weather(2);
    weather_high_alt = weather(3);
    weather_type = TYPE_LIST{weather(1)};
    name = strcat(engagement_list.RadarArray(engage_ind),'_',...
        num2str(engagement_list.Frequency(engage_ind)),'_',...
        engagement_list.atmosphereType(engage_ind),'_',...
        engagement_list.standardType(engage_ind),'_WX_Num_',...
```

156

```matlab
        num2str(weather(1)),'_',num2str(weatherLowAlt),'_',...
        num2str(weatherHighAlt),'_platAlt_',num2str(platAlt),...
        '_look_',num2str(platAngle));

else
weather_low_alt = [];
weather_high_alt = [];
weather_type = [];
weather = [];
name = strcat(engagement_list.RadarArray(engage_ind),'_',...
num2str(engagement_list.Frequency(engage_ind)),'_',...
engagement_list.atmosphereType(engage_ind),'_',...
engagement_list.standardType(engage_ind),'_platAlt_',...
num2str(platAlt),'_look_',num2str(platAngle));

end



engagement_info = v2struct(platform_altitude,weather,...
weather_high_alt, weather_low_alt,weather_type,...
atmosphere_type,std_type, platAngle);



fileName = [radar_folder, '\', name{1}];
matfile(fileName, 'Writable', true);
save(fileName, 'pib');
save(fileName, 'irradiancepeak', '-append');
save(fileName, 'trans', '-append');
save(fileName, 'zeniths', '-append');
save(fileName, 'azimuths', '-append');
save(fileName, 'los_range', '-append');
```

```matlab
save(fileName, 'targAlt', '-append');

save(fileName, 'powers', '-append');

save(fileName, 'engagement_info', '-append');

disp(['Complete with radar file ' name{1}])



end % For engagement list


end
```

3.1   inputRadarData MATLAB Function (Needed By Script)

```matlab
function [azimuths, zeniths, powers] = inputRadarData(array,frequency, ...
    radar_folder, threshold, max_azimuth, max_zenith)
%Get the name of the radar data file in question
baseFilename = strcat(array,'_',num2str(frequency),'_Watts-1.mat');
baseFilename = baseFilename{1};
%read radar data file
radarData = load([radar_folder '/' baseFilename]);
azimuths = radarData.AZ_ANG;
zeniths = radarData.EL_ANG;
powers = radarData.PAT_W_SQ_MET;


%If negative, convert to positive equivalent
% azimuths(azimuths < 0) = azimuths(azimuths < 0) + 360;
% zeniths(zeniths < 0) = zeniths(zeniths < 0) + 360;


% Throw away data outside the cone
zeniths = zeniths((91 - max_zenith):(91 + max_zenith));
azimuths = azimuths((181 - max_azimuth):(181 + max_azimuth));
powers = powers((91 - max_zenith):(91 + max_zenith),...
```

```matlab
        (181 - max_azimuth):(181 + max_azimuth));


    %Cut off data where power is less than the threshold
    [azimuths, zeniths] = meshgrid(zeniths, azimuths);
    zeniths = zeniths(powers >= threshold);
    azimuths = azimuths(powers >= threshold);
    powers = powers(powers >= threshold);
    % Take transpose to rotate 90 degrees so ULAs slice vertically
    % powers = powers;
end
```

Appendix D. MATLAB Script for Generating Plots from Calculated Data

```matlab
function final_image_processing(userin)


% This function plots a set of .mat files in a folder and plots the dB

% attenuation with respect to the PIB/IRR value that user defines


% Richard D Cook - AFIT/ENP


% Note for using v2struct and userin structure - Example Structure creation

%

% savefigtoggleon = true; % Toggles save .fig and .png if true

% xy_res = 1000; % Resolution for interpolation in the plane perpendicular to the range

% interpolate = 0; % 1 if you want to interpolate according to xy_res (not currently fun

% datatype = 'irr'; % Either irr or pib for irradiance or power in the bucket

% inputFolder = '/Users/Richard_Cook_MBP/Documents/MATLAB/Thesis Data/Results_20_deg_cor

% figpath = '/Users/Richard_Cook_MBP/Documents/MATLAB/Thesis Data/Results_20_deg_cone/ne

% pt_size = 60; % Size of each filled circle in scatter3 plot

% ref_value_35 = 1.4e6; % dB reference value for a 35 GHz file

% ref_value_94 = 1.56e6; % dB reference value for a 94 GHz file


% userin = v2struct(savefigtoggleon,xy_res,interpolate,datatype,...

% inputFolder,figpath,pt_size);



format long g % So no Sci Not in altitude coordinate


%% **** Begin User Inputs ****
v2struct(userin) % v2struct.m can be found on File Exchange
```

```matlab
% **** End User Inputs ****

%% Inport the Data Files

rawDataFiles = dir(fullfile(inputFolder,'*.mat'));

for ii = 1:length(rawDataFiles) % Loop through all data files


% Get name of file

name = rawDataFiles(ii).name;

[~,basename,~] = fileparts([inputFolder '/' name]);

% Load the actual atmosphere file
load([inputFolder '/' name]);

if strcmp(datatype,'irr')
data = irradiancepeak;
else
data = pib;
end

% Trim off last azimuth/elevation pair (goes to full range)
data = data(1:end-1,:);
azimuths = azimuths(1:end-1,:);
zeniths = zeniths(1:end-1,:);
los_range = los_range(1:end-1,:);
targAlt = targAlt(1:end-1,:);
```

```matlab
% Setup the colormap
cmap = load('/Users/Richard_Cook_MBP/Documents/MATLAB/functions/fireCMAP.mat');
cmap = cmap.FireCMAP/255;


%% Plot Data
bs_ranges = [5:500:10005]';


for i = 1:size(los_range,2) % Loop through each range value


data_temp = data(:,i);
targAlt_temp = targAlt(:,i);
azimuth_temp = azimuths;
zenith_temp = zeniths;
los_range_temp = ones(size(zenith_temp));
los_range_temp = bs_ranges(i) * los_range_temp;



% Pull out NaN Values if there is a NaN in any of the three arrays
% (data, az, or zenith)
ix = isnan(data_temp);
azimuth_temp(ix) = [];
zenith_temp(ix) = [];
los_range_temp(ix) = [];
targAlt_temp(ix) = [];
data_temp(ix) = [];


% Calculate dB attenuation based off what vacuum value would have been
% at that point


if strcmp(basename(5:6),'35')
dB_atten = log10(data_temp/ref_value_35);
```

162

```matlab
elseif strcmp(basename(5:6),'94')
dB_atten = log10(data_temp/ref_value_94);
else
error('Data did not include a 35 or 94 GHz file name')
end


% Convert to Cartesian coordinates for scatter3 plot
[x,y,z] = sph2cart(deg2rad(azimuth_temp),deg2rad(zenith_temp),los_range_temp);
z = (z+targAlt_temp)/1000 ; % Correct for actual altitude and send to kilometers
x = x/1000; % Range to km
y = y/1000;


scatter3(x,y,z,pt_size,dB_atten,'filled');
hold on
colormap(cmap);
colorbar
h = colorbar;
if strcmp(datatype,'irr')
ylabel(h, 'dB Attenuation of Irradiance (Watts/m^2)')
else
ylabel(h,'dB Attenuation Power in the Bucket (Watts)')
end


end

% title([basename,descriptor],'interpreter','none');
ylabel('Lateral Distance from Aperture (in kilometers)')
xlabel('Range (in kilometers)')
zlabel('Above Ground Level (in kilometers)')
view(-18,6) % Standardize look angle
% set(gca,'YTickLabel','')
```

163

```matlab
% set(gca,'DataAspectRatio',[1 1 1]) % Standardize aspect ratio
caxis([-11,0]) % Standardize colorbar axis
xlim([0,10]);
sdf(1,'spotsize'); % See fileexchange for sdf.m subfunction
pause % Wait for user to adjust image and final approval


%% Save Figure
if savefigtoggleon
if strcmp(datatype,'irr')
saveas(gcf, fullfile(figpath, [basename,'_irr_',descriptor]));
print(gcf,fullfile(figpath,[basename,'_irr_',descriptor]),'-dpng','-r500');
else
saveas(gcf, fullfile(figpath, [basename,'_pib_',descriptor]));
print(gcf,fullfile(figpath,[basename,'_pib_',descriptor]),'-dpng','-r500');
end

close all;
else
end



end
```

Bibliography

1. C. Donald Ahrens. *Meteorology Today: An Introduction to Weather, Climate and Environment.* Brooks/Cole, 1988.

2. B. R. Bean, E. J. Dutton, and Central Radio Propagation Laboratory (U. S.). *Radio Meteorology.* US Government Printing Office, 1966.

3. Ronald Bohlander, Robert W McMillan, James J Gallagher, et al. Atmospheric Effects on Near-Millimeter-Wave Propagation. *Proceedings of the IEEE*, 73(1):49–60, 1985.

4. RK Crane and DW Blood. Handbook for the Estimation of Microwave Propagation Effects: Link Calculations for Earth-Space Paths (Path Loss and Noise Estimation). *NASA STI/Recon Technical Report N*, 82:12301, 1979.

5. Nicholas C. Currie. *Millimeter-Wave Radar Clutter.* Artech House, Boston, 1992.

6. G Daniel Dockery. Development and Use of Electromagnetic Parabolic Equation Propagation Models for U.S. Navy Applications. *Johns Hopkins APL Technical Digest*, 19(3):283–292, 1998.

7. ST Fiorino, RJ Bartell, GP Perram, DW Bunch, LE Gravley, CA Rice, ZP Manning, MJ Krizo, JR Roadcap, and GY Jumper. The HELEEOS Atmospheric Effects Package: A Probabilistic Method for Evaluating Uncertainty in Low-Altitude High Energy Laser Effectiveness. *J. Dir. Energy*, 1(4):347–360, 2006.

8. S.T. Fiorino and K.J. Keefer. Atmospheric Propagation Subject Matter Experts. Personal Correspondence. October 2015.

9. Steven T Fiorino, Richard J Bartell, Matthew J Krizo, Gregory L Caylor, Kenneth P Moore, Thomas R Harris, and Salvatore J Cusumano. A First Principles Atmospheric Propagation & Characterization Tool: the Laser Environmental Effects Definition and Reference (LEEDR). In *Lasers and Applications in Science and Engineering*, pages 68780B–68780B. International Society for Optics and Photonics, 2008.

10. Steven T Fiorino, Richard J Bartell, Matthew J Krizo, and Salvatore J Cusumano. Propagation Variability Assessments of Ship Defense HEL and HPM Performance in Worldwide Maritime Boundary Layer Environments at Wavelengths of 1.0642 μm, 2.141 μm, 3.16 mm and 12.2 cm. In *SPIE Defense and Security Symposium*, pages 69510G–69510G. International Society for Optics and Photonics, 2008.

11. Steven T. Fiorino, Richard J. Bartell, Matthew J. Krizo, Kenneth P. Moore, and Salvatore J. Cusumano. Validation of a Worldwide Physics-Based, High Spectral Resolution Atmospheric Characterization and Propagation Package for UV to RF Wavelengths, 2008.

12. Center for Directed Energy. LEEDR Equations and Principles. Wright-Patterson AFB OH, August 2015.

13. Adrian K. Fung. *Microwave Scattering and Emission Models and Their Applications.* Artech House, Boston, 1994.

14. Liesebet E Gravley. *Comparison of Climatological Optical Turbulence Profiles to Standard, Statistical, and Numerical Models Using HELEEOS.* PhD thesis, Air Force Institute of Technology, 2006.

15. K. L. S. Gunn and T. W. R. East. The Microwave Properties of Precipitation Particles. *Quarterly Journal of the Royal Meteorological Society*, 80(346):522–545, 1954.

16. A.E. Barrios K.D. Anderson, G.E. Lindem. Advanced Propagation Model (APM) Analysis of VHF Signals in the Southern California Desert. *Technical Report* 1945, SPAWAR Systems Center San Diego, August 2006.

17. K.J. Keefer. Directed Energy and Atmospheric Propagation Subject Matter Experts. Personal Correspondence. December 2015.

18. Fred Levien. IMOM Field Test Study and Accuracy Verification Engineering Report. Technical report, Monterrey CA. Naval Postgraduate School, 1998.

19. M. Levy. *Parabolic Equation Methods for Electromagnetic Wave Propagation.* The Institution of Engineering and Technology, 2000.

20. E. P. Magee M. R. Whiteley and A. M. Ngwele. *Scaling for High Energy Laser and Relay Engagement (SHaRE) User Guide.* MZA Associates, Dayton OH, 2011.

21. Sergey Makarov. *Antenna and EM Modeling with MATLAB.* Wiley-Interscience, 2002.

22. W.L. Patterson. Advanced refractive effects prediction system (areps). In *Radar Conference, 2007 IEEE*, pages 891–895, April 2007.

23. Grant W. Petty. *A First Course in Atmospheric Radiation.* Sundog Publishing, Madison WI, 2004.

24. Mark A. Richards, James A. Scheer, and William A. Holm. *Principles of Modern Radar: Basic Principles.* SciTech Publishing, Edison NJ, 1st edition, 2010.

25. James A. Scheer and William L. Melvin. *Principles of Modern Radar Volume 3: Radar Applications.* SciTech Publishing Inc, Edison NJ, 1st edition, 2013.

26. I Sirkova and M Mikhalev. Parabolic Wave Equation Method Applied to the Tropospheric Ducting Propagation Problem: A Survey. *Electromagnetics*, 26(2):155–173, 2006.

27. Merrill Skolnik, editor. *Radar handbook.* McGraw-Hill, New York, 2008.

28. G.W. Stimson, H.D. Griffiths, C. Baker, and D. Adamy. *Stimson's Introduction to Airborne Radar.* SciTech Publishing, Incorporated, 2013.

29. Barron Stone. IMOM Engineer Overview. Presentation, August 2013.

30. V. I. Tatarski. *Wave Propagation in a Turbulent Medium.* McGraw-Hill, New York, 1st edition, 1961.

31. Weather Underground. Historical Weather Conditions for Panama City, Panama.

32. J. H. van Vleck. The Absorption of Microwaves by Oxygen. *Phys. Rev.*, 71:413–424, Apr 1947.

33. H. B. Wallace. Millimeter-wave propagation measurements at the Ballistic Research Laboratory. *IEEE Transactions on Geoscience and Remote Sensing*, 26:253–258, May 1988.

34. John M. Wallace and Peter V. Hobbs. *Atmospheric Science, Second Edition: An Introductory Survey (International Geophysics).* Academic Press, 2006.

35. Warren J Wiscombe. Improved Mie Scattering Algorithms. *Applied optics*, 19(9):1505–1509, 1980.

List of Abbreviations

List of Symbols

REPORT DOCUMENTATION PAGE

1. REPORT DATE *(DD–MM–YYYY)*	2. REPORT TYPE	3. DATES COVERED *(From — To)*
03–24–2016	Master's Thesis	Sept 2014 — Mar 2016

4. TITLE AND SUBTITLE

Capturing Atmospheric Effects on 3-D
Millimeter Wave Radar Propagation Patterns

5a. CONTRACT NUMBER

5b. GRANT NUMBER

5c. PROGRAM ELEMENT NUMBER

6. AUTHOR(S)

Cook, Richard D, 2nd LT, USAF

5d. PROJECT NUMBER

5e. TASK NUMBER

5f. WORK UNIT NUMBER

7. PERFORMING ORGANIZATION NAME(S) AND ADDRESS(ES)

Air Force Institute of Technology
Graduate School of Engineering and Management (AFIT/EN)
2950 Hobson Way
WPAFB OH 45433-7765

8. PERFORMING ORGANIZATION REPORT NUMBER

AFIT-ENP-MS-16-M-063

9. SPONSORING / MONITORING AGENCY NAME(S) AND ADDRESS(ES)

Air Force Research Laboratory
2241 Avionics Circle, Bldg 600
WPAFB OH 45433-7765
(937) 528-8200 (DSN 798)

10. SPONSOR/MONITOR'S ACRONYM(S)

AFRL/RY

11. SPONSOR/MONITOR'S REPORT NUMBER(S)

12. DISTRIBUTION / AVAILABILITY STATEMENT

DISTRIBUTION STATEMENT A:
APPROVED FOR PUBLIC RELEASE; DISTRIBUTION UNLIMITED.

13. SUPPLEMENTARY NOTES

This work is declared a work of the U.S. Government and is not subject to copyright protection in the United States.

14. ABSTRACT

The need to model millimeter wave (MMW) radar propagation is imperative to proper design of aeronautical, civil, and military systems. As radar advances into the MMW regime, atmospheric effects, such as attenuation and refraction, become more pronounced than at traditional radar wavelengths. The High Energy Laser End-to-End Operational Simulation (HELEEOS), in combination with the Laser Environmental Effects Definition and Reference (LEEDR) code, is a powerful tool for simulating laser propagation and effects tied to atmospheric phenomena such as turbulence and extinction. This research attempts to extend HELEEOS to characterize radar patterns in three dimensions as a signal propagates from an antenna through realistic atmospheres and weather conditions. Realistic atmospheres are derived using numerical weather prediction models or climatological databases. The results from these simulations are compared to those from traditional radar propagation software packages. In summary, this research explored adapting a laser propagation model to extend understanding of MMW propagation through various atmospheric and weather conditions.

15. SUBJECT TERMS

Millimeter Wave Radar, Atmospheric Propagation Effects, HEL Laser Modeling, HELEEOS, Radar Propagation Modeling

16. SECURITY CLASSIFICATION OF:			17. LIMITATION OF ABSTRACT	18. NUMBER OF PAGES	19a. NAME OF RESPONSIBLE PERSON
a. REPORT	b. ABSTRACT	c. THIS PAGE			Dr. S.T. Fiorino, AFIT/ENP
U	U	U	UU	185	**19b. TELEPHONE NUMBER** *(include area code)* (937) 255-3636; steven.fiorino@afit.edu